The prostaglandin 15-deoxy- $\Delta^{12,14}$ -PGJ$_2$ inhibits CRM1 mediated protein export

Analysis of nuclear import of human telomerase reverse transcriptase

Dissertation

for the award of the degree

„Doctor rerum naturalium"

Division of Mathematics and Natural Sciences

of the Georg-August University Göttingen

Grundprogramm Biologie

of the Georg-August-University School of Science (GAUSS)

submitted by

Cornelia Frohnert

from Göttingen

Göttingen 2013

Member of the Thesis Committee (First Reviewer):

Prof. Dr. Ralph H. Kehlenbach

Department of Molecular Biology

Center for Biochemistry and Molecular Cell Biology

Georg-August University, Göttingen

Member of the Thesis Committee (Second Reviewer):

Prof. Dr. Ralf Ficner

Department of Molecular Structural Biology

Institute for Microbiology and Genetics

Georg-August University, Göttingen

Statutory declaration:

I herewith declare, that this thesis has been written independently and with no other sources and aids than explicitly quoted.

I would like to use the term 'We' instead of 'I', because during my PhD thesis I was supported by other persons, in particular my supervisor and coworkers. However, the presented work in this dissertation (if not explicitly quoted differently) and the writing were done by myself.

This thesis was not submitted in the same or in a substantially similar version to any other authority to achieve an academic grading.

Cornelia Frohnert

To science
and
to my parents

Content

Abstract

Nuclear import and export of macromoloecules are essential processes in eukaryotic cells. In consequence, different mechanisms of transport developed in the cell, resulting in the involvement of different monodirectional or bidirectional transport receptors, which recognize specific sequences or regions in their cargos.

CRM1, the major cellular export receptor can be specifically inhibited by the fungal compound leptomycin B (LMB). The inhibitor binds to a sensitive cysteine residue (at position 528) in CRM1 resulting in a blockade of the NES recognition site (Kudo et al., 1999; Sun et al., 2013). The question arose whether endogenous substances exist, which also have the ability to inhibit CRM1 mediated protein export in a similar way. The prostaglandin 15-deoxy-$\Delta^{12,14}$-PGJ$_2$ (15d-PGJ$_2$) was found to exhibit a partly similar structure like LMB and CRM1 was identified as a target of 15d-PGJ$_2$. Mass spectrometry analysis identified 15d-PGJ$_2$ to modify CRM1 at the same cysteine residue like LMB. After incubation of cells with 15d-PGJ$_2$, inhibition of CRM1-dependent export was observed. Also kinetic measurements of CRM1 mediated protein export in living cells showed a clear decrease in export capability of endogenous CRM1 after incubation of cells with 15d-PGJ$_2$. Rescue experiments using an LMB insensitive CRM1 with a mutation at cysteine 528 also suggested that 15d-PGJ$_2$ modifies CRM1 at the same residue as LMB (Hilliard et al., 2010). As a conclusion we present a CRM1 inhibitor which can be produced endogenously by cells e.g. during an inflammatory response.

In contrast to export, import of proteins is largely mediated by import receptors from the importin-β superfamily. Import receptors recognize their cargos at specific sequences and some of these sequences are already mapped and classified as nuclear localization signals (NLS). For some of import receptors, no specific consensus sequence for cargo recognition could be identified so far. In consequence, the import pathways of many nuclear proteins still remain elusive.

In this work we gained further insights into the nuclear import of the protein subunit of telomerase reverse transcriptase (TERT), which catalyzes the de novo synthesis of telomeric chromosome ends. Previous studies identified the cytoplasmic filament nucleoporin Nup358 to be involved in TERT nuclear import (Hutten, 2007). After depletion of Nup358, TERT showed an import defect, resulting in a cytoplasmic or equal cellular localization instead of a

nuclear localization. In this work, we were able to identify a zinc finger region in Nup358 to play a crucial role in TERT nuclear import. Using mutagenesis, we discovered two independent NLS sites in the TERT protein, which contribute to nuclear import of TERT. By siRNA mediated depletion of major eukaryotic import receptors we were able to identify importin-7 as a responsible import receptor of TERT. FLIP experiments, measuring the import kinetics of TERT showed a clear decrease in TERT nuclear import upon depletion of importin-7. Rescue experiments using a siRNA resistant mutant of importin-7 confirmed these results.

Together, our findings provide further detailed insights into the nuclear import pathways of TERT pointing to important roles of Nup358 and importin-7.

1. Introduction

1.1 General mechanisms of nucleocytoplasmic transport

In contrast to prokaryotic cells the eukaryotic cell contains several compartments and its genome in the nucleus is isolated from the cytoplasm. The nucleus is surrounded by two lipid bilayers, forming the inner and the outer nuclear membrane, which is non-permeable for proteins or RNAs. However, several types of RNAs have to leave the nucleus to build a ribosome or to be translated into proteins in the cytoplasm. Therefore a mechanism had to evolve that selectively permits entrance to the nucleus for a certain subset of proteins and also selectively exports proteins and mRNAs to the cytoplasm. To achieve this, the nuclear envelope contains pores through which transport of proteins and different RNAs in both directions can occur. While small molecules up to 50 kDa can diffuse freely through the pore larger molecules utilize specific recognition sequences that can bind a transport receptor to enable transport of the cargo through the pore in an energy dependent manner (reviewed by Chook et al., 2011; Wente et al., 2010; Pemberton et al., 2005).

1.1.1 The nuclear pore complex and its translocation models

The nuclear pore complex (NPC) is a large cylindrical protein complex that spans the nuclear envelope from the outer nuclear membrane to the inner nuclear membrane, creates a channel-like structure. The NPC consists of several copies of around 30 different nucleoporins (Nups) which form an eight fold rotational symmetry and give the NPC a mass of ~ 125 mDa (Akey et al., 1993; reviewed in Alber et al., 2007a; Schooley et al., 2012). As shown in figure I the NPC can be divided into several sections. The cytoplasmic one contains seven nucleoporins that are located close to the outer nuclear membrane e.g. Nup214 or Nup88 (reviewed in Hoelz et al., 2011). These Nups form an outer ring of the NPC, which connects the cytoplasmic filaments formed by Nup358 (RanBP2) (Walther et al., 2002; Bernad et al., 2004). The middle part is arranged to give rise to a scaffold that forms a central transport channel, the so-called spoke ring (Goldberg et al., 1996). The scaffold forming nucleoporins consist of four channel Nups which are connected to five adaptor Nups, which are again

linked to nine coat nucleoporins. Three pore membrane (POM) proteins connected to the coat Nups are also linked to pore membrane nucleoporins (POMs) that anchor the NPC into the nuclear envelope (Alber et al., 2007b; reviewed in Hoelz et al., 2011). At its nuclear face the NPC harbors three Nups forming a basket-like structure ending in a distal ring (reviewed in Terry et al., 2009).

Nucleoporins can also be divided into FG (phenylalanine-glycine)-nucleoporins and non-FG-nucleoporins. Nearly one third of all Nups belong to the group of FG nucleoporins which contain several phenylalanine-glycine repeats (reviewed in Burns et al., 2012). FG-Nups facilitate trafficking through the NPC and they are present at the cytoplasmic filaments, among the channel Nups where they form the spoke ring as well as in the basket structure (Alber et al., 2007b). During passage through the NPC, transport receptors can transiently interact with the FGs of the nucleoporins via hydrophobic regions on their surface (Ribbeck et al., 2001; reviewed in Pemberton et al., 2005). There are currently several different models in the literature describing how transport receptors with their cargos could translocate through the pore.
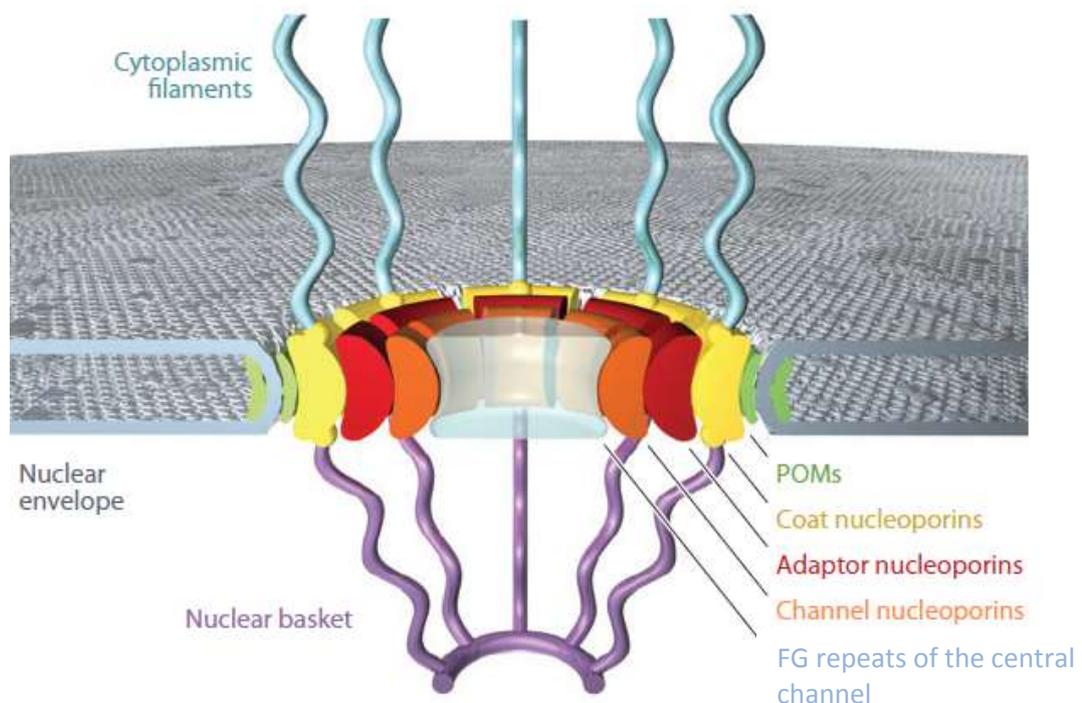
Figure I: The nuclear pore complex (Hoelz et al., 2011)
A schematic model of the vertebrate nuclear pore complex with its sub compartments. The pore is constructed of several different nucleoporins with different properties which form cytoplasmic filaments, the translocation channel and the nuclear basket. The nuclear pore provides a selective barrier between nucleus and cytoplasm, permitting transport of only certain proteins.

The "hydrogel-model" for example suggests that FGs of different nucleoporins form a gel-like meshwork within the central channel of the NPC. Transport receptors can interact with the FGs through hydrophobic regions on their surface, disrupt the inter FG connections and thus translocate through the pore (Ribbeck et al., 2001; Frey et al., 2006; Frey et al., 2007).

Observations during atomic force microscopy indicates, that FG repeats collapse after binding of transport factors. By this interaction, transport factors open up their own channel through the FG meshwork and translocate through the pore (Lim et al. 2007a; Lim et al. 2007b; reviewed in Wente et al., 2010)

The "reduction in dimensionality"-model hypothesizes that the inner surface of the transport channel is coated by FG repeats. Transport receptors entering the channel can bind to the FGs and move by a random walk on the inner surface of the transport channel. They have full access and can pass the NPC easily. Molecules that are unable to bind FGs cannot pass the tube easily and are excluded when they are too large to pass the FG-free central part of the NPC channel (Peters 2005; reviewed in Wente et al., 2010).

All models mentioned above have in common that solely the interactions of FG repeats with transport receptors are responsible for translocation of receptor-cargo complexes through the pore. There are hints that several classes of FG repeats exist depending on their charge, density and FG repeat motif, hence exhibiting different physical behavior (Krishnan et al., 2008). Different transport factors then may preferentially bind to only certain FG repeats. In consequence, very diverse, functionally independent, and yet specific transport pathways through the pore might exist (reviewed in Tran et al., 2006).

In contrast, the "virtual gate"- model proposes the NPC to function as an energetic barrier with non- cohesive FG-nups reaching into the transport channel (Rout et al., 2003). Soluble molecules possess a certain defined energy state. Following this model, the NPC requires a certain energy state for molecular transition. Smaller molecules may possess this energy and can reach this required "transition state" and translocate through the pore. Larger molecules are restricted from this strategy because the energy required for their translocation is too high. In contrast, transport factors with their cargos bind to the FG repeats, decreasing the required energy, and can so reach the transition state.

Apart from the described single models hybrid models also exist, combining at least two models and theories. A very recent hybrid model is the "forest-model", combining the "virtual gate"- and "hydrogel-models" (Yamada et al., 2010). This model suggests that FG-Nups form a

"forest"-like landscape within the nuclear pore channel enabled by their diverse structure and interactivity, and dependant on their ability to collapse or to form longer relaxed stretches. Using these different behaviors the authors classify FG-Nups into "shrubs" with only collapsed coils and "trees", bearing an extended structure with coils sitting on it. These "trees" reach into the central part of the transport channel, where transport receptors bound to large substrates translocate, creating a permeability barrier described by the "hydrogel"-model. In contrast, the "shrubs" create a different zone close to the wall of the transport channel where small molecules and transport receptors with smaller cargos can translocate. There translocation depends on the required entropic energy level, corresponding to the "virtual gate"-model.

1.1.2 Signal-and receptor-mediated nucleocytoplasmic transport through the pore

Cargoes are bound by soluble transport receptors through specific sequences and are transported in an energy dependent manner. Among eukaryotes transport receptors are evolutionary conserved and exhibit a size of 90-145kDa. Around 20 transport receptors are known and most of them belong to the importinβ-like family (reviewed by Pemberton et al., 2005; Fried et al., 2003). Import from the cytoplasm into the nucleus is mediated by several importins while export out of the nucleus into the cytoplasm occurs through binding of exportins to their cargo. Importins bind their substrates via small recognition sequences, so called nuclear localization signals (NLS), within the cargo. Via interaction with components of the nuclear pore, this import complex translocates to the nucleus. In the nucleus, the import substrate is released by binding of RanGTP to the receptor. The receptor-RanGTP complex is later translocated back to the cytoplasm (Jäkel et al., 1998; Izaurralde et al., 1997).

One of the first and very well characterized import sequences is the classical nuclear localization sequence (cNLS) which is composed of the amino acids lysine and arginine [K(K/R)X(K/R)] (Conti et al., 2000; Kalderon et al., 1984). It can either occur as a monopartite cNLS which comprises one basic region or as a bipartite cNLS which consists of two basic regions (Dingwall et al., 1982; Robbins et al., 1991). A cNLS is recognized by importin-α which again is recognized by importin-β. Importin-β binds importin-α at its IBB (Importinβ-binding domain) and the complex is then translocated through the pore (Görlich et al., 1996). Importin-β is also able to bind to other NLSs directly. It is known that cyclin B1 or the

parathyroid hormone-related protein (PTHrP) are importin-β dependent cargos (Moore et al., 1999; Cingolani et al., 2002).

Other nuclear localization signals exist that bind to import receptors other than importin-β or importin-α. Another well characterized import signal is the glycine rich M9-sequence containing a PY-motif which is recognized by transportin directly (Siomi et al., 1997; Nakielny et al., 1996). This sequence is defined by the existence of positively charged amino acids within the motif with the consensus sequence R/K/HX$_{(2-5)}$PY (Lee et al., 2006).

Besides this signals also exist that are recognized by multiple import receptors like the BIB (beta-like import receptor binding) domain in rpL23a (Jäkel et al., 1998). The HIV-1 Rev protein has also been shown *in-vitro* to be imported by several import receptors via an arginine-rich region (Arnold et al., 2006).
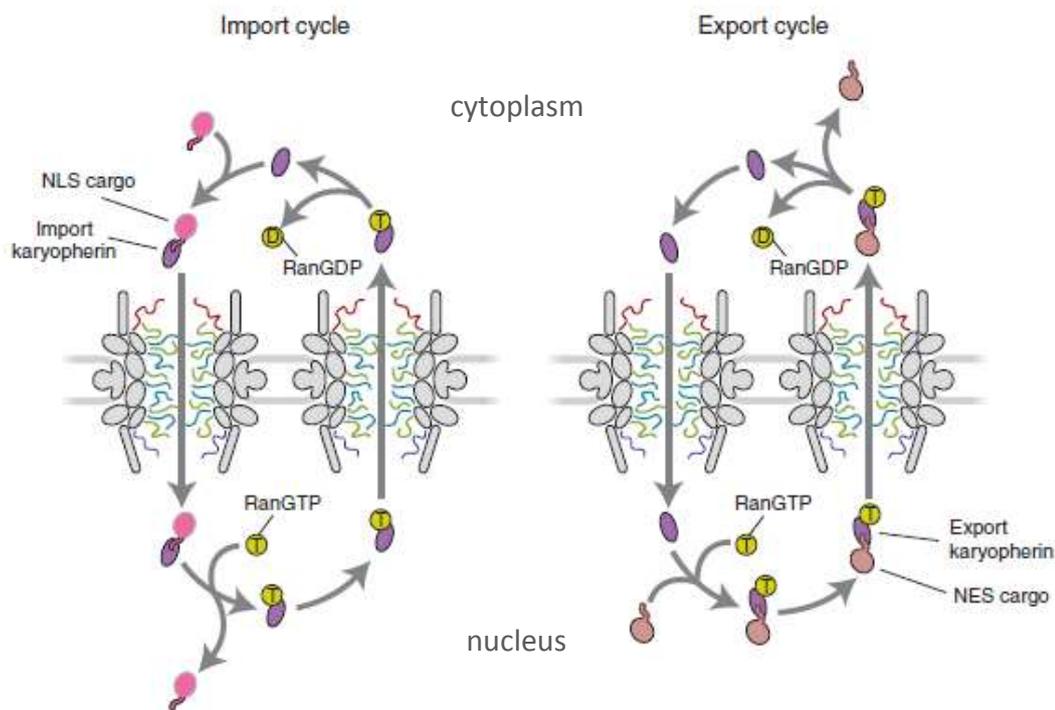
Figure II: The transport cycle (Wente et al., 2010)
A schematic depiction of the import and export cycle in a vertebrate cell depending on the cofactor Ran. RanGTP bound import receptors translocate from the nucleus into the cytoplasm and are freed from Ran following the hydrolysis of GTP to GDP. They recognize their substrate in the absence of Ran in the cytoplasm, translocate through the pore into the nucleus where the cargo is then released by RanGTP binding to the receptor. In contrast to import receptors, binding of substrates to export receptors requires RanGTP. This trimeric export complex translocates through the pore into the cytoplasm where the cargo is released after GTP hydrolysis to GDP. The export receptor is recycled alone back to the nucleus.

Nuclear export is mediated by exportins, which recognize their substrates via a nuclear export signal (NES). Among the importin β-like family of nuclear transport receptors, there are eight nuclear export receptors known (reviewed in Fried et al., 2003; Weis, 2003). Most of them are highly specialized receptors transporting just a few cargos. They also mediate export of several endogenous RNAs and viral RNAs (reviewed in Carmody et al., 2009, Wente et al., 2010).

The main export receptor in the eukaryotic cell is a very well characterized export factor CRM1 (chromosome region maintenance 1) (Stade et al., 1997; Fornerod et al., 1997). CRM1 recognizes its substrates in the nucleus at a hydrophobic leucine-rich region with the consensus sequence (ϕ^1 X$_{2-3}$ ϕ^2 X$_{2-3}$ ϕ^3 X ϕ^4) consisting of hydrophobic amino acids (ϕ) with a regular interval of random amino acids (X) (Fornerod et al., 1997a; Kosugi et al., 2008). Additionally to the NES the receptor binds a cofactor called RanGTP forming a trimeric complex. Formation of this trimer is assisted by Ran-binding protein 3 (RanBP3) that links Crm1 to the Ran guanine nucleotide exchange factor (RCC1/ RanGEF) (Fornerod et al., 1997a; Fried et al., 2003; Lindsay et al., 2001; Nemergut et al., 2002).

(see also 1.2.2 for detailed description of CRM1)

1.1.3 The cofactor Ran

The small protein Ran belongs to the Ras family of GTPases and is involved in nucleocytoplasmic transport (Bischoff et al., 1991; reviewed in Pemberton et al., 2005; Stewart, 2007). Ran exhibits a weak intrinsic GTPase activity, which is enhanced after binding to RanGAP (Ran-GTPase activating protein) (Bischoff et al., 1994). Ran can exist in a GTP bound state as well as in a GDP bound state (Bischoff et al., 1991). In the cytoplasm only low RanGTP levels are detectable, Ran is present predominantly in a GDP bound state. In the nucleus, GDP exchanged by the chromatin bound nucleotide exchange factor RCC1 (RanGEF) to yield GTP. This asymmetric distribution of GDP and GTP loaded Ran between cytoplasm and nucleus contributes to the directionality of transport in the cell (Mattaj et al., 1998; Görlich et al., 1999; Bischoff et al., 1991a). This Ran gradient is involved in regulation of transport since RanGTP binds to the incoming import complexes and releases the cargo from its receptor (Rexach et al., 1995; Görlich et al., 1996a; Floer et al., 1997). RanGTP binding to the import receptor in the nucleus also contributes to its retranslocation to the cytoplasm

(Jäkel et al., 1998). In contrast to import complexes which bind their cargos in the absence of Ran in the cytoplasm, export receptors require RanGTP to bind their cargos. In the nucleus the export receptors form trimeric complexes with their cargos and the cofactor RanGTP. Following the formation of a trimeric export complex, the complex translocates through the pore into the cytoplasm (reviewed in Wente et al., 2010). There, the cargo has to be released from the export receptor. In the trimeric complex RanGTP is insensitive towards RanGAP mediated nucleotide hydrolysis of RanGTP and therefore additional factors become necessary for release of the cargo. The soluble cytoplasmic protein RanBP1 (Ran-binding protein1) and also the nucleoporin Nup358 with its four Ran-binding sites contribute to the dissociation of trimeric export complexes in the cytoplasm (Bischoff et al., 1997; Matunis et al., 1996). The export factor is recycled back to the nucleus to be available for another round of transport. RanGDP is also imported back into the nucleus via the nuclear transport factor2 (NTF2) where RCC1 triggers the nucleotide exchange from GDP to GTP again (Ribbeck et al., 1998; Smith et al., 1998).

1.2 Transport receptors and their mechanisms

1.2.1 The importin-β-like superfamily

The importin-β-like superfamily of transport receptors contains the largest number of import receptors in the eukaryotic cell. All members of this family contain an N-terminal Ran-binding domain and possess a similar overall structure (reviewed in Fried et al., 2003). A very well characterized import receptor is importin-β. This import receptor consists of 19 tandemly repeated HEAT (Huntington, elongation factor 3, 'A' subunit of protein phosphatase 2A and TOR1) repeats. One HEAT repeat comprises 2 helices which are connected by a loop (reviewed in Pemberton et al., 2005; Cingolani et al., 1999; Cingolani et al., 2002). Among the import receptors importin-β shows an exceptional behavior since it can form heterodimers with importin-α (Görlich et al., 1995) or importin-7 (Görlich et al., 1997; Jäkel et al., 1999). The importin-β/ importin-7 heterodimer for example imports the histone H1 (Jäkel et al., 1999).

Importin-7 is a Ran-binding protein of 119kDa with few identified cargos for example the murine zinc finger protein called EZI, ERK-2, MEK1 and Smad3 (Saijou et al., 2007; Chunderland et al., 2008; reviewed in Chook et al., 2011). Other cargos e.g. the ribosomal proteins rPL23a, rPS7 and rPL5 are also known substrates of importin-7, but interestingly they are also substrates of other transport receptors e.g. importin-5, -9, -α/β and transportin (Jäkel et al., 1998).

Although binding regions for several importin-7 cargos have been mapped, a specific recognition motif has not been determined until now. Very often importin-7 cargos are bound by the import receptor at various domains and long stretches of 50 amino acids or more are involved in binding (see figure III) (Chook et al., 2011). In EZI for example, a region between zinc fingers 9-12 could be identified as the essential import region (Saijou et al., 2007). It could therefore be that importin-7 recognition motifs are structurally very diverse (Chook et al., 2011). In this work we present a new import substrate of importin-7.

1.2.2 CRM1 recognizes its cargo via a nuclear export signal (NES) and thereby undergoes conformational changes

CRM1 is a very well-studied export receptor in the mammalian cell forming a trimeric export complex consisting of the receptor, RanGTP and a CRM1 specific cargo. CRM1 recognizes proteins containing a hydrophobic, mostly leucine-rich NES motif (Fischer et al., 1995; Zhang et al., 1998). Very recently a structure of *Chaetomium thermophilum* CRM1 which possesses 50% homology towards *human* CRM1 has been solved in the absence of additional factors such as RanGTP or snurportin (Monecke et al., 2013). The export receptor comprises a structure often referred to be ring-like and consists of 21 HEAT repeats (Monecke et al., 2013; Monecke et al., 2009; Dong et al., 2009). For a long time it remained unclear whether the binding of RanGTP causes changes in the CRM1 conformation. As shown by Monecke et al., 2013, Ran binds to CRM1 and interacts with an acidic loop between heat repeat 9A and 9B. This binding causes structural changes within the receptor. Upon binding, the C-terminal heat repeat H21 flips towards the N-terminus, interacting with heat repeats H2 to H5, providing space in the middle of the CRM1-ring for RanGTP binding (figure III B/D). In contrast to this change in conformation the authors showed that empty CRM1 exhibits a more relaxed and extended conformation with a free N-terminus and the C-terminus interacting with a region

close to the hydrophobic cleft of CRM1 (figure III A). When CRM1 binds NES substrates e.g. snurportin1 (SPN1) or RanBP1 the conformation of the receptor also changes.
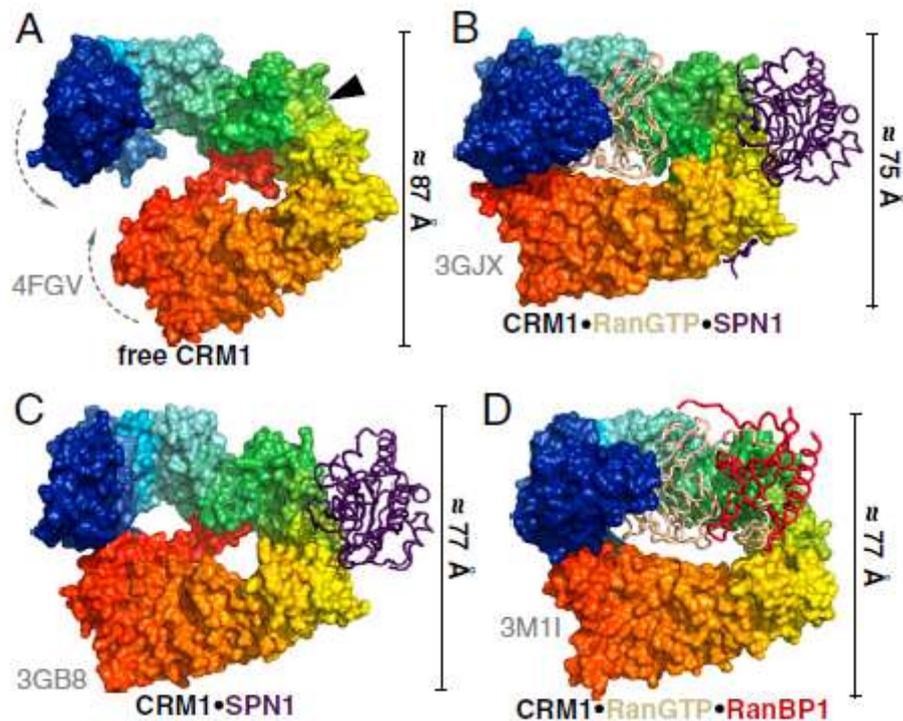
Figure III: Conformational changes in CRM1 after binding of NES-cargos and RanGTP (taken from Monecke et al., 2013)
(A) Free *ct*CRM1 exhibiting a relaxed conformation with a blocked hydrophobic cleft, indicated by the arrow head. **(B)** CRM1*RanGTP*SPN1 complex **(C)** CRM1*SPN1 complex **(D)** CRM1*RanGTP*RanBP1 complex **(B-D)** Upon binding of substrates to the CRM1 molecule, N- and C- termini move closer together, therefore opening the hydrophobic cleft and enhancing its availability for export substrates.

N- and C- termini of CRM1 move closer together and opens helices 11A and 12A, making the hydrophobic cleft accessible for NES-cargos (figure III C/D) (Koyama et al., 2010; Monecke et al., 2013).

The hydrophobic cleft in the region of HEAT repeats 11A and 12A, providing the NES binding site, locates at the convex surface of CRM1. Although there is no common binding mechanism and NES sequences differ among proteins they all bind to this hydrophobic cleft (Güttler et al., 2010). The binding affinity of most NES-cagos to the cleft is low (Askjaer et al., 1999). The CRM1 cargo SPN1 is an exception, it binds to CRM1 even in the absence of RanGTP (figure IV C) (Paraskeva et al., 1999).

Other studies show the involvement of an α-helical C-terminal part of CRM1 in substrate binding. After binding of RanGTP to CRM1 the loop of HEAT repeat 9 becomes an ordered β-hairpin that interacts with HEAT repeats 12-15. As a result, the α-helix and the loop of HEAT repeat 9 can contribute to NES-substrate binding (Dong et al., 2009; Fox et al., 2011).

Besides proteins, CRM1 can also export several RNAs e.g. some mRNAs, uridine-rich small nuclear RNAs, viral RNAs and ribosomal RNAs with the help of NES containing adaptor proteins (Moy et al., 2002; Gadal et al., 2001; Fisher et al., 1995; reviewed in Rodriguez et al., 2004). It is known that the 60S pre-ribosomal RNA is exported by CRM1 (Gadal et al., 2001) and there are hints of an involvement of CRM1 in intranuclear trafficking of snpRNPs (Pradet-Balade et al., 2011).

The complete mechanism of translocation of the trimeric export complex has not yet been completely solved. But, it is known that the complex translocates through the pore by interacting with the nucleoporins Nup88/Nup214 (Kehlenbach et al., 1999; Hutten et al., 2006; Roloff et al., 2013). The trimeric complex is then dissociated with the help of Nup358, NTX1, RanBP1 and RanGAP1 (Black et al., 2001; Bischoff et al., 1997; Mahajan et al., 1997).

1.2.3 Specific inhibition of CRM1 by LeptomycinB

Leptomycin B (LMB) is an unsaturated fatty acid derived from a fungus (Hamamoto et al., 1983a; Hamamoto et al., 1983b). It is also known to be a highly specific and potent inhibitor of CRM1 mediated protein export. It covalently modifies a sensitive cysteine residue at position 528 located in the hydrophobic cleft and thus abolishing docking of export substrates to the receptor (Kudo et al., 1999).

In a very recent study it was shown that not only LMB alone is responsible for attacking the cysteine, but furthermore CRM1 itself contributes and enhances binding of LMB to cysteine 528 by driving a chemical reaction. Following the initial CRM1-LMB interaction the export receptor drives lactone hydrolysis, thereby strengthening the modification by LMB. This step enhances the inhibitor potency and results in irreversibility of this modification (Sun et al., 2013). This extraordinary behavior of the CRM1-LMB interaction can also help to explain the very high specificity of LMB towards CRM1.

1.3 The prostaglandin 15-deoxy-$\Delta^{12,14}$-PGJ$_2$

Prostaglandins are small signaling molecules, involved in inflammatory response, thrombosis, gastrointestinal secretion and in apoptosis (Shin et al., 2009; Ho et al., 2008). Prostaglandins derive from arachidonic acid, which is released from lipid plasma membranes by phospholipase A2.

Arachidonic acid is then processed by cyclooxygenase1 and -2 to form prostaglandinH$_2$ (PGH$_2$), a precursor in the synthesis of many other prostaglandins. PGH$_2$ is further processed by Hematopoietic-prostaglandinD$_2$ synthase (H-PGDS) and/or the Lipocaline-type PGDS (L-PGDS) to prostaglandinD$_2$ (PGD$_2$). Hydrolysis of PGD$_2$ forms the prostaglandin J$_2$ -series such as 15-deoxy-$\Delta^{12,14}$-PGJ$_2$ (15d-PGJ$_2$) (reviewed in Uchida et al., 2008; Scher et al., 2004).

Prostaglandin 15d-PGJ$_2$ seems to be unique among the prostaglandins. In contrast to other prostaglandins which bind to extracellular receptors and trigger a signal transduction cascade, 15d-PGJ$_2$ acts mainly intracellular. In addition, 15d-PGJ$_2$ displays anti-inflammatory effects (Straus et al., 2001). This can be explained by the action of 15d-PGJ$_2$ as a high-affinity ligand for the peroxisome proliferator-activated receptor γ (PPARγ) (Straus et al., 2000). PPARγ interacts with inflammation stimulating transcription factors in the nucleus but can be also involved in complex formation with transcriptional coactivators and corepressors. It has been shown that PPARγ also modulates the activity of kinases involved in pro-inflammatory pathways (reviewed in Uchida et al., 2008). The PGJ$_2$ anti-inflammatory effect can be also enhanced by its involvement in cellular apoptosis (Shin et al., 2009; Ho et al., 2008).

PGJ$_2$ and its metabolites e.g. 15d-PGJ$_2$ are structurally characterized by a cyclopentenone ring that contains an electrophilic group. The prostaglandin 15d-PGJ$_2$ is also described as an electrophile having the ability to covalently modify nucleophiles by a Michael addition via a free reactive group, affecting the functionality of its targets (reviewed in Uchida et al., 2008; Straus et al., 2000). Another explanation for its anti-inflammatory effect is that 15d-PGJ$_2$ targets for example IκB kinase. In the inflammatory response IκB kinase is activated and phosphorylates IκB at two serines. IκB can then be degraded NF-κB is released and can migrate to the nucleus to activate gene expression. After 15d-PGJ$_2$ has targeted IκB kinase it inhibits DNA binding of NFκB and transcription of the cyclo-oxygenase 2- gene (COX2), which catalyses the synthesis of pro-inflammatory prostaglandins, (Straus et al., 2000; Rossi et al., 2000). This also means that 15d-PGJ$_2$ supports a self-regulating mechanism (Scher et al.,

2004). Another target of covalent 15d-PGJ$_2$ modification seems to be the HIV transactivating protein Tat, which is inhibited by the modification (Kalantari et al., 2009).

Due to its modifying behavior towards sensitive cysteine residues it is likely that 15d-PGJ$_2$ has many targets within a cell and may therefore strongly influence cell fate. In this work we show evidence that 15d-PGJ$_2$ covalently modifies the export receptor CRM1 and inhibits CRM1 mediated protein export.
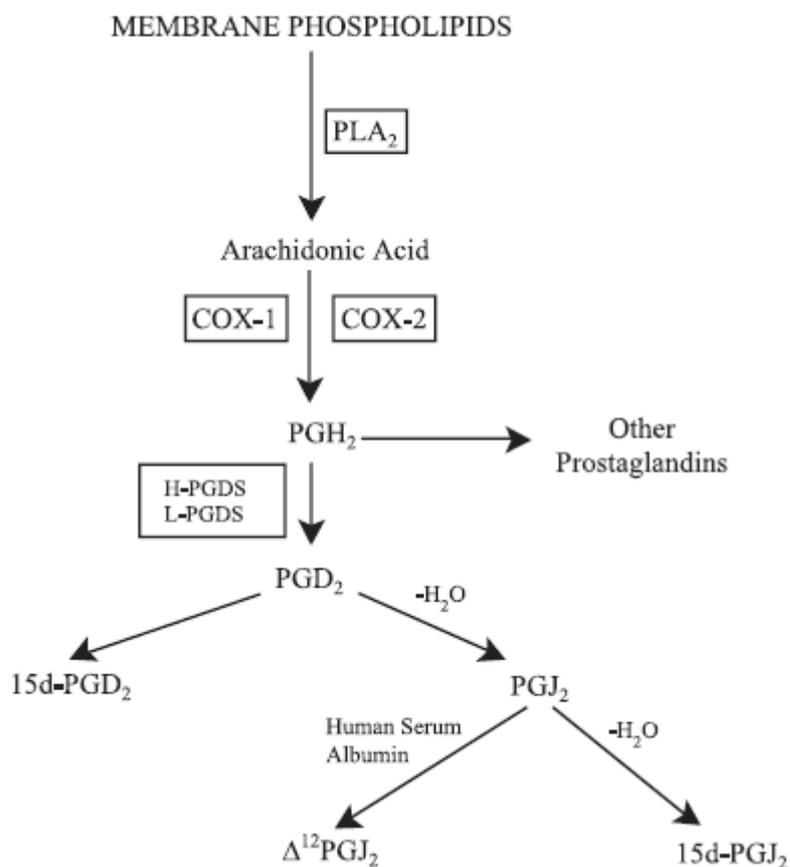
Figure IV: Synthesis way of 15d-PGJ$_2$ (taken from Scher et al., 2004)
Phospholipase A$_2$ releases arachidonic acids from plasma membranes. Cyclooxygenases-1 and -2 process arachidonic acids to the precursor prostaglandin H$_2$. Further enzymatic processes and hydrolysis forms the prostaglandin 15d-PGJ$_2$.

1.4 Telomerase reverse transcriptase

Telomeres are the ends of eukaryotic chromosomes and consist of proteins and TTAGGG DNA repeats in humans (Morin et al., 1989). After each round of cell division telomeres shorten, due to the inability of the replication machinery to complete duplication, termed the "end replication problem". As a consequence, cells with incomplete replication at their chromosome termini would later be unable to divide anymore and die (Harley et al., 1990; Hastie et al., 1990; reviewed in Autexier et al., 2006). With the help of telomerase activity, cells overcome this problem. Telomerase exhibits enzymatic activity and is a conserved enzyme among various species. This ribonucleoprotein is involved in chromosome maintenance and telomere elongation.

Telomerase catalyzes the *de novo* addition of lost telomeric sequences and therefore helps to regenerate telomeres, contributes to cell cycle progression and enhances the life-span of cells (Greider et al., 1989; Morin 1989, Blackburn et al. 1989; Counter et al., 1992). The enzyme is also involved in ageing, cancer development and diseases like dyskeratosis congenital (Mitchell et al., 1999; Harley et al., 1990).

Human telomerase reverse transcriptase is a ribonucleoprotein that comprises two subunits. The 126kDa protein subunit (TERT) binds an RNA component (TR) with a conserved secondary structure (reviewed in Lamond 1989; Shippen-Lentz et al., 1990; Bhattacharyya et al., 1994).

To restore lost telomeric sequences during a cell cycle, TR contains a template sequence which is used to sequentially add the telomeric repeats (Shippen-Lentz 1990; Morin 1989).

Telomerase activity was first discovered in ciliated protozoa e.g. *Tetrahymena thermophila* which posesses 10^4-10^7 macronuclear telomeres. Later, telomerase activity was also demonstrated in a human HeLa cell lysate (Greider et al., 1985; Morin 1989; Avilion et al., 1992; reviewed in Autexier et al., 2006).

1.4.1 Domains and structure of TERT

TERT contains several domains which are largely conserved in several species (Figure V). The most prominent and best characterized domains are the N-terminal extension domain (NTE) and the reverse transcriptase (RT) domain. The NTE consists of several conserved telomerase specific motifs which form the telomerase RNA binding domain (TRBD) and are therefore required for TR binding to TERT (Bachand et al., 2001; Moriarty et al., 2002). These motifs also

affect the rate of template copying during telomere synthesis (reviewed in Wyatt et al., 2010). The TEN-domain is also involved in TR binding although it possesses a weak affinity towards TR (Jakobs et al., 2006). Furthermore, the TEN-domain exhibits binding affinity towards single stranded telomeric DNA and contributes to the enzymatic activity (reviewed in Wyatt et al., 2010).

The RT-domain is crucial for the enzymes catalytic activity (Lingner et al., 1997) and contains evolutionary conserved RT motifs (Harrington et al., 1997; reviewed in Autexier et al., 2006). For *tribolium castaneum* TERT, it has been shown that the RT domain is separated into the "fingers" and "palm" subdomains (Gillis et al., 2008). The IFD (insertion in fingers domain) in between helps to organize and stabilize the RT region (Gillis et al., 2008; Nakamura et al., 1997; Lingner et al., 1997).

Endogenous TERT localizes to the nucleus. The enzyme is found in the nucleoplasm as well as in nucleoli, nucleoplasmic foci and at the telomeres. In contrast, TR is known to accumulate in Cajal bodies and to associate with nucleoli. It remains unclear in which cellular compartment assembly of TERT and TR finally occurs (Wong et al., 2002; reviewed in Collins 2006). Nevertheless it is known that assembly of TERT and TR requires additional factors that link both subunits tightly together. For *tetrahymena* TERT and TR assembly it has been shown that the telomerase specific p65 holoenzyme protein, which belongs to the La family, contributes to the assembly of both units (Witkin et al., 2007).
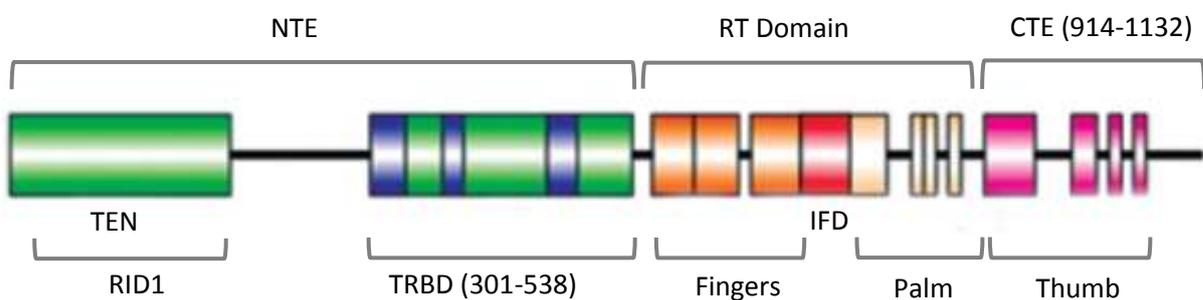
Figure V: **Human TERT and its domains** (taken from Wyatt et al., 2010 and modified)
Human TERT consists of several conserved domains. The telomerase specific (TS) motif and CP, QFP motifs form the TR binding domain (TRBD).The RID1 RNA interaction domain1 lies within the TEN domain. Both RNA interaction motifs are required for binding of TR.

1.4.2 Biogenesis of *human* TERT holoenzyme

The TR binding H/ACA trimeric protein complex consist of dyskerin, NOP10 and NHP2 and forms in the cytoplasm. Additionally, NAF1 is recruited to the complex. In the nucleus NAF-1 recruits the RNA polymerase II and its specific transcription factors and mediates the co-transcription loading of the H/ACA complex (Darzacq et al., 2006; reviewed in Hukezalie et al., 2013). NAF-1 is released from the complex and substituted with Gar-1 which mediates the
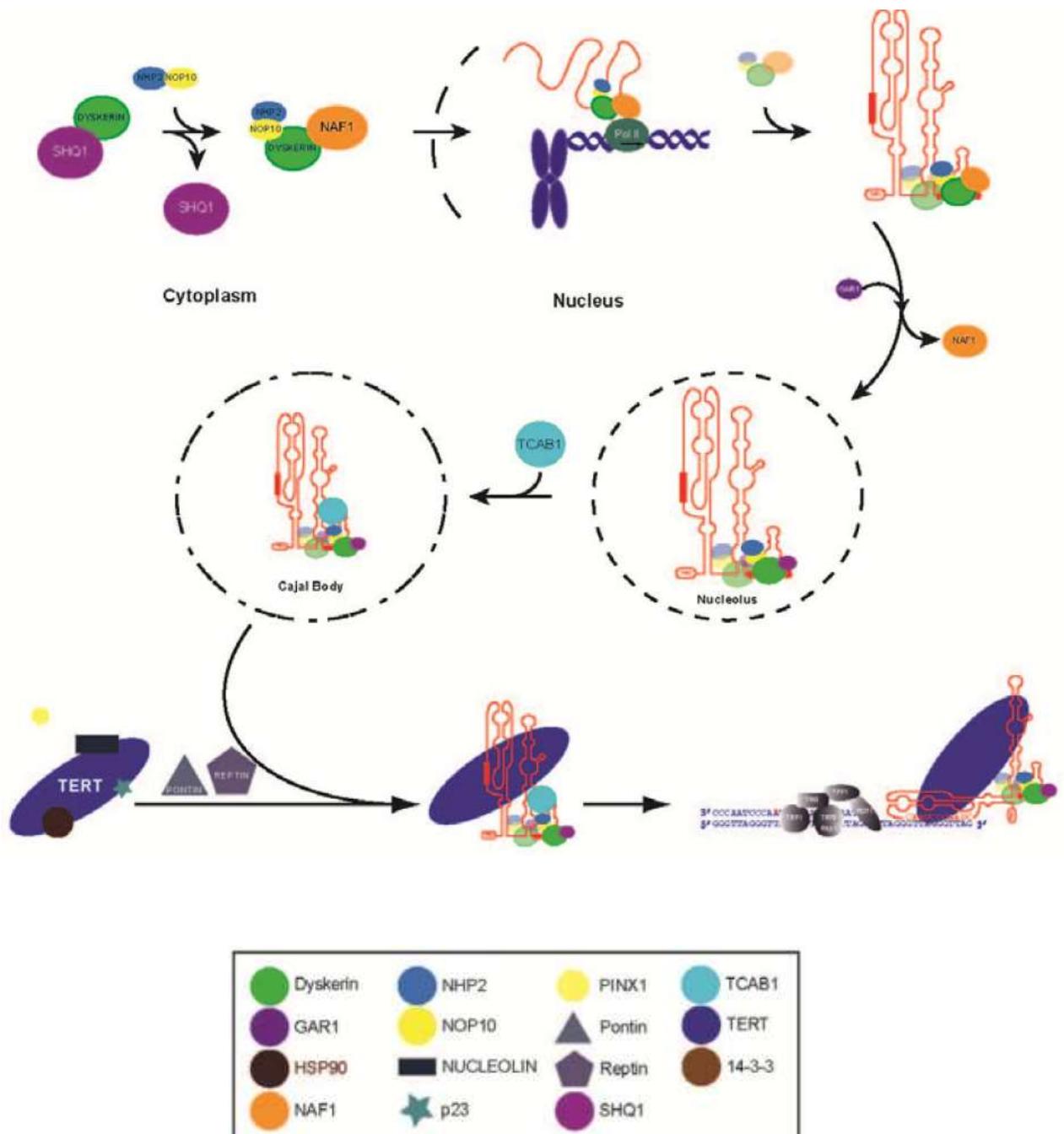
Figure VI: Biogenesis of telomerase (taken from Hukezalie et al., 2013)
Biogenesis of TR and complexing of it as a TR-RNP is mediated under involvement of H/ACA- proteins. The assembly of TERT-TR holoenzyme requires additional proteins and nuclear compartments such as Cajal bodies or the nucleolus.

recruitment of the TR-ribonucleoprotein complex at the nucleoli (Darzacq et al., 2006). There, a Cajal body localization factor mediates the translocation of the TR-ribonucleoprotein to the Cajal bodies (reviewed in Hukezalie et al., 2013). The H/ACA complex is essential for the TR stability and essential for biogenesis and assembly of TR with TERT. The H/ACA proteins also remain at the TERT/TR ribonucleoprotein complex during its catalytic cycle (Egan et al., 2012). Prior to assembly of TERT with TR-RNP, TERT passes the nucleolus, due to its interaction with the nucleolar proteins PinX1 and nucleolin (Banik et al., 2004).

Assembly of the TERT/ TR-RNP complex involves the ATPases pontin and reptin (Venteicher et al., 2008) which dissociate from active telomerase again (reviewed in Hukezalie et al., 2013).

The nucleolar proteins NAT10 and GNL3L assemble with the active holoenzyme, suggesting that telomerase travels between nucleolus and Cajal bodies (Fu et al., 2007). Regeneration of telomeric DNA ends is believed to be synthesized at the Cajal bodies (reviewed in Hukezalie et al., 2013).

In yeast the telomerase RNA was found to colocalize with telomeres in G1- to S-phase but lacking of any one of the telomerase holoenzyme-forming Est proteins leads to TLC1 RNA accumulation in the cytoplasm (Gallardo et al., 2008). The authors could show that endogenous TLC1 RNA traffics between nucleus and cytoplasm and associates with the Crm1p exportin and the nuclear importins Mtr10p–Kap122p (Gallardo et al., 2008; Ferrezuelo et al., 2002).

1.4.3 Nucleocytoplasmic transport of *human* TERT

Not much is known about transport pathways of TERT and import of telomerase specially remaines unclear. However, it was already suggested that *human* TERT can be exported by CRM1 in a Ran dependent manner (Haendeler et al., 2003; Seimiya et al., 2000). It has also been shown that exogenously or endogenously triggered oxidative stress can initiate Ran dependent nuclear export of TERT, through the nuclear pores and can be inhibited by the addition of LMB (Haendeler et al., 2003). The authors could also demonstrate that the

phosphorylation by the Src kinase family of a tyrosine at position 707 is involved in export of TERT triggered by reactive oxygen species (ROS) (Haendeler et al., 2003). Another study mentions the involvement of the tyrosine phosphatase Shp2 in nuclear retention of TERT (Jakob et al., 2008).

As already mentioned, overexpressed as well as endogenous *human* TERT localize to the nucleus. It could also be demonstrated that overexpressed GFP-tagged TERT shows a subnuclear shuttling in several fibroblasts (Wong et al., 2002). TERT therefore needs to be transported into the nucleus and it could be shown that nuclear localization of *human* TERT is enhanced by the interaction of 14-3-3 signaling proteins with the telomerase C-terminus (Seimiya et al., 2000). The 14-3-3s blocks a CRM1 binding site, and as a consequence CRM1 mediated export of telomerase is prevented (Seimiya et al., 2000).

A very recent publication identified a functional bipartite NLS motif in the N-terminal part of TERT which is required for nuclear import of TERT mediated by Akt phosphorylation at serine 227 (Chung et al., 2012). However the authors did not show an involvement of an import receptor in TERT nuclear import. Independently from the study mentioned above, the same NLS motif was also discovered in this work and was found to be a functional motif. We are also able to demonstrate the involvement of the import receptor importin-7 in TERT nuclear import.

2. Material

2.1) Technical equipment

Agarose gel documentation	Intas
Autoclave DX200	Systec
Bacteria incubator Heraeus function line	Heraeus Instruments
Bacteria shaker Innova 4430	New Brunswick scientific
CASY 1	Schärfe System
Cell culture hood HERAsafe KS	Thermo scientific
Cell culture incubator HERAcell 150i	Thermo scientific
Centrifuge 5415D	Eppendorf
Centrifuge 5415R	Eppendorf
Developer machine CURIX60	Agfa
Emulsiflex	GE Healthcare
Heat blocks	Eppendorf
HPLC (Äkta)	GE Healthcare
LSM 510 meta confocal microscope	Zeiss
Nanodrop	PeqLab
SDS Gel eletrophoretsis system	Biometra
Thermocycler Tprofessional gradient	Biometra
Thermocycler Primus MWG	Biometra
Ultracentrifuge	Beckmann Coulter
UV cross linker	Biometra

2.2 Consumables

Amersham Hyperfilm ECL	GE Healthcare
Cell culture plastic ware	Sarstedt, Starlab
Chemiluminescence Immobilon Western	Millipore
Coverslips (12mm Ø)	Marienfeldt
GFP Nanotrap	Chromotek
GST- sepharose	GE Healthcare
Medix XBU medical x-ray film	FOMA Bohemia
Microscope slides	Thermo scientific
Ni-NTA Agarose	Qiagen
Nitrocellulose PROTRAN	Whatman, GE Healthcare
Reaction tubes	Sarstedt
Safe view	Gemtaur
SpinX-UF	Corning

2.3 Software

LSM Image Browser	Zeiss
LSM Software	Zeiss
Photoshop CS 5.1	Adobe
Serial cloner	Serialbasics

2.4 Kit systems

NucleoBond Xtra Midi	Macherey-Nagel
Nucleo Spin Plasmid (Mini)	Macherey-Nagel
Silica Bead DNA Gel Extraction Kit	Fermentas

2.5 Buffers, solutions, media

Buffers

Antibody elution buffer	500mM NaCl in 0.2M acetic acid, pH 2.7
Buffer P1	50 mM Tris-HCl (pH 8), 10 mM EDTA, 100 µg/ml RNase A
Buffer P2	200 mM NaOH, 1 % (v/v) SDS
Buffer P3	3 M KOAc (pH 5.5)
Carbonate buffer	0.2M carbonate pH 8.9
Colloidal coomassie	0.02% brilliant blue G250, 5% aluminiumsulfate, 10% ethanol, 2% orthophosphoric acid
DNA loading dye 10x	50% (v/v) glycerin, 0.1% (w/v) bromphenol blue, 0.1% (w/v)xylencyanole
GFP nanotrap dilution buffer	10mM Tris, 150mM NaCl, 0.5mM EDTA, pH 7.2, 1% BSA freshly supplemented with 2mM DTT, 1mM PMSF, 1µg/ml aprotinine, pepstatin, leupeptine, *Complete* (protease inhibitor)
GFP nanotrap lysis buffer	10mM Tris, 150mM NaCl, 0.5mM EDTA, 0.5% NP-40, 1% BSA pH 7.2 freshly supplemented with 2mM DTT, 1mM PMSF, 1µg/ml aprotinine, pepstatin, leupeptine, *complete* (protease inhibitor)

Immunoprecipitation lysis buffer	20mM Tris, 150mM NaCl, 0.5mm EDTA, 1% NP-40, 1% BSA pH 7.3 freshly supplemented with 2mM DTT, 1mM PMSF, 1µg/ml aprotinine, pepstatin, leupeptine, *complete* (protease inhibitor)
Immunoprecipitation washing buffer	20mM Tris, 150mM NaCl, 0.5mm EDTA, 1% BSA pH 7.3 freshly supplemented with 2mM DTT, 1mM PMSF, 1µg/ml aprotinine, pepstatin, leupeptine, *complete* (protease inhibitor)
Importinβ lysis buffer	50mM Tris, 2mM $MgCl_2$, 250mM NaCl, 10% Glycerol, 4mM β-mercaptoethanol, pH 7.4 freshly supplemented with 1mM PMSF, 1µg/ml aprotinine, pepstatin, leupeptine
Importinβ washing buffer	50mM Tris, 2mM $MgCl_2$, 250mM NaCl, 10% Glycerol, 4mM β-mercaptoethanol, 10mM imidazole, pH 7.4 freshly supplemented with 1mM PMSF, 1µg/ml aprotinine, pepstatin, leupeptine
Laemmli- Buffer 10x	25 mM Tris, 192 mM glycine, 0.01 % (w/v) SDS
Optimem	used without any additives
Paraformaldehyde	3.7% (w/v) paraformaldehyde
Phoshate buffered saline (PBS)	140 mM NaCl, 2.7 mM KCl, 10mM Na_2HPO_4, 1.5 mM KH_2PO_4 (pH 7.5)
PBS- tween	PBS supplemented with 0.1% (v/v) tween
Ponceau S	0.5 % (w/v) ponceau S, 1 % (v/v) acetic acid
Pull down buffer	50mM Tris, 200mM NaCl, 1% BSA 1mM $MgCl_2$, 5% glycerol pH 7.3

SDS-PAGE loading buffer 4x	4 % (w/v) SDS, 125 mM Tris (pH 6.8), 10% (v/v) glycerol, 0.02 % (w/v) bromphenol blue, 10 % (v/v) β-mercaptoethanol
TAE- buffer 50x	40 mM Tris acetate (pH 7.7), 1 mM EDTA
TFB-I-buffer	100 mM RbCl, 15 % (v/v) glycerol, 0.5 mM LiCl (pH 5.8)
TFB-II-buffer	10 mM MOPS (pH 7), 10 mM RbCl, 75 mM $CaCl_2$, 15 % (v/v) glycerol
Transfection buffer 1	250mM $CaCl_2$
Transfection buffer 2 (HEPES)	50mM HEPES, 250mM NaCl, 1,5mM Na_2HPO_4, pH 6.95
Western blot transfer buffer	25 mM Tris-HCl, 192 mM glycine, 20 % (v/v) methanol, 0.036% (v/v) SDS

Stock solutions

Ampicillin	100 mg/ml
Aprotinin	1 mg/ml
Chloramphenicol	30 mg/ml
Dithiothreitol (DTT)	1 M
Hoechst 33258	10 mg/ml
Kanamycin	50 mg/ml
Leupeptin/Pepstatin	1 mg/ml each, in DMSO
Phenylmethylsulfonyl fluoride (PMSF)	100 mM in 2-propanol
Penicillin-Streptomycin	Penicillin 10.000 U/ml Streptomycin 10 mg/ml

Bacterial media

LB	1 % (w/v) bacto-tryptone, 0.5 % (w/v) yeast extract, 1 % (w/v) NaCl (pH 7)
LB agar plates	LB supplemented with 1.5 % (w/v) bacto-agar
SOC	2 % (w/v) tryptone, 5 % (w/v) yeast extract, 50 mM NaCl, 2.5 mM KaCl, 10 mM $MgCl_2$, 10 mM $MgSO_4$

Cell culture media

CO_2 independent medium (Invitrogen)	used without additives
DMEM (high) Invitrogen	DMEM high glucose (4500mg/ml), 10% FCS, 2mM glutamine

2.6 Enzymes, chemicals and reagents

Enzymes

Restriction enzymes	Fermentas
Fast alkaline phosphatase (FastAP)	Fermentas
Phusion polymerase	Fermentas
Pfu-Ultra polymerase	Agilent
T4- DNA ligase	Fermentas
Vent polymerase	NEB
Trypsin/ EDTA	Invitrogen
RNase A	AppliChem

Chemicals and reagents

All standard chemicals used within this work were obtained from AppliChem (Darmstadt), Carl Roth (Karslruhe), Serva (Heidelberg), Sigma-Aldrich (Taufkirchen), or Merck (Darmstadt).

15-deoxy-$\Delta^{12,14}$-prostaglandin J2	Cayman Chemical
Acrylamid (30 %)	AppliChem
Advanced protein assay reagent 5x	Cytoskeleton Inc.
Aprotinin	Biomol
BSA, fraction V	PAA
Cay 10410	Cayman Chemical
Dako mounting medium	invitrogen
Dimethylsulfoxide (DMSO)	AppliChem
Dithiothreitol (DTT)	AppliChem
DNA ladder, 1 kb	Fermentas
dNTPs	Fermentas
ECL	Milipore
Ethanol (analytic grade)	Roth
FCS	Gibco
Fluorescence mounting medium	Dako Cytomation, Linaris
GDP, GTP	Sigma-Aldrich
Glutamine (cell culture grade)	Invitrogen
H_2O_2	Roth
Hoechst 33258	Sigma-Aldrich
IPTG	Fermentas
Leptomycin B	Sigma-Aldrich
Leupeptin	Biomol
Methanol (technical grade)	Roth
Oligofectamine	Invitrogen
Oligonucleotides	Sigma-Aldrich
OptiMEM	Invitrogen
Pepstatin	Biomol
PMSF	Sigma-Aldrich

Poly-L-lysine	Sigma-Aldrich
Prostaglandin A	Cayman Chemical
Prostaglandin E	Cayman Chemical
Protein ladder PAGE ruler	Fermentas
siRNA oligonucleotides	Ambion, Santa Cruz, Eurofins
β-Mercapthoethanol	Roth
Tris (buffer grade)	Applichem

2.7 Antibodies

Primary antibodies

Name	Immunogen	Species	Origin	Dilution
α CRM1	affin., c-terminus H20672	goat	Kehlenbach lab	WB 1:1000 IF 1:1000
α GFP	GFP 1-238	rabbit	Santa Cruz	WB 1:1000
α HA	clone 16B12	mouse	Covance	WB 1:1000 IF 1:1000
α HIS (penta)	HIS-tag	mouse	Qiagen	WB 1:1000
α importin-α (Karyopherin α2)	Rch-1 254-497	mouse	BD Transduction Laboratories	WB 1:1000
α importin-β	importin-β	rabbit	Kehlenbach lab	WB 1:1000
α importin-7	c-terminal peptide	rabbit	Görlich lab	WB 1:10000
α importin-7-1	c-terminal peptide CLADQRRAAHESKMIEKHG	rabbit	Kehlenbach lab	WB 1:500
α importin-9	clone EP1353Y	rabbit	Abcam	WB 1:1000
α Myc	clone 9E10	mouse	Abd Serotec	IF 1:1000
α NUP358	AA 2553-2838	goat	Kehlenbach lab	WB 1:1000 IF 1:1000
α RanBP1	clone35	mouse	BD Transduction Laboratories	IF 1:100
α tubulin	ag1727	rabbit	Proteintech	WB 1:1000

Secondary antibodies

Secondary antibodies for Western blotting were horseradish peroxidase-conjugated (HRP) and used in a dilution of 1:10000. The antibodies were obtained either from Dianova or Jackson ImmunoResearch Laboratories.

Secondary antibodies for immunofluorescence were obtained from Molecular Probes and were either Alexa488, Alexa594 or Alexa647 conjugated as indicated. The dilution used was 1:1000.

2.8 siRNAs

SiRNAs were purchased from Ambion, Eurofins or Santa Cruz. The importin-7-1 siRNA from Eurofins was selected from a list of predesigned and validated siRNAs. Importin-β and importin-9 siRNAs, also obtained from Eurofins, were designed with the online siMAX™ Design Tool provided on the webpage. All siRNAs were diluted in nuclease free water to a stock concentration of 100µM.

Name	siRNA sequence 5'→3'	Target sequence	company
siRNA importin-7	GAUGGAGCCCUGCAUAUGA	nct. 1288-1306 NM_006391	Ambion
siRNA importin-7-1	UGAUGACCUUACCAAUGUA	nct. 1665-1683 NM_006391	Eurofins MWG Operon
siRNA importin-9	UCACUGAGGAGCAGAUUAA	nct. 1109-1127 NM_018085	Eurofins MWG Operon
siRNA importin-β	ACAGUGCCAAGGATTGTTA	nct. 1613-1631 NM_002265	Eurofins MWG Operon
siRNA non-targeting	GAGCUUCAACUAACAGGAATT	Scrambled sequence	Ambion
siRNA NUP358-1	CACAGACAAAGCCGUUGAAUU	Nct. 351-369 NM_006267	Ambion
siRNA transportin	Pool of 3 target-specific siRNAs Sc-35737	Transportin1 NM_002270.3	Santa Cruz Biotechnology

2.9 Oligonucleotides

Oligonucleotides used in this work were ordered at Sigma-Aldrich and used at a working concentration of 10µM.

Oligonucleotides used for mutagenesis

Name	Sequence 5'⟶ 3'
Mutate Xen IPO7 Ha rev	TCATCTGTAGAGCGCCGTCTTT
Mutate Xen IPO7 Ha for	AAAGACGGCGCTCTACAGATGA
TERT K236A R237A only for	AGTCTGCCGTTGCCCGCGGCGCCCAGGCGT
TERT K236A R237A only rev	ACGCCTGGGCGCCGCGGGCAACGGCAGACT
TERT K649A R650A for	TTCCGCAGAGAAGCGGCGGCCGAGCGT
TERT K649A R650A rev	ACGCTCGGCCGCCGCTTCTCTGCGGAA

Oligonucleotides used for cloning

Name	Sequence 5'⟶ 3'
Ran for pEF-HA EcoRI	ACGAATTCATGGCTGCGCAGG
Ran rev pEF-HA SpeI	TTACTAGTTCACAGGTCATCATC
TERT NT for HindIII	TTTTAAGCTTCATGCCGCGCGCTCC
TERT NT 300 rev BamHI	TTTTGGATCCTCAGCCCACGGATGG
TERT NT 150 rev BamHI	TTTTGGATCCTCAAACCAGCACGTCG
TERT NT 301 for HindIII	TTTTAAGCTTCCGCCAGCACCACG
TERT NT 600 rev BamHI	TTTTGGATCCTCACTCCCGCAGCTG

Oligonucleotides used for sequencing

Sequencing was performed by GATC sequencing service. The DNA samples were diluted to a concentration of 100ng/µl and a sample of 20µl was sent for sequencing. Required customer primers were diluted to a concentration of 10pmol/µl and were also sent as a 20µl sample.

Name	Sequence 5'⟶ 3'
EF FOR (pEF-Ha)	GCCATCTATTGCTTACATTTGCTTCTGACACAACTG
GFP 3' MCS	CCACAACTAGAATGCAGTGAAAA
Importin 7 seq. 1211-1229	CACATCCTTGCAGTAAAAG

seqXen_Imp7_1632_F	CAGACTGCTCTGGAACTGAC
seqXen_Imp7_2133_F	CTAACGTGCCAGCAGGTTTC
seqXen_Imp7_2635_F	TTGGGTTACATGATCGGAAG
seqXen_Imp7_630_F	TACAAGAAGCCTGAGGAGCG
TERT 605 EcoR1 F_pGEX KG	TTTGAATTCAAGAGGTCAGGCAGCATCGG
TERT 606-623 seq.Primer	CTCGGAACCATAGCGTCAG
TERT 707 for EcoR1 pmal	TTTTGAATTCTACTTTGTCAAGGTGGATGTG
TERT 927 for EcoR1 pmal	TTTTGAATTCCTATTCCCCTGGTGCGG
TERT EcoRI for	TTTTTGAATTCGGGATGCCGCGCGCTCCC
TERT_seq_881f	ACTCCCACCCATCCGTGGGC

2.10 Vectors and plasmids

All vectors used in this work were available in the lab.

Name	Tag	Expression	Source
dGFP-C2	2x EGFP	mammalian	Based on Clontech pEGFP-C2 containing additional EGFP Dr. Saskia Hutten
pEF-Ha	2x Ha (N-terminal)	mammalian	Dr. O. T. Fackler (Gasteier et al., 2003)
pEGFP-C2	EGFP	mammalian	Clontech
pEGFP-N1	EGFP	mammalian	Clontech

Available plasmids

Tags are always located as shown in the plasmid construct.

#	Name	Tag	Expression	Source
503	GFP-TF II A alpha	GFP	mammalian	Dr. Jörg Kahle
514	NC2ß-RFP	RFP	mammalian	Dr. Jörg Kahle
532	pcDNA3.1 HA- CRM1	HA	mammalian	Christiane Spillner

545	pCDNA3.1 TERT-HA	HA	mammalian	Dr. Sarah Wälde
628	pcDNA3.1(+)-Crm1-HA-C528S h.s.	HA	mammalian	Dr. Stephanie Roloff
495	pEF-HA importin-7	HA	mammalian	Wälde et al., 2011
454	pEF-HA-importin-β	2x HA	mammalian	Hutten et al.,2008
795	pEF-HA-Nup358 aa 1-1810	2x HA	mammalian	Wälde et al. 2011
794	pEF-HA-Nup358 aa 1-2148	2x HA	mammalian	Wälde et al 2011
801	pEF-HA-Nup358 aa 806-1306	2x HA	mammalian	Wälde et al. 2011
455	pEF-HA-transportin	2x HA	mammalian	Christiane Spillner (Hutten et al., 2008)
487	pGFP-NES(Rev)	GFP	mammalian	Christiane Spillner
1126	pME18S myc-EZI (mouse)	myc	mammalian	Tohru Itoh (Saijou et al., 2007)
623	Rev 68-90-GFP2-M9core	2x GFP	mammalian	Dr. Saskia Hutten (Hutten et al., 2008/2009)
504	Rev(68-90)-GFP2-cNLS	2x GFP	mammalian	Hutten et al., 2008, Wälde et al., 2011

Generated plasmids within this work

Plasmid inserts were amplified by PCR reaction, digested with the indicated enzymes and ligated in the respective vector. Tags are located at the respective termini as indicated in the plasmid name.

#	Name	Insert	Vector	Species	Primer
833	TERT-GFP	TERT	pEGFP-N1	human	Cloned via HindIII and EcoRI from TERT-YFP
1127	HA-importin-7 (siRNA resistant)	importin-7 (mutagenesis)	pEF-HA	Xenopus	Template vector: pEF-Ha importin-7 xen Mutate Xen IPO7 Ha rev Mutate Xen IPO7 Ha for
1130	TERT KR 236/237 AA-GFP	TERT (mutagenesis)	pEGFP-N1	human	TERT K236A R237A only for TERT K236A R237A only rev

1131	TERT KR 236/237AA KR 649/650 AA-GFP	TERT (mutagenesis)	pEGFP-N1	human	TERT K649A R650A for TERT K649A R650A rev
1132	GFP TERT 1-150	TERT 1-150	pEGFP-C2	human	TERT NT for HindIII TERT NT 150 rev BamHI
1133	GFP TERT 1-300	TERT 1-300	pEGFP-C2	human	TERT NT for HindIII TERT NT 300 rev BamHI
1134	GFP TERT 301-600	TERT 301-600	pEGFP-C2	human	TERT NT 301 for HindIII TERT NT 600 rev BamHI
1135	dGFP TERT 1-150	TERT 1-150	2xGFP	human	TERT NT for HindIII TERT NT 150 rev BamHI
1136	dGFP TERT 1-300	TERT 1-300	2xGFP	human	TERT NT for HindIII TERT NT 300 rev BamHI
1137	dGFP TERT 301-600	TERT 301-600	2xGFP	human	TERT NT 301 for HindIII TERT NT 600 rev BamHI

2.11 Proteins

The proteins listed below belong to the common lab stock.

Protein	Source
His-importin-7	Kehlenbach lab, (Wohlwend et al., 2007)
GST NUP 358 aa806-1000	Kehlenbach lab, (Annegret Nath)
GST NUP 358 aa806-1133	Kehlenbach lab, (Annegret Nath)
GST NUP 358 aa806-1170	Kehlenbach lab, (Annegret Nath)
GST NUP 358 aa806-1306	Kehlenbach lab, (Annegret Nath)
GST NUP 358 aa2011-2445	Kehlenbach lab, (Annegret Nath)
Ran Q69L	Kehlenbach lab, (Melchior et al., 1995b)

2.12 Cell lines

Mammalian cell lines

HeLap4   This cell line is an adherent immortal human cervix carcinoma cell line and stably expresses human CCR-5 and CD4 (Charneau et al., 1994). It was used as a standard cell line for immunofluorescence, because it is easy to transfect.

NIH AIDS Research and Reference Reagent Program, catalog number 3580

293T HEK   293T HEK derived from the adherent and immortal embryonic kidney line HEK 293. This line is useful for protein expression by supporting the replication of plasmids with the Epstein-Barr virus oriP or SV40 origin of replication.

ATCC, CRL-2828

Bacterial strains

DH5α

This strain was used for DNA preparation and cloning. For transformation it was provided chemically competent. The genotype of the strain is: F− Φ80lacZΔM15 Δ(lacZYA-argF) U169 recA1 endA1 hsdR17 (rK−, mK+) phoA supE44 λ− thi-1 gyrA96 relA1

BL21 (DE3) codon+

The BL (DE3) codon+ strain was used for protein induction and preparation. Protein expression was induced by addition of IPTG (0.15-1mM) which induced the expression of T7 polymerase. The genotype of the strain is: *E. coli* B F$^−$ *ompT hsdS*(r$_B$ $^−$ m$_B$ $^−$) *dcm*$^+$ Tet^r *gal* λ (DE3) *endA* Hte [*argU ileY leuW* Cam^r]

3) Methods

3.1 Prokaryotic cells

Cultivation of *E.coli* strains

E.coli strains were grown large scale in conical flasks containing LB-medium, or as mini cultures in falcon tubes. Colonies were grown on LB-agar plates. Cultures were incubated at 37°C and liquid cultures with shaking at 150-170 rpm. For plasmid selection the corresponding antibiotics were added as followed: ampicillin 100 µg/ ml, kanamycin 60 µg/ ml, chloramphenicol 30 µg/ ml.

Preparation of chemical competent bacteria

Under sterile conditions, *E.*coli cells were spread onto an LB-agar plate without antibiotics and incubated overnight at 37°C. A single colony was picked and inoculated in 200ml of LB-medium without antibiotics. The culture was grown at 37°C with shaking till it reached an OD_{600} of 0.5. The culture was incubated on ice for 10 minutes and then harvested by centrifugation at 5.000 g for 5 min at 4°C. The pelleted cells were resuspended in 200ml of ice-cold sterile TFB-I-buffer and further incubated on ice for 2 hours. Cells were again pelleted at 5000 g for 5 min at 4°C and carefully resuspended in 8 ml of ice-cold sterile TFB-II-buffer. Resuspended competent bacteria were aliquoted in 100µl, snap frozen in liquid nitrogen and stored at -80°C.

3.2) Molecular biology techniques

3.2.1 Transformation of plasmid- DNA into *E.coli* DH5α

For plasmid transformation, chemically competent cells were used. Cells were defrosted on ice, mixed with the plasmid DNA then incubated on ice for a further 30 minutes. Following this incubation step, cells were heat shocked at 42°C for 90 seconds and then chilled on ice for one minute. During the heat shock DNA is brought into the cells. Cells were recovered in SOC medium without antibiotics for 30-45 minutes. Subsequently cells were plated on LB-agar supplemented with the appropriate antibiotics and incubated over night.

3.2.2 Isolation of plasmid-DNA

Plasmid DNA was extracted from bacteria in different amounts and quality. For isolation, one single colony was picked from a plate and inoculated in LB-media. Cells were incubated at 37°C until they reached stationary phase and were then prepared as follows.

Mini-prep (Birnboim et al., 1979)

Colonies were grown in 6ml of LB-Media overnight and harvested by centrifugation. Cells were resuspended in 200µl P1 buffer containing RNase. Subsequently, 200µl of alkaline lysis buffer P2 was added to lyse the cells for 3-5 minutes. To stop the reaction, 200µl of neutralization buffer P3 was added to the lysate. Precipitated proteins were pelleted by centrifugation at 16 000 g for 10 min. The supernatant was transferred into a fresh tube and plasmid DNA was precipitated by adding 400µl 2-propanol. After centrifugation for 30 minutes at 16 000 g, the DNA pellet was washed with 70% ethanol twice, dried and disolved in 50µl of water.

Midi and Mini prep with kit

Plasmid preparation in large scale was performed according to the protocol of the Nucleo Bond Xtra Midi kit provided by Macherey-Nagel. Also Mini-preps were performed using the Nucleo spin plasmid kit from Macherey-Nagel according to the manufacturer protocol. The concentration and purity of the obtained DNA was monitored by measurement with a Nanodrop and was then adjusted to 1µg/µl.

3.2.3 Polymerase chain reaction (PCR)

Polymerase chain reaction (PCR) is a technique used to amplify defined regions of a DNA molecule. For this purpose, primers, small oligonucleotides of a length of <20 nucleotides, which are complementary to known sequences of the DNA were used to define the region to be amplified. Primers can exhibit an overhang at their 5' ends that does not hybridize with the DNA to provide sequences for later endonuclease restriction. For a complete PCR reaction also dNTPs, a thermally stable DNA polymerase and a template DNA (100ng) are needed. In this work, proof-reading polymerases, e.g. the Phusion polymerase (Fermentas) and the Pfu-Ultra polymerase (Agilent) were used. PCR reactions were carried out in a volume of 50µl with a primer concentration of 200nM and a dNTP concentration of 200µM. To the reaction 0.5-1U of the polymerase was added. The polymerase buffer was diluted according to the manufacturers manual. The PCR reaction was run in several consecutive steps, beginning with a denaturation step of 95°C and followed by the annealing phase of the primers to the single strand DNA. The annealing temperature was usually determined analog to the G/C content of the annealing primer part. The elongation phase was then carried out by the polymerase at 72°C. The primers were elongated using the existing DNA as a template. A typical PCR protocol is shown:

5 min 95°C initial denaturation

1 min 95°C denaturation
30 s T_m primer annealing   } 34 cycles
1min/ kb 72°C elongation

10min 72°C final elongation
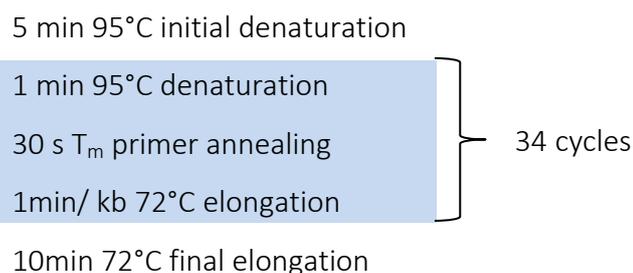
3.2.4 Site-directed mutagenesis

Mutations were introduced in a gene by site-directed mutagenesis. Complementary primers carrying up to 4 nucleotide exchanges were designed and applied in a PCR reaction to introduce the mutations into the gene. For this kind of PCR reaction only the Pfu-Utra polymerase was used. The reaction volume was set to 50µl and contained 200nm of each primer, 250µM dNTPs, 100ng template DNA, 2U polymerase, 10x Pfu-Ultra buffer and 3% DMSO to lower the annealing temperature and to facilitate wobble-pairing of bases. The annealing temperature was applied in a gradient from 55°C to 80°C. For every mutagenesis, 10 reactions were pipetted. Nine reactions were subjected to thermocycling while one was incubated at room temperature representing the negative control to test the efficiency of the following DpnI digestion. After the PCR reaction 1U of the restriction enzyme DpnI and its corresponding buffer were added to every sample and incubated for one hour at 37°C. DpnI digested the methylated template DNA and left the newly synthesized unmethylated DNA intact. Each reaction was transformed into competent *E.coli* DH5α. Clones were prepared and sent for sequencing to identify clones positive for the mutations. A standard PCR protocol for mutagenesis is shown below:

5min 95°C initial denaturation

1min 95°C denaturation
30s 55°C-80°C primer annealing   29 cycles
1min/ kb 72°C elongation

20min 72°C final elongation
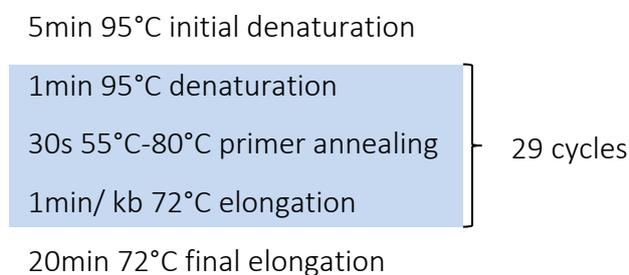
3.2.5 Agarose-gel electrophoresis

In this work, gels with an agarose concentration of 1% were used. Agarose-gel electrophoresis was used to purify digested DNA. To visualize DNA 5µl of the fluorescent DNA intercalating dye Safe View was added to 100ml gel and DNA bands were detectable under UV-light. To load DNA into the pockets of a gel it was previously mixed with the appropriate amount of 10x DNA loading dye. 6µl of a DNA ladder was run in parallel as a marker. The gel was run with a current of 120V for at least 45 minutes. After separation, DNA bands were imaged.

Isolation of DNA bands from agarose gels

After separation, DNA bands were cut out and were purified with the Silica Bead DNA Gel Extraction Kit from Fermentas, according to the manufacturer protocol. DNA was eluted in 50µl water.

3.2.6 Restriction of DNA fragments

DNA can exhibit specific sequences that are recognized, bound and cut by prokaryotic restriction enzymes. These enzymes bind to a recognition motif and cut the double-strand DNA between 2 defined bases. This is used to create specific overhangs to clone inserts into the multiple cloning site of the vector. Digestion of DNA was carried out in a volume of either 30µl or 50µl using the recommended buffer for the enzymes used. Enzymes were used at a concentration of 1-2U per reaction depending on their activity in the buffer system. For the purpose of cloning 2-6µg of DNA was used in the digestion reaction. In contrast, analytical digestion was carried out using 0.5-1µg of DNA. Digestion was performed at 37°C for 2 hours. The DNA fragments were subsequently purified by agarose gel-electrophorese. All restriction enzymes used in this work were obtained from Fermentas.

Dephosphorylation of vectors

In the process of cloning, vectors were dephosphorylated to prevent religation of linearized vectors. Dephosphorylation removes phosphates from the 5' end of DNA molecules and supports ligation of the insert. Dephosphorylation was performed after agarose gel-electrophoresis which follows a restriction digestion with the Fast-AP from Fermentas and its respective buffer. The reaction was carried out at 37°C for 15 minutes followed by a thermal inactivation at 75°C for 20 minutes.

3.2.7 Ligation of DNA

DNA ligases catalyze the joining of double strand DNA molecules by creating an ester bond between a phosphate residue and the desoxyribose. In this work, T4 DNA ligase from

Fermentas was used. The reaction was set up in 50µl containing the T4 DNA ligase specific buffer, the DNA fragments to be ligated and 2,5U of the enzyme. Ligation was either carried out at room temperature for 2 hours or overnight at 8°C. The whole reaction was transformed into competent *E.coli* DH5α.

3.2.8 Sequencing of DNA

Probes were sent for sequencing to GATC in Konstanz. DNA concentration was adjusted to 30-100ng/ µl in a volume of 20µl. Standard primers were provided by GATC. When using a specific customer primer they were also sent in a volume of 20µl with a concentration of 10pmol/ µl in water.

3.3) Biochemical techniques

3.3.1) Detection of proteins and separation

SDS-Page

The SDS-PAGE of Laemmli describes a technique to separate proteins from each other in high resolution via a 2-layer gel system consisting of a stacking gel and a resolving gel (Laemmli 1970). The proteins are separated in the gel according to their mass in an electric field under denaturing and reducing conditions in a buffer system. The resolution and separation of protein bands is determined by the pore size of the gel and is dependant on the concentration of acrylamide used. In this work, gels of an acrylamide concentration from 8% - 12% were used.

Samples were combined with SDS-PAGE loading buffer (final concentration 1x) and heated at 95°C for 5min. In addition to the samples a protein ladder was loaded onto the gel to later determine the molecular weight of the separated proteins. The gels were run in 1x Laemmli buffer at 20-25 mA.

Coomassie staining

Via unspecific binding of the dye coomassie brilliant blue G-250 to cationic amino acids, proteins can be detected directly in a gel. The method used in this work was a colloidal staining and did not require any previous fixation protocol (Dyballa et al 2009 based on Kang et al 2002). The solution was prepared 24h prior to use in the following order:

After the aluminiumsulfate was dissolved in deionized water, 10% ethanol was added and the whole solution was homogenized. Next, coomassie G-250 and phosphoric acid were added under stirring. Finally the solution was made up to the desired volume with deionized water and stirred.

After running, gels were washed in deionized water with agitation for 2 x 10 minutes to reduce background to a minimal level. After washing, gels were placed into the staining solution with agitation for at least 3 hours or overnight. Minimal excess of dye was removed by washing with water.

3.3.2) Protein transfer via Western blot and immunological detection of proteins

Western blot

Western blotting was performed under wet conditions to transfer proteins following SDS-PAGE onto a nitrocellulose membrane in order to detect them with antibodies. For this pupose a nitrocellulose membrane and several sheets of whatman paper were equilibrated in transfer buffer. The gel and the membrane were then layered with the whatman-paper in a blotting cassette. The cassette has to be placed into the blotting tank with the membrane facing the positive electrode. Finally, the tank was filled with transfer buffer. Blotting was carried out at 400 mA for 2h at 4°C.

Ponceau stain

To detect marker bands of an unstained ladder and to confirm equal blotting on a membrane, a Ponceau-S stain was applied directly after blotting under slight agitation for 1-2 minutes. Excess of dye was washed with an aqueous solution containing 1% (v/v) acetic acid.

Immunological detection of proteins on a western blot

After being transferred onto a membrane, proteins can be visualized via antibody binding and a following chemiluminescent reaction.

First, unspecific binding epitopes on the membrane are blocked with 5% (w/v) milk in PBST for 30-45 min at room temperature. To detect the proteins of interest specific primary antibody were applied in an appropriate dilution in milk and incubated either over night at 4° or for 1-2 hours at room temperature with slight agitation. Excess of antibody was eliminated by washing for 3-5 times with PBST for 5 min each. The HRP (horseradish-peroxidase) coupled secondary antibody was used to detect the primary antibody. The secondary antibody was also diluted in milk and used at a dilution of 1:10000 and was incubated with agitation for 45 minutes at room temperature. The blot was again washed 5 times with PBST for 5 minutes each. Subsequently, protein bands were visualized by application of a chemiluminescent substrate (ECL kit from Millipore), followed by exposure of a light sensitive film and development in an automated development machine (AGFA Curix 60).

In certain cases a membrane was reused for immunological detection, signals were then quenched by drying the membrane and leaving it for 2 days at room temperature. Following quenching, the membrane was incubated with 1% acetic acid for 15 minutes and blocked in 5% milk again.

3.3.3 Expression and purification of recombinant proteins (named below)

One day prior to expression, the corresponding plasmid was transformed into BL21 DE3 codon+ cells. The transformed cells were incubated on LB-agar containing chloramphenicol and the selection antibiotic appropriate for the plasmid used. All colonies were inoculated in LB medium, supplimented with appropriate antibiotics. The culture was grown at 37°C with shaking to a cell density of OD_{600} 0.6-0.8 and induced with IPTG for protein expression. The culture was further incubated at 16°C- 20°C over night.

Cells were harvested by centrifugation and resuspended in the respective lysis buffer depending on the protein to be purified. For complete cell lysis, the resuspended culture was treated in an emulsiflex 3-6 times, there cells break according to high pressure applied. The lysate was then centrifuged at 100 000 g for 30 minutes at 4°C to pellet insoluble

components. The supernatant was incubated with beads for 2-3 hours at 4°C. Following three washing steps, the recombinantly expressed protein was eluted from the beads and concentrated in a SpinX-UF concentrator previously blocked with 1% BSA. The protein was aliquoted and its purity and concentration was checked on a coomassie gel.

Importin7, NUP358 fragments, RanQ69L

The proteins His-importin-7, GST NUP 358 aa806-1000, GST NUP 358 aa806-1133, GST NUP 358 aa806-1170, GST NUP 358 aa806-1306, GST NUP 358 aa2011-2445 and Ran Q69L have been previously purified according to the references shown in 2.11 and were available in a communal stock.

Loading of RanQ69L with GTP (Nachury et al., 1999, modified)

Equal volumes of 5mM GTP and 5μg RanQ69L were incubated together in presence of 30mM EDTA for 20 minutes at room temperature in a volume of 30μl. 15mM $MgCl_2$ was then added and the reaction incubated for a further 15 minutes on ice.

3.3.4 Affinity purification of antibodies

In this work, a rabbit α importin-7 antibody was raised and purified. The antibody was raised using a peptide from the C-terminal region of importin-7, specifically aa 998-1015 with an additional cysteine residue at its n-terminus (CLADQRRAAHESKMIEKHG). The antibody was raised in rabbits and the complete immunization of 2 rabbits and the collection and processing of the blood was done by Proteintech group.

For the affinity purification of the importin-7 antibody 1mg of full length importin-7 protein was coupled to the CnBr beads. Firstly, 0.4g of CnBr beads were rehydrated in 1mM HCl for 10 minutes and then equilibrated with 0.2M carbonate buffer pH 8.9. In 0.2M carbonate buffer the protein was added to the beads and was then incubated with rotation at 4°C overnight. Beads were then washed twice with carbonate buffer for five minutes with rotation and were then incubated with 100mM ethanolamine for 1 hour at room temperature

to saturate free binding sites. After incubation, beads were washed again with carbonate buffer as described above, followed by equilibration with 500mM NaCl in PBS. Beads were then incubated with 15ml of the relevant serum overnight at 4°C. Subsequently, beads were collected carefully and all serum removed by washing twice for five minutes with 500mM NaCl/PBS in 50ml volume. Beads were then packed into a column and washed until no protein could be detected in the flow-through. Protein detection and later antibody detection from flow- through was carried out with Advanced protein reagent (Cytoskeleton Inc.). Purified antibodies were eluted with antibody elution buffer under low pH conditions in 500µl aliquots. Fractions were neutralized immediately after elution with 100µl Tris-base. After elution, fractions were analyzed on nitrocellulose- membrane with a Ponceau-S stain and antibody containing fractions were pooled and concentrated. Antibody validation was carried out by Western blotting of recombinant protein and cell lysate with subsequent immunological.

3.3.5 Immunoprecipitation

Immunoprecipitation was used as a technique to isolate proteins and their interacting factors from a whole cell lysate. Sepharose was equilibrated shortly and then blocked with immunoprecipitation washing buffer containing 1% BSA for 1.5 hours at 4°C.

In this work a specific antibody against the target protein was coupled to sepharose by incubation. Cells were lysed with immunoprecipitation lysis buffer on ice for 30 min. Cellular debris was then removed by centrifugation at 16.000 g for 10 min. Next, the supernatant was collected and incubated on the sepharose for 1-2 hours at 4°C. Beads were washed three times with immunoprecipitation washing buffer and boiled in SDS-PAGE loading buffer.

GFP- Immunoprecipitation using GFP- nanotrap

A GFP immunoprecipation kit was used to immunoprecipitate GFP tagged proteins. 293T HEK cells in 10cm cell culture plates were used for expression. Cells were transfected with the relevant plasmid coding for a GFP-fusion protein and incubated for 24-48h. For harvesting, cells were trypsinized, pelleted, washed with PBS and pelleted again. For cell lysis, 200µl of GFP lysis buffer/ 10cm plate, was used. The lysis buffer was supplemented with protein

inhibitors, 1% BSA and DNaseI. Cells were lysed for 30 minutes on ice with pipetting every five minutes. A small sample was taken as input control. Following lysis the lysate was centrifuged at 16. 000 g for 10 minutes to pellet insoluble components. The supernatant was diluted with 2.5 volumes of GFP dilution buffer, yielding a tolerable NP-40 concentration of 0.2%. For each immunoprecipitation 8µl of GFP-beads were equilibrated in GFP dilution buffer and blocked with 1% BSA for 1 hour at 4°C. The supernatant was then incubated with the beads for 2.5 hours at 4°C. After incubation, the beads were washed three times with GFP dilution buffer without BSA and spun down. Beads were resuspended in 20µl 2x SDS-PAGE loading buffer and heated to 95°C for 5 minutes. The samples could now be stored at -20°C or directly analyzed on SDS-PAGE.

Immunoprecipitation using protein G- sepharose

Immunoprecipitations are performed from 3-5 10cm plates per experiment using 2µl of goat α NUP358 antibody per plate. The antibody was coupled over night to equilibrated protein G sepharose, previously blocked with 1% BSA, with rotation at 4°C. After coupling, excess of antibody was washed off with immunoprecipitation washing buffer. Per 10cm plate, 5µl of sepharose was used. Cells were lysed with 200µl immunoprecipitation lysis buffer per 10cm plate on ice for 30 minutes with pipetting every 5 minutes. A small sample referred to as input was taken from the lysate and boiled in 2x SDS-PAGE loading buffer for 5 minutes. Subsequent to lysis, the lysate was centrifuged at 16.000 g to pellet insoluble components. The supernatant was then incubated with the beads for 3 hours at 4°C with rotation. Beads were washed with washing buffer without BSA to eliminate unbound proteins. Finally, beads were resuspended in 20µl 2x SDS-PAGE loading buffer and heated to 95°C for 5 minutes. The samples could now be stored at -20°C or analyzed directly on SDS-PAGE.

3.3.6 In vitro binding assays with GST- and His- tagged proteins (pull down)

In vitro binding assays using recombinant proteins were performed to demonstrate direct interactions between proposed binding partners. In this work, all in vitro binding assays were performed at 4°C and in 1mL volume of pull-down buffer. GST- sepharose was equilibrated in

pull down buffer and subsequently blocked with 1% BSA for 1 hour at 4°C with rotation. 5µg of a GST- tagged protein was coupled to 10µl of sepharose for 2 hours under rotation. Excess of protein was removed in three washing steps with pull down buffer. 5µg of a His- tagged binding partner was added and incubated for 1 hour. When indicated, reactions also contained 2.5µg of GTP-loaded RanQ69L. Unbound protein was removed by performing three washing steps with pull-down buffer. The last washing step was performed without BSA. Samples were then resuspended in 2x SDS-PAGE sample buffer and heated for 5 minutes at 95°C. They were now analyzed on an SDS-PAGE or stored at -20°C. Analysis of the in vitro binding assays was performed either by colloidal staining or Western blotting.

3.4 Cell biological techniques

3.4.1 Cultivation and passaging of adherent cells

HeLa P4 and HEK 293T cells were grown adherently in Dulbecco's modified Eagle medium (DMEM) supplemented with 10% (v/v) fetal calf serum (FCS) and 2mM glutamine. Both cell types were kept without antibiotics permanently. Cells were incubated in a humidified HERAcell 150i incubator at 37°C with 5% CO_2 atmosphere.

Cells were passaged by transferring 1/10 of the cells to a new plate every 3-4 days or when they reached confluency. Cells were washed with sterile PBS and detached from the culture plate by applying prewarmed trypsin/ EDTA. Subsequently cells were diluted in fresh medium and were further cultured.

3.4.2 Coating cover slides with Poly-L-lysine

To facilitate adherence of cells, cover slides were coated with the positively charged Poly-L-lysine. Slides were washed with 2-propanol, rinsed with sterile water and then incubated with

a 1/10 dilution of Poly-L-lysine in sterile water for 20 minutes. Coverslides were dried and sterilized with UV light for 3min at 0.12 J/cm^2.

3.4.3 Transient transfection of DNA

Transient transfection of mammalian HeLa P4 cells was used for localization experiments. The method was also used to transfect HEK 293T cells in order to overexpress protein for immunoprecipitation experiments. An appropriate amount of DNA (see table below) was mixed with 250mM calcium chloride (transfection buffer 1) and vortexed for 5 seconds at half power. Subsequently, an equal volume of 2x HEPES- phosphate buffer (transfection buffer 2) was added and again vortexed for 10 seconds at full speed. The reaction was incubated for 20 minutes at room temperature and was then added to cells of 50-60% confluency. Cells were further incubated for 20 hours to express the gene of interest and then processed for immunofluorescence or immunoprecipitation. Transfection of 10cm plates was performed using 3 samples for one plate.

Table for transfection:	24 well	10 cm plate (prepare 3 samples)
CaCl$_2$ (µl)	25	215
DNA (µg)	1,5	15-20
2x HEPES (µl)	25	215

3.4.4 RNA-interference (Tuschl et al., 1999; Tuschl, 2001)

RNA-interference provides a highly specific and efficient method to suppress the expression of proteins. A 21 nucleotides long double stranded oligo was designed specifically for the protein to be silenced. The sequence of the small interference (siRNA) oligo had to be homologous to the coding part of the proteins mRNA.

Transfection of siRNAs with Oligofectamine (Invitrogen)

siRNAs were transfected with the Oligofectamine transfection reagent. Cells were plated at a confluency of 30-40%, prior to transfection in 24 well plates with 500µl cell-suspension each well. SiRNAs were kept at a working concentration of 20µM in nuclease free water. Only the transportin siRNA was kept at 10µM according to the manufacturers protocol. 2µl of siRNA (final conc. 80nM) was transfected with 1.5µl Oligofectamine and 45µl Optimem per 24-well. The reaction was incubated for 25 min at room temperature, added to the cells in 500µl medium, and was incubated for 72 h. Cells were then split in a 1:3 or 1:4 ratio on coverslides in the morning and were transfected with the relevant plasmids in the evening. Experimental analysis was performed the day after, resulting in a total siRNA incubation of 96h. The silencing for transportin was done the same way except that 8µl (final conc. 160nM) of siRNA was used.

Silencing of NUP358 was achieved with a retransfection after 2 days of incubation. Cells at 30% confluency were transfected with 2µl of NUP358 siRNA, 1.5µl Oligofectamine and 45µl Optimem as described before on day 1. Cells were then incubated for 48 hours and split depending on their density in a 1:5 or in a 1:6 ratio on coverslides on day 3. Splitting was then followed immediately by a further transfection of NUP358 siRNA as described before. Reporter proteins were transfected in the evening of day 4. Analysis was performed at day 5. Silencing efficiency was confirmed by western blot.

3.4.5 Immunofluorescence

Indirect Immunofluorescence was used to quantify and analyze localization of proteins within cells in steady state. Cells were shortly washed with PBS twice and fixed with 4% paraformaldehyde in PBS supplemented with Hoechst 33258 at a concentration of 1:4000. Fixation was performed for 15 minutes at room temperature. Cells were again washed two times for 1 minute with PBS and then permeabilized with 0.5% triton X-100 in PBS for 10 minutes at room temperature. The detergent was washed off with two PBS washes. Afterwards, unspecific epitopes in the cells were blocked with 1% BSA in PBS for 30 minutes at room temperature. For protein detection, cells were incubated with primary antibodies at the appropriate dilution in PBS for 1 h at room temperature in a humid atmosphere. The

primary antibody was washed off with PBS twice. Subsequently, the appropriate secondary antibody was applied at a dilution of 1:1000 and incubated for 45 minutes. Cells were again washed two times in PBS, dried and mounted with Dako mounting medium.

Incubation of compounds

Cells were washed with PBS and prostaglandins were applied in an appropriate final concentration of 1µM-15µM in 400µl medium without FCS and incubated on the cells for 1 hour at 37°C. The prostaglandins were kept as a 10mM ethanol stock. LMB was applied at a final concentration of 5nM from a stock solution of 5µM also in medium lacking FCS. Cells were also incubated for 1 hour at 37°C. Since ethanol was a solvent for the compounds it was applied in the negative control.

3.5 Microscopy techniques

3.5.1 Confocal microscopy

Confocal microscopy was performed using a LSM 510 meta confocal microscope from Zeiss. Images were taken with the 63x Plan-Neofluar 1.3 NA water-corrected objective. The filter settings were adjusted to the type of fluorescence used in the experiment. For visual illumination and analysis, an x-site series 120 lamp was used. Images were taken using different lasers for excitation of dyes or fluorescent proteins. The Diode laser provided an excitation at 405nm and was used to detect the Hoechst stain. EGFP, YFP and Alexa Fluor488 antibodies were detected with the Argon 488 laser while the HeNe 594 was used to excite Alexa 594-conjugated antibodies. For far red antibodies such as Alexa 647and Alexa 633 the HeNe633 was used. While imaging fixed specimen, the pinhole was set between 1-1.5 airy units depending on the strength of fluorescence. The scan speed was set to a pixel time of 3.2µs -6.4µs. Signal to noise ratio was reduced by averaging several images, so the number of

scans was set to 4. In order to avoid bleaching, the laser transmission was set to 8% for the Diode laser and 12-15% for the Argon and HeNe lasers.

3.5.2 Measurement of import and export kinetics (reviewed in Shawn et al., 2005)

Import and export kinetics of HeLap4 cells were measured by live cell imaging at the confocal microscope using a technique called fluorescence loss in photobleaching (FLIP). Cells grown on coverslides were transfected with the respective plasmids expressing GFP-fusion proteins. The slide was put into a chamber fitting into the attachment of the microscope and cells were supplied with CO_2- independent medium. The microscope chamber was preheated to 37°C. For kinetic measurement, two equally fluorescent cells in close proximity to each other were chosen. In one cell the measurement was performed while the other one was referred to as a reference cell. The measurement was carried out as a photometric analysis using a set of 200 single photographs taken between 180 defined bleaching steps within 148 seconds. The first 20 images were performed without a bleaching interval in between. Once a GFP is bleached, it cannot recover within 146 seconds and therefore also not be measured again. Loss of fluorescence in a certain compartment of the cell is then due to protein diffusion or active transport.

For this kind of experiment, the pinhole was set to 2.0 airy units to collect as much light as possible. Imaging scan speed was set to a minimum pixel time of 1.27µs with an image number of 1 which resulted in an image interval of 154ms. The image was taken with a laser transmission of 1%. Between the images bleach intervals of 650ms were performed with 100% laser transmission and an iteration of 70. The bleaching intervals were performed within the measured cell in a small ROI (region of interest) of 30x10 pixels. When import kinetics were measured, the bleached region ROI-1 was set inside the nucleus of the analyzed cell. In contrast, export kinetics were analyzed with the bleached region ROI-1 set in the cytoplasm. After performing the measurement, other ROIs were encircled to measure their fluorescence intensity. In case of import analysis, ROI-2 was set by encircling the cytoplasm of the analyzed cell, ROI-3 was set by encircling the cytoplasm of the reference cell, ROI-4 marked the background (also see figure S6). For analysis of export kinetics ROI-2 was defined by encircling the nucleus of the analyzed cell, ROI-3 was defined inside the nucleus of the reference cell and ROI-4 also marked the background. Due to the 200 images taken of a single

FLIP sample, the computer program analyzed the loss of fluorescence within the defined ROIs in pixel intensities. For each experiment 30-45 FLIPs were performed.

FLIP data analysis

The data from FLIP experiments were analyzed using Microsoft Office Excel 2010. Data were plotted by analyzing signal intensities from nuclear regions of a bleached (Fb) and a neighboring unbleached cell as a reference (Fr), and a background region (Fc). Nuclear fluorescence intensities for each time point were expressed as $F(t) = (Fb - Fc)/(Fr - Fc)$. Fluorescence intensities were normalized to 1. Per condition 10–20 cells were analyzed.

Data analysis and quantification

Cellular localization of reporter proteins under different conditions was determined either by immunofluorescence or using fluorescent GFP-fusion proteins. For that purpose, cells were counted and subdivided into three categories: N>C majority of the reporter protein localizes in the nucleus, N<C majority of the reporter localizes in the cytoplasm, N=C equal distribution of the reporter. For every analyzed condition, 100 cells were counted and quantification was performed from at least three independent experiments. Error bars indicated the standard deviation calculated from these three experiments. Statistical significance of the data was determined applying a two-tailed and heteroscedastic student´s t-test (White, 1980) All calculations were done using Microsoft Office Excel 2010. Images were processed using the LSM Image Browser and Adobe Photoshop CS 5.

4 Results

4.1 Prostaglandin 15-deoxy-$\Delta^{12,14}$-PGJ$_2$ inhibits CRM1 mediated protein export

Prostaglandins are derivatives of arachidonic acids and contribute mainly to inflammatory responses. Cells that produce prostaglandins therefore belong to the immune system of an organism, such as T-cells or macrophages. During an inflammatory response these cells produce a subset of prostaglandins after stimulation. In this work HeLa cells were used to investigate effects of 15d-PGJ$_2$ on CRM1 mediated protein export.

4.1.1 15-deoxy-$\Delta^{12,14}$-PGJ$_2$ accumulated in the nucleus

The fungal inhibitor leptomycin B (LMB) is known for its inhibitory effect on CRM1-mediated protein export in mammalian cells (Kudo et al., 1999). LMB binds covalently and highly specifically to an evolutionary conserved cysteine residue at position 528 of the CRM1 sequence. The binding occurs at the sulfhydryl group of the cysteine via Michael addition (Kudo et al. 1999). Since LMB is an exogenous factor it was interesting to investigate whether endogenous compounds exhibiting a similar structure were also able to show comparable effects. In a binding assay using biotinylated 15-deoxy-$\Delta^{12,14}$-PGJ$_2$ (15d-PGJ$_2$) as a bait, CRM1 was detected as one of the prey proteins (Hilliard et al., 2010). Interestingly, 15d-PGJ$_2$ exhibits a very similar structure like LMB (figure 1B). It also contains a fatty acid tail and a cyclopentenone ring with a free α,β unsaturated carbonyl group which can potentially react in a Michael addition. In previous studies it was shown that biotinylated LMB enters the nucleus to target CRM1 (Kudo et al. 1999). If 15d-PGJ$_2$ is able to bind covalently to CRM1 it seemed to be possible that also 15d-PGJ$_2$ can be detected in the nucleus. Therefore, HeLa cells were incubated with biotinylated 15d-PGJ$_2$ to determine its subcellular localization. Incubation was performed in serum-free medium, because 15d-PGJ$_2$ shows a preference to target BSA (Rajakariar, 2007).

To detect the biotinylated 15d-PGJ$_2$ cells were fixed and incubated with streptavidin 488. A negative control was performed using untreated cells. In 15d-PGJ$_2$- biotin treated cells, the prostaglandin clearly accumulated in the nucleus, which led to the assumption that 15d-PGJ$_2$

**Figure1: 15-deoxy-Δ^{12,14}-PGJ$_2$ accumulates in the nucleus**

(A) HeLa p4 cell were treated with 15µM biotinylated 15d-PGJ$_2$ for 1 hour at 37°C and 5% CO$_2$. Incubation was performed in serum-free medium. Cells were fixed, permeabilized and blocked. Biotin was detected using Strepavidin488. The control cells were not treated with biotinylated 15d-PGJ$_2$ but were incubated with Streptavidin488 to detect possible cross-reactions. Images of the control were taken using the reuse function. (Hilliard et al. 2010) **(B)** Structures of 15d-PGJ$_2$ and LMB. The asterisks mark the free electrons in both cyclic compounds available for a Michael addition.

is able to target nuclear proteins (figure 1 A). Within this experiment it became clear that 15d-PGJ$_2$ entered the nucleus very quickly. The prostaglandin was detectable in cell after only 15 minutes of incubation (data not shown).

4.1.2 CRM1 can be covalently modified by 15d-PGJ$_2$

Since it became obvious that 15d-PGJ$_2$ can target nuclear proteins it is possible that it can bind covalently to the export receptor CRM1 as LMB is known to do. In order to identify a binding of 15d-PGJ$_2$ to CRM1 a cell lysate was incubated with biotinylated 15d-PGJ$_2$. The prostaglandin was bound to neutravidin beads and proteins modified by 15d-PGJ$_2$ could be

precipitated. Samples were then subjected to SDS-PAGE, followed by Western blotting and

CRM1 was detectable on the nitrocellulose membrane showing that it is definitely a target of

A

B

identified peptide	aa in CRM1
YYGLQILENVIK	77-88
LLSEEVFDFSSGQITQVK	173-190
AVGHPFVIQLGR	701-712
IYLDMLNVYK	713-722
DFEEYPEHR	837-845
EFAGEDTSDLFLEER	1024-1038

C
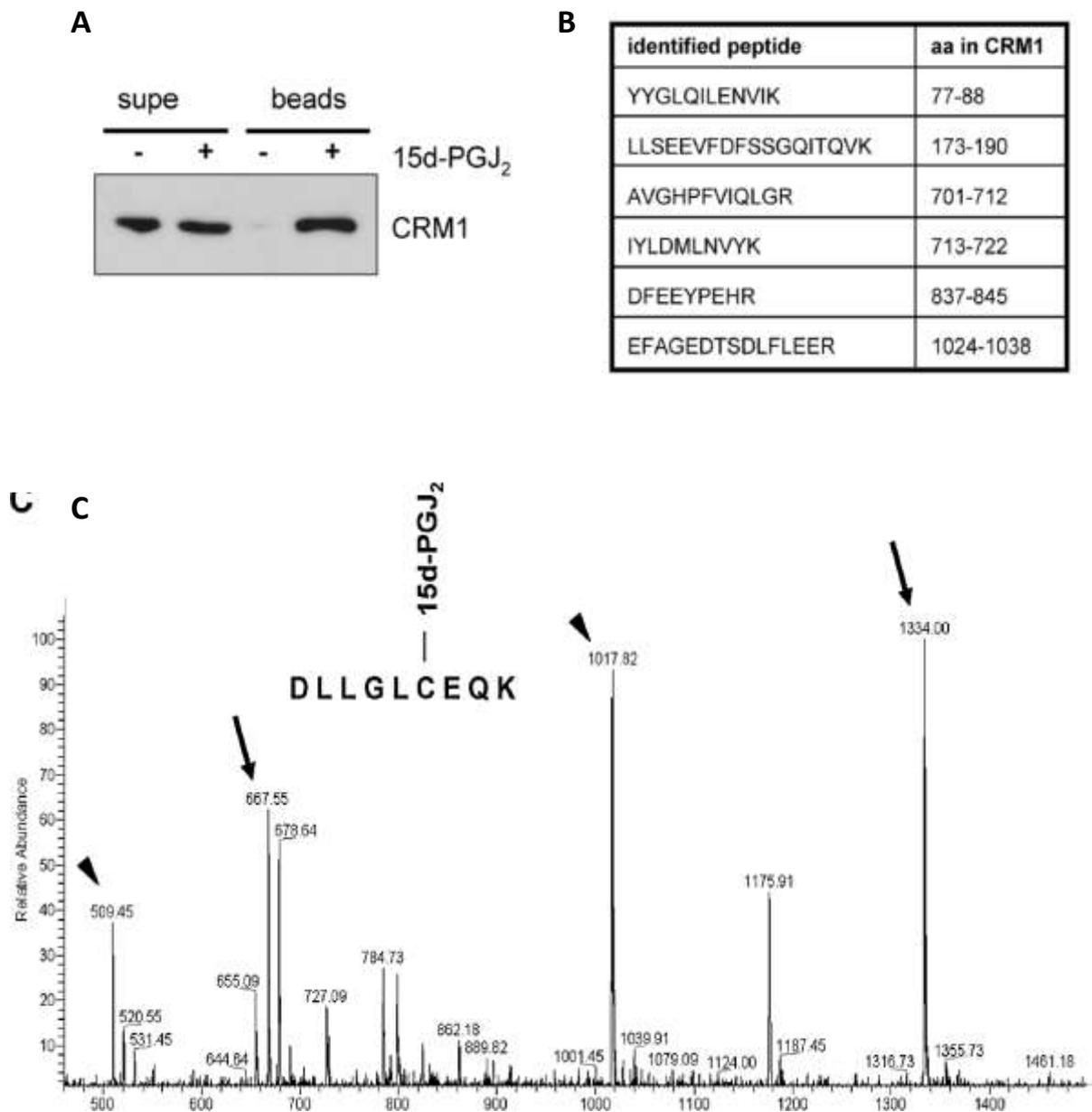
**Figure 2: 15-deoxy-Δ^{12,14}-PGJ₂ can target CRM1**
All data shown in this figure were published in Hilliard et al., 2010. **(A)** Western blot analysis of immunoprecipitation of a cell lysate incubated with (+) or without (-) biotinylated 15d-PGJ₂ bound to neutravidin beads. CRM1 was detected by rabbit αCRM1 antibody. 1% of the supernantant (supe) was loaded as an input control. This experiment was carried out by Annegret Nath **(B)** Identified CRM1 peptides out of a pool of 15d- PGJ₂ modified proteins from a HeLa-cell lysate. Peptides were analyzed by LC-MS/MS. Identitiy of peptide LLSEEVFDFSSGQITQVK was confirmed by sequencing. The experiments of figure 2B and 2C were carried out by Marc Hilliard. **(C)** Full mass spectrum of the modified CRM1 peptide DLLGLCEQK treated with 15d-PGJ₂. Arrows indicate the peaks of the modified peptide double charged (667.55) and singly charged (1334.00). Arrowheads indicate peaks of the same peptide unmodified. The difference in weight of the unmodified single charged peptide at 1017.82 and the 15d-PGJ₂ modified single charged peptide at 1334.00 corresponds to the molecular weight of 15d-PGJ₂.

15d-PGJ$_2$ (figure 2 A). To confirm results that CRM1 was targeted by the prostaglandin, a LC-MS/MS mass spectrometry approach was performed from precipitated proteins using the same precipitation method as described above. Indeed several CRM1 peptides were found, identifying the nuclear export receptor as a target of 15d-PGJ$_2$ (figure 2 B).

To further analyze whether the modification by 15d-PGJ$_2$ occured at the same amino acid (528) of CRM1 as the modification by LMB, a synthetic peptide (aa at position 523-531) carrying the sensitive cysteine was incubated with 15d-PGJ$_2$ and later analyzed by mass spectrometry. The full mass spectrum showed peaks at m/z 1017 corresponding to the unmodified peptide and m/z 1334 corresponding to the modified peptide, both of single positive charge (figure 2 C). The difference in weight between the peptides corresponded to the molecular weight of 15d-PGJ$_2$, showing that this CRM1 peptide was modified by 15d-PGJ$_2$. The peaks shown at m/z 509 and m/z 667 correspond to the unmodified and modified peptide with a double positive charge. Taken together, these data showed that the nuclear export receptor CRM1 can be targeted by 15d-PGJ$_2$ at the same cysteine residue as LMB. This led us to the hypothesis that also 15d-PGJ$_2$ can inhibit CRM1 mediated protein export (Hilliard et al., 2010).

4.1.3 15d-PGJ$_2$ inhibits nuclear export of overexpressed CRM1 substrates

To monitor a putative inhibitory effect of 15d-PGJ$_2$ on CRM1 mediated protein export in vivo, experiments with overexpressed reporter proteins were performed. The GFP-tagged transcription factor TFIIAα was overexpressed and tested for changes in localization after treatment with 15d-PGJ$_2$. TFIIAα-GFP was known from previous experiments to be localized predominantly to the cytoplasm and to respond to LMB treatment with nuclear accumulation. As shown in figures 3A, the CRM1 inhibitor LMB led to an accumulation of the reporter in the nucleus while cells treated with the ethanol control showed the original localization of the reporter in the cytoplasm. This suggested that export of GFP-TFIIAα is mediated by CRM1. Application of 15d-PGJ$_2$ also led to an accumulation of TFIIAα-GFP in the nucleus (figure 3 A). Figure 3B shows a quantification of this experiment. After treatment with the very potent CRM1 inhibitor LMB, quantification showed a strong localization of the reporter in the nucleus. Quantification of 15d-PGJ$_2$ treated cells showed a nuclear localization of the reporter in around 30% of the analyzed cells while more than 60% showed an equal distribution of the

A

B
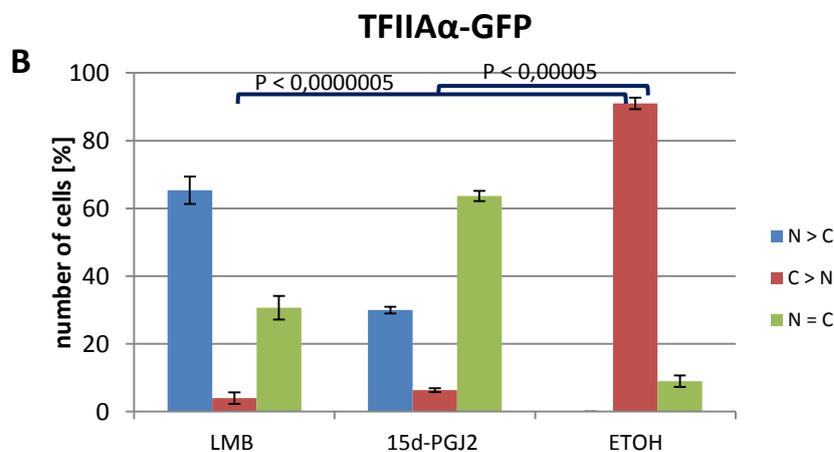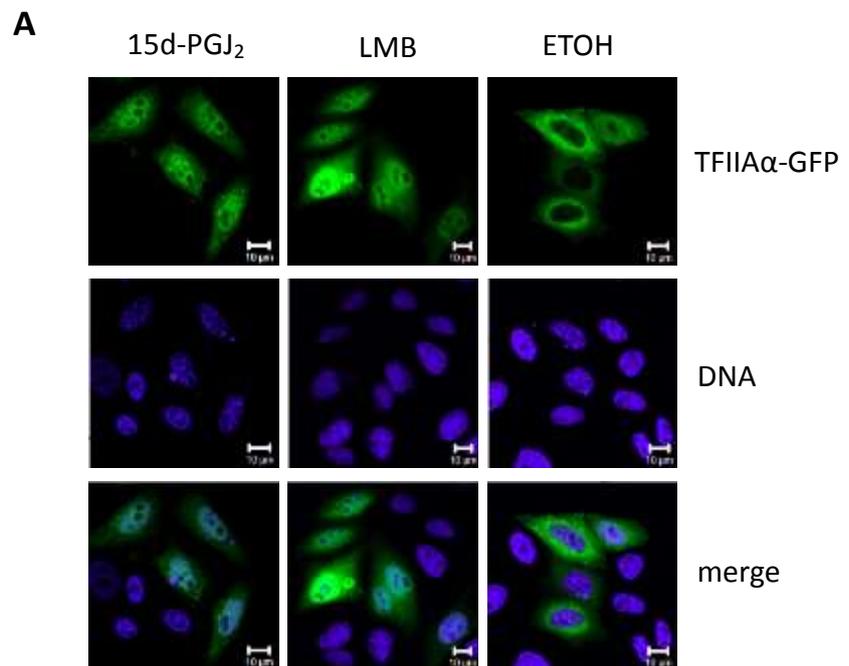
Figure 3: Export of TFIIAα is inhibited by 15d-PGJ$_2$

(A) Prior to fixation TFIIAα-GFP transfected HeLa p4 cells were treated with either 15µM 15d-PGJ$_2$ or 5nM leptomycin B (LMB) in serum-free medium for 1 hour. Ethanol (ETOH) was used as a solvent control. **(B)** Quantification of TFIIAα-GFP after treatment with the compounds mentioned above. For every condition 100 cells were counted from 3 independent experiments.

reporter between cytoplasm and nucleus. In less than 10% of the cells GFP-TF2Aα still localized to the cytoplasm. This suggested that 15d-PGJ$_2$, like LMB, can also impair the export function of CRM1.

To strengthen evidence that CRM1 can be modified by 15d-PGJ$_2$ an artificial reporter protein solely exported by CRM1 was used. The protein corresponding to the plasmid GFP$_2$-NES was overexpressed in HeLa cells which were then treated with either 15d-PGJ$_2$ or different prostaglandins (figure 4 A). Incubation with other prostaglandins was performed to test whether the previous shown inhibitory effect of CRM1 is due to a specific modification by 15d-PGJ$_2$ or whether prostaglandins in general can modify the protein. Therefore, a subset of endogenously produced cyclic prostaglandins with and without a free electron pair in their cyclopentenone ring, were tested (figure 4 A). As a negative control, the compound Cay 10410 was used which has a similar structure to 15d-PGJ$_2$ but lacks a free electron pair in its cyclopentenone ring (figure 4 A). To control the dependency of the reporter on CRM1, LMB was again used as a positive control. It was also useful to control the quality of export inhibition and to compare and quantify the putative inhibitory effect of 15d-PGJ$_2$.

Figure 4 A shows the different localizations of GFP$_2$-NES in steady state after treatment with different prostaglandins. Representative images are shown in figure 4A, the quantification of the experiment is shown in figure 4 B. As is obvious in the ethanol control, the reporter plasmid predominantly showed an equal distribution between nucleus and cytoplasm or localized to the cytoplasm exclusively. Following LMB treatment more than 60% of the analyzed cells the reporter accumulated in the nucleus. Also after 15d-PGJ$_2$ treatment more than 45% of the cells showed a nuclear accumulation of GFP$_2$-NES whereas the rest of the cells showed an equal distribution and only in few cells the reporter still localized to the cytoplasm (figure 4 B).

The other tested prostaglandins showed little or no influence on localization of the reporter protein. In case of prostaglandin E$_2$ (PGE$_2$) localization did not change significantly. The non-reactive 15d-PGJ$_2$ analog CAY 10410 and prostaglandin A (PGA) showed an equal distribution of the reporter with little influences on its localization. Although PGA also exhibits a free electron pair in its cyclopentenone ring it apparently cannot inhibit CRM1 mediated protein export in the same way like 15d-PGJ$_2$. Taken together, these in vivo data with an artificially designed CRM1 export substrate showed 15d-PGJ$_2$ can inhibit CRM1 mediated protein export.

A

B

Figure 4: CRM1 export substrate GFP$_2$-NES is inhibited by 15d-PGJ$_2$
(A) Prior to fixation GFP$_2$-NES transfected HeLa p4 cells were treated with different compounds for 1 hour in serum-free medium. Structures of the relevant compounds are shown next to the images. Asterisks mark free electron pairs in the cyclopentenone ring structure. LMB was used as a final concentration of 5nM while prostaglandins and CAY 10410 were used at 15µM. Ethanol (ETOH) was used as a solvent control. **(B)** Quantification of localization of GFP$_2$-NES after treatment with the compounds mentioned above. For each condition, 100 cells were counted from at least 3 independent experiments. Error bars showed the standard deviation of these three experiments.

4.1.4 15d-PGJ$_2$ inhibits CRM1 mediated export of endogenous RanBP1

Since 15d-PGJ$_2$ was able to impair the export of overexpressed proteins in vivo, the question arose whether the prostaglandin treatment also led to the nuclear accumulation of endogenous CRM1 export substrates. Therefore, RanBP1 a known NES containing CRM1 substrate (Richards et al. 1996) was analyzed. HeLa cells were incubated with several prostaglandins, LMB, Cay10410, ethanol and hydrogen-peroxide for 1 hour in serum-free medium. Hydrogen-peroxide was used to exclude changes in protein localization due to oxidative stress, which is known to occur after 15-PGJ$_2$ treatment (Kondo et al., 2001) and therefore validate the inhibitory effect of 15d-PGJ$_2$ on CRM1. After treatment with the different compounds cells were subjected to immunofluorescence and RanBP1 was detected using a specific antibody. Localization of RanBP1 was subsequently quantified. RanBP1 localized exclusively to the cytoplasm in the ethanol control as well as in the hydrogen-peroxide treated sample implying no influences on protein localization after induction of oxidative stress. After treatment with LMB, RanBP1 strongly accumulated in the nucleus (figure 5A, 5B). As shown in the quantification, all prostaglandins had a clear effect on localization of RanBP1. But compared to the effects of PGA and 15d-PGJ$_2$ the prostaglandin PGE$_2$ showed the weakest effect on RanBP1 localization. Still more than 50% of the analyzed cells showed a cytoplasmic localization of RanBP1. After incubation with PGA localization of RanBP1 was shifted to a 50% equal distribution of the export factor between cytoplasm and nucleus. The inhibitory effect of 15d-PGJ$_2$ was again stronger showing that this prostaglandin can also inhibit CRM1-dependent export of endogenous proteins. The modification of CRM1 through a Michael-addition by 15d-PGJ$_2$ appeared more likely considering the localization of RanBP1 after CAY10410 treatment, which lacked the α,β unsaturated carbonyl-group in the cyclopentenone-ring. In contrast to 15d-PGJ$_2$, CAY10410 did not change the localization of RanBP1, suggesting a Michael- addition of the reactive group at CRM1.

A

B
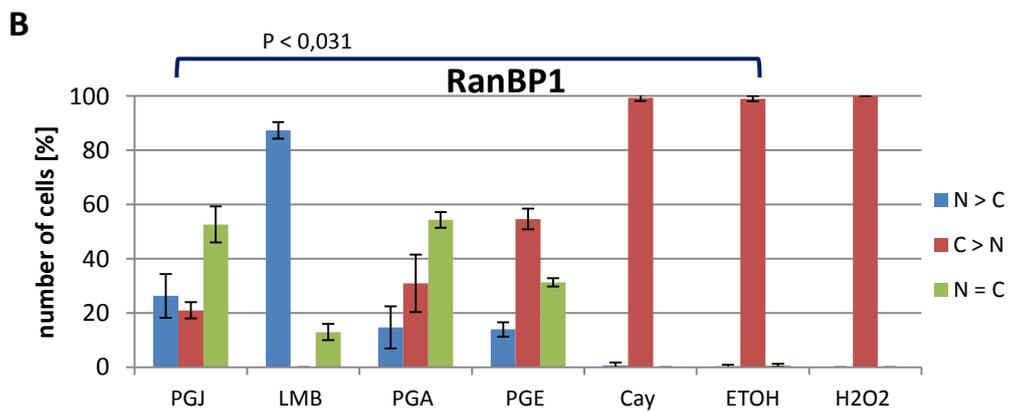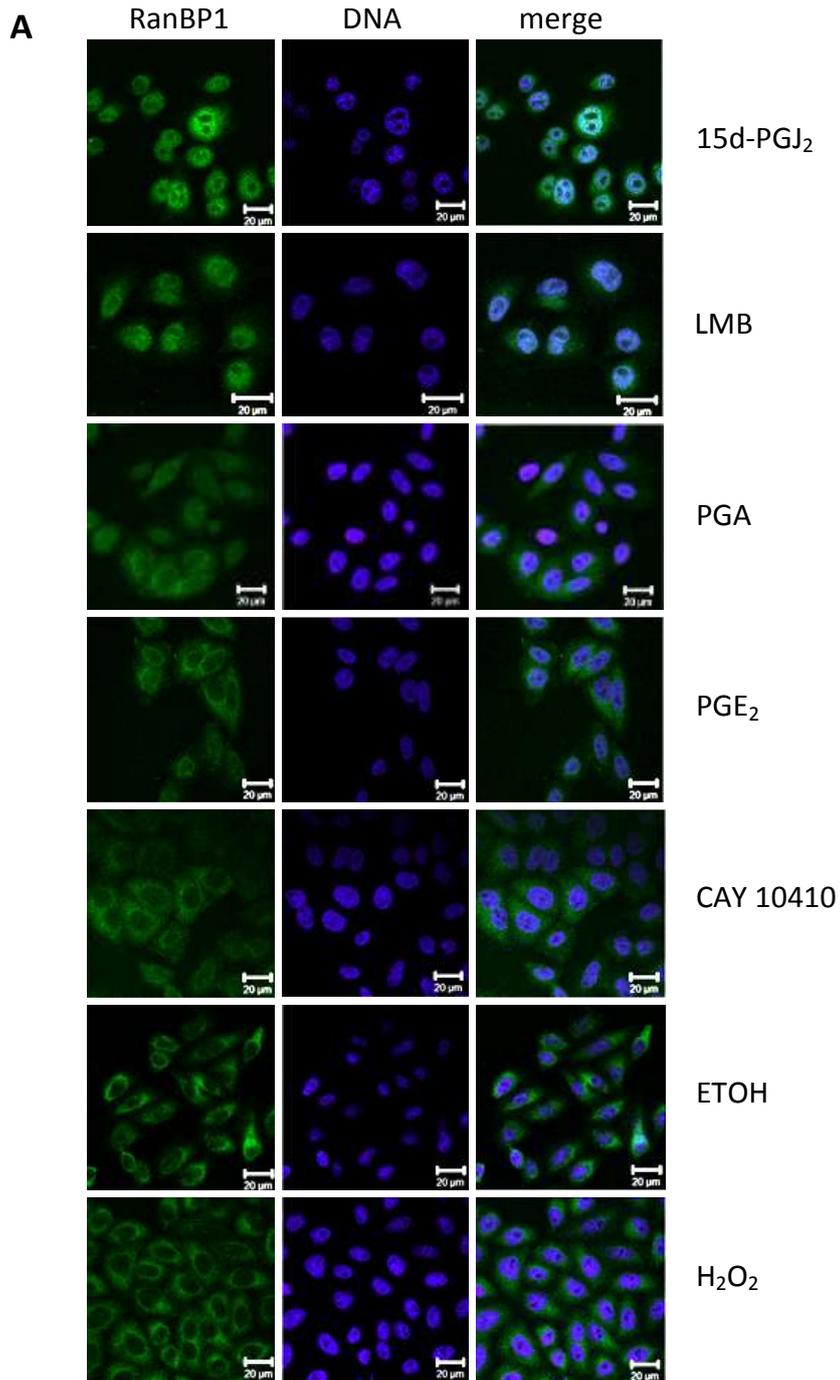
Figure 5: 15d-PGJ₂ inhibits CRM1 mediated export of endogenous RanBP1
(A) Prior to fixation, HeLa p4 cells were treated with 15d-PGJ₂, LMB, Prostaglandin A (PGA), ProstaglandinE₂ (PGE₂), CAY 10410, ethanol as a solvent control and H₂O₂ for 1 hour at 37°C in serum-free medium. All prostaglandins and CAY were used at a final concentration of 30µM. LMB was used at a final concentration of 5nM and hydrogen-peroxide was incubated in a final concentration of 10µM. RanBP1 was detected using a mouse α RanBP1 antibody at a concentration of 1:100 at 4°C overnight. **(B)** Quantification of RanBP1 distribution after incubation of compounds on cells. For each condition, 100 cells were counted from at least three independent experiments. Error bars indicate the standard deviation from the mean.

4.1.5 The CRM1 export substrate NC2β is very sensitive towards 15d-PGJ₂ export inhibition

In the previous experiments, 15d-PGJ₂ was used in high, non-physiologically relevant concentrations. Since prostaglandins are synthesized by cells in low nanomolar concentrations (Rouzer et al. 2005) it was interesting to find export substrates which responded to much lower concentrations of 15d-PGJ₂.

To investigate this, different CRM1 substrates were tested and the transcription factor RFP-NC2β (negative cofactor 2β) was found to differ in its subcellular localization after incubation with comparatively low levels of 15d-PGJ₂. NC2β was described as a nuclear-cytoplasmic shuttle and as a CRM1 dependent export substrate exhibiting a functional NES in its N-terminus (Kahle et al. 2009).

In control cells treated with ethanol, RFP-NC2β localized to the nucleus and cytoplasm quite homogenously. Transfected cells were treated with LMB to detect CRM1 mediated export. After treatment with LMB, RFP-NC2β accumulated very strongly in the nucleus (figure 6A) confirming a CRM1 mediated export of the substrate. 15d-PGJ₂ was incubated with RFP-NC2β transfected HeLa cells using different final concentrations ranging from 100nM to 2µM. Figure 6B shows a quantification of cells where RFP-NC2β accumulated in the nucleus. After incubation with a final 15d-PGJ₂ concentration of 200nM, around 12% of the transfected cells showed a nuclear accumulation of the reporter protein. When the 15d-PGJ₂ concentration was raised to 500nM one third of the analyzed cells showed a nuclear accumulation of RFP-NC2β (figure 6B).

Taken together, these data showed that indeed even low concentrations of 15d-PGJ₂ can affect the localization of certain CRM1 substrates.

A

B

C
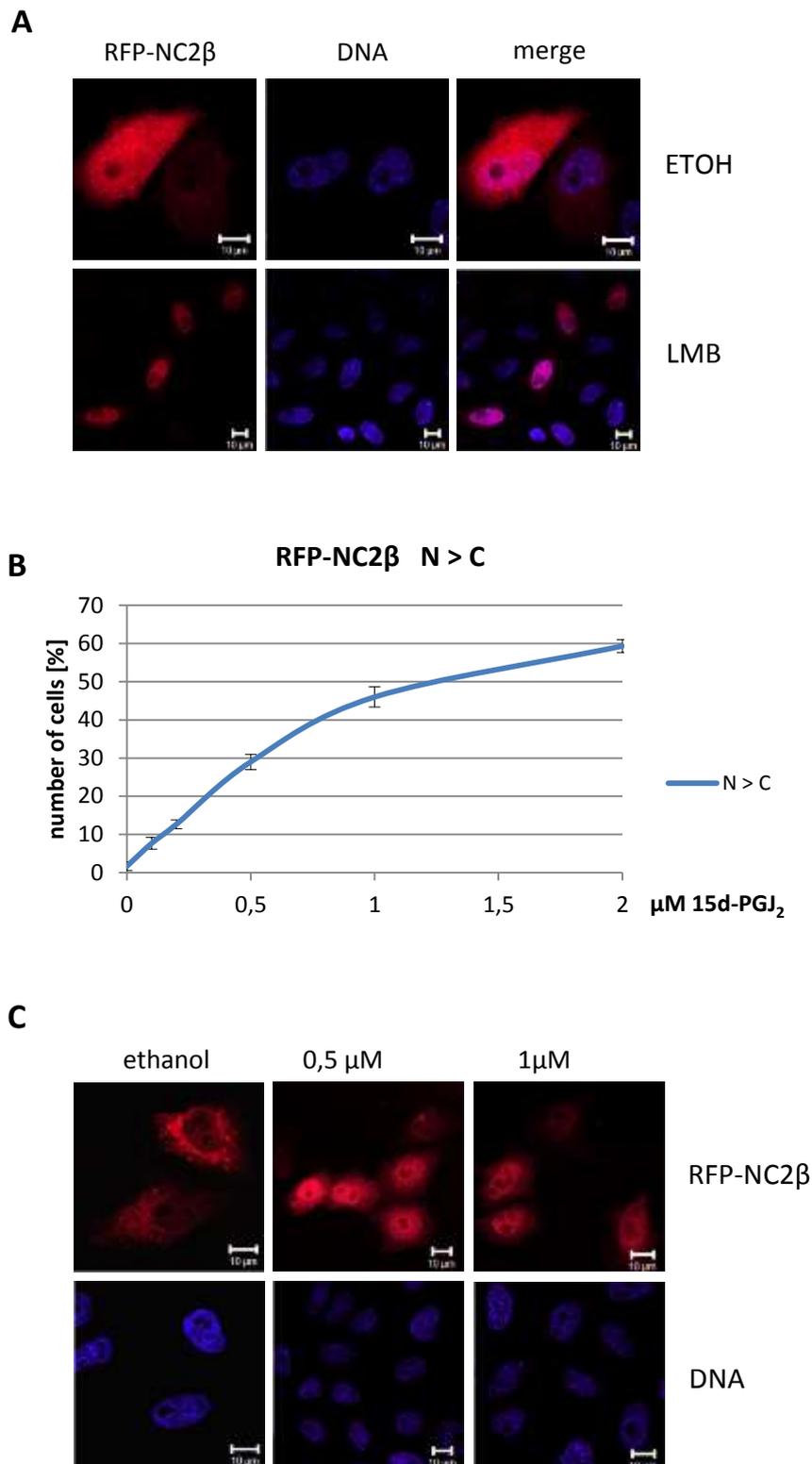
Figure 6: RFP-NC2β accumulates in the nucleus at low concentrations of 15d-PGJ$_2$
(A) HeLa p4 cells were transfected with RFP-NC2β and treated with either a final concentration of 5nM LMB or ethanol as a solvent control for 1 hour at 37°C in serum-free medium. Cells were then fixed and their DNA stained with Hoechst. **(B)** Quantification of RFP-NC2β transfected cells following a titration of 15d-PGJ$_2$ and fixation. Only numbers of N>C cells are shown in this graph. Prior to fixation cells were treated with ethanol as a solvent control (0nM 15d-PGJ$_2$), 100nM 15d-PGJ$_2$, 200nM 15d-PGJ$_2$, 500nM 15d-PGJ$_2$, 1µM 15d-PGJ$_2$ and 2µM 15d-PGJ$_2$. Quantification was carried out by counting 100 cells per experiment which was repeated at least three times. Error bars represent the standard deviation. **(C)** Representative images of quantification.

4.1.6 In vivo analysis of export kinetics by live cell imaging

To further analyze inhibition of CRM1 mediated export by 15d-PGJ$_2$ treatment export kinetics were performed with life cell imaging using the FLIP (fluorescence loss in photo bleaching) method. This method documents the loss of fluorescence of a GFP-tagged protein in one cell compartment (nucleus) while another one (cytoplasm) is bleached. The loss of fluorescence in a cellular compartment is either due to diffusion or active transport of the fluorescent protein. For this kind of analysis, the reporter plasmid coding for NES-GFP$_2$-M9 was transfected into HeLa cells. This construct contained a functional NES from the HIV-1 Rev protein, which is recognized and exported by CRM1 while it is imported by transportin via its
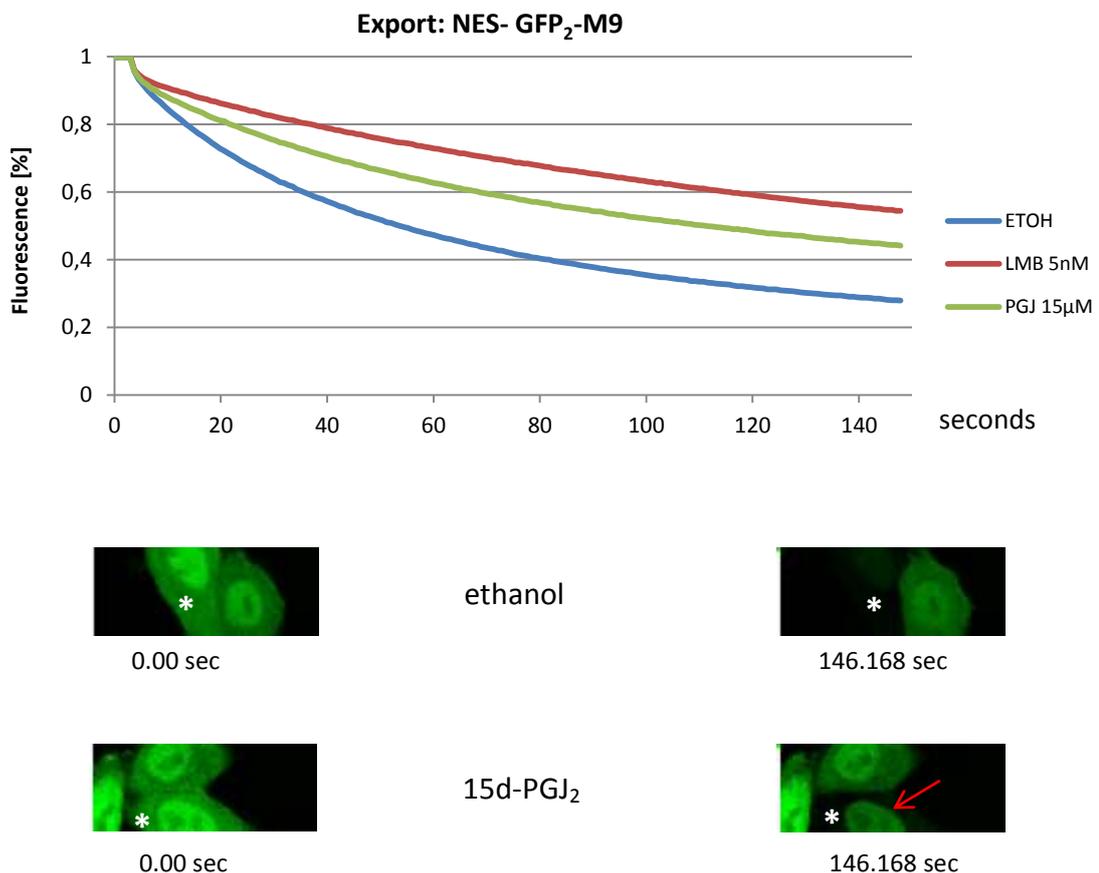
Figure 7: Life cell imaging performance showing CRM1 export inhibition by 15d-PGJ$_2$ using FLIP
HeLa p4 cells were transfected with the shuttling reporter protein NES-GFP$_2$-M9. Prior to analysis, cells were treated with either LMB (5nM), 15d-PGJ$_2$ (15µM) or ethanol as a solvent control. The compounds were incubated with the cells in serum-free medium for 1 hour at 37°C and 5% CO_2. Before starting the analysis the medium was changed to CO_2 independent medium. Asterisks in the images mark the bleached region in the cytoplasm. The assay was performed in three independent experiments analyzing 15-20 cells each. Error bars in the diagram were left out for better clarity of experimental data.

M9 sequence. In control cells, this protein showed a nuclear localization so the loss of fluorescence in the nucleus could be measured easily. After transfection, cells were either incubated with LMB, 15d-PGJ$_2$ or ethanol as a solvent control.

In control cells, it took 52.8 seconds until nuclear fluorescence was reduced to 50%. In cells treated with 15d-PGJ$_2$ it took 110.7 seconds, (figure 7). This showed that nuclear export of CRM1 can be inhibited by 15d-PGJ$_2$ in living cells. The well-established CRM1 inhibitor LMB gave a fluorescence of 54% after 146.3 seconds at the very end of the measurement. The import of the shuttling protein was not affected (figure S3). The images taken from the FLIP analysis show the retention of the reporter protein in the nucleus after 15d-PGJ$_2$ treatment (arrow).

4.1.7 The CRM1 mutant C528S can rescue CRM1 substrate mis-localization due to export inhibition by 15d-PGJ$_2$

LMB inhibits CRM1-mediated protein export by binding to its sensitive cysteine at amino acid 528 of the *human* sequence. The CRM1 protein from the yeast Saccharomyces pombe is resistant to LMB targeting due to the presence of a serine at this position (Kudo et al., 1999). To investigate whether 15d-PGJ$_2$ used the same mechanism to modify CRM1, a LMB resistant Ha-tagged CRM1 C528S mutant was used. The mutation of the cysteine to a serine has no influences on CRM1 export capabilities. CRM1 C528S was cotransfected with CRM1 dependent export substrates and the localization of the substrates was analyzed after treatment with LMB, 15d-PGJ$_2$ or ethanol. To control and quantify the effect, wild-type Ha-CRM1 was also cotransfected with the same reporter proteins. If CRM1 modification by 15d-PGJ$_2$ occured at the same residue as in LMB, then CRM1 C528S should be able to rescue the inhibitory effect of 15d-PGJ$_2$ on the reporter proteins. One day after transfection the cells were treated with either 15d-PGJ$_2$, LMB or ethanol for 1 hour. After fixation cotransfected cells were imaged and quantified. In the ethanol control the CRM1 dependent reporter protein TFIIAα-GFP localized to the cytoplasm in the presence of CRM1 WT as well as CRM1 C528S (figure 8A/B) showing that overexpressed CRM1 did not influence its localization (compare figure 3). After treatment with the CRM1 inhibitor LMB, a clear nuclear accumulation of the reporter in cells with CRM1 WT was detectable and quantifiable, while cells with CRM1 C528S showed rescue of the localization of the reporter (50% less nuclear

accumulation) (figure 8A/B). After 15d-PGJ$_2$ treatment, localization of GFP-TFIIAα in cells with CRM1 WT was equally distributed between nucleus and cytosol in 60% of cells. However, in cells expression the CRM1 C528S mutant almost 70% of cells showed cytoplasmic localization of GFP-TFIIAα due to the inhibitory effect of 15d-PGJ$_2$. This experiment showed that the exchange of the cysteine to a serine at position 528 can rescue CRM1 mediated protein export after export inhibition with 15d-PGJ$_2$.
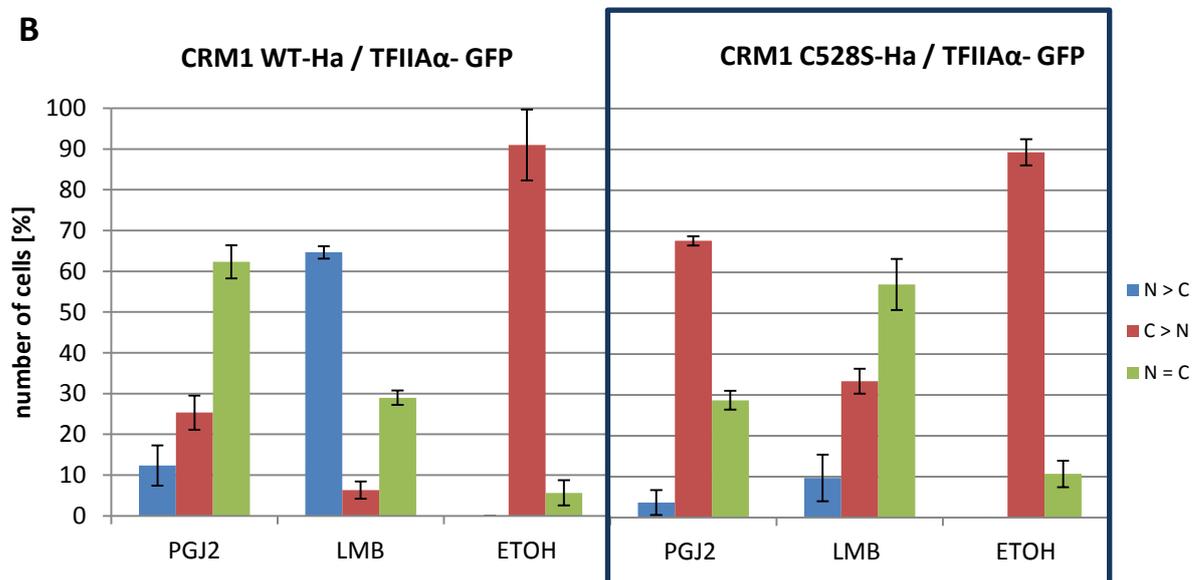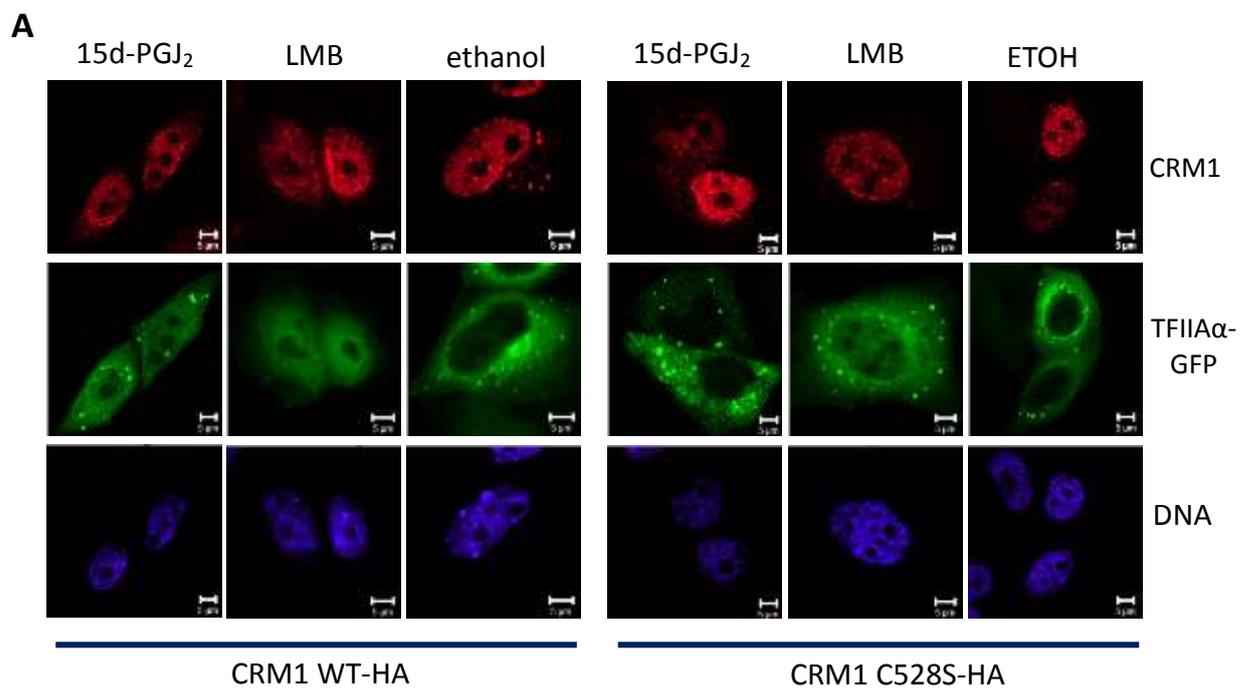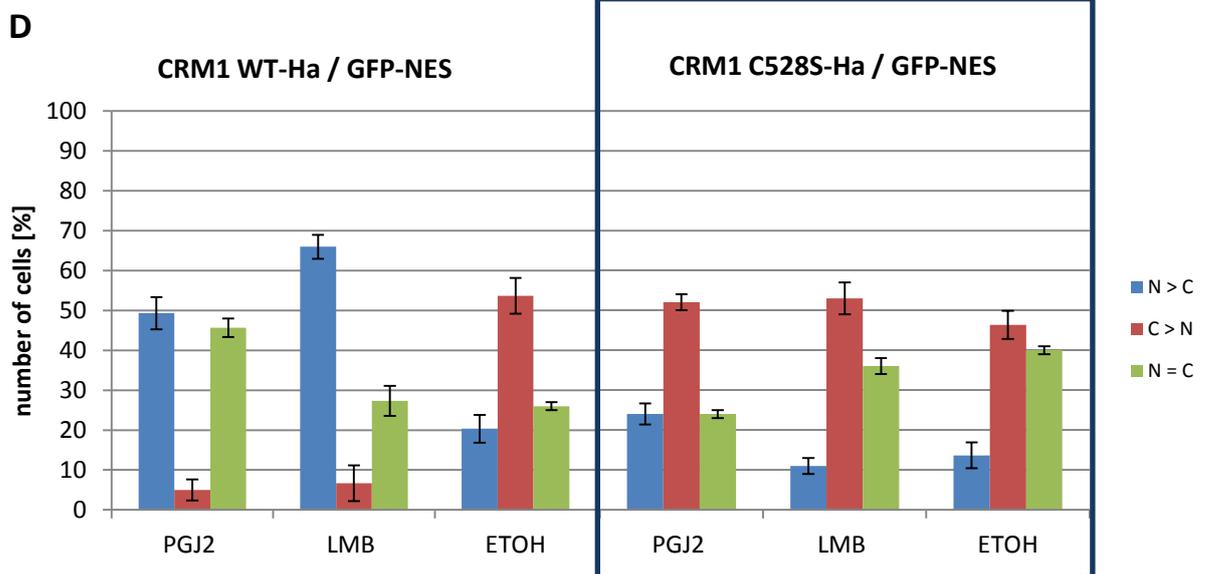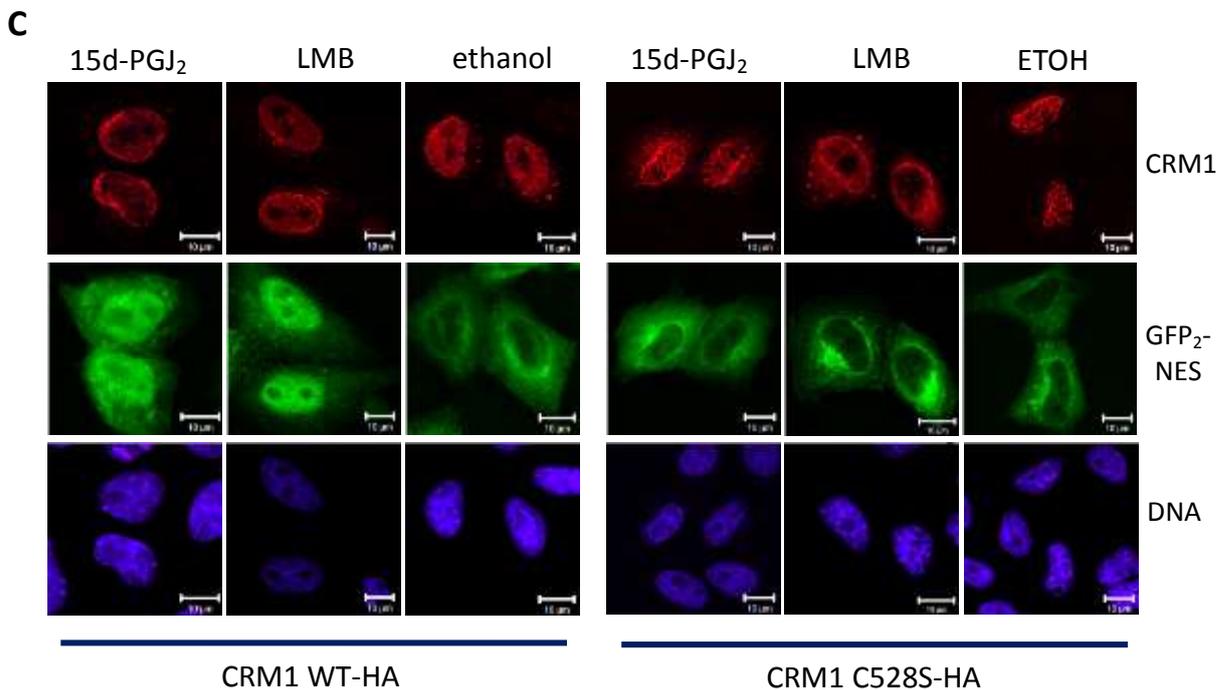
Figure 8: CRM1 C528S rescues CRM1 export substrates from 15d-PGJ$_2$ inhibitory effects.
(A) Rescue of GFP-TFIIAα localization by CRM1 C528S mutant. HeLa p4 cells were cotransfected with GFP-TFIIAα and Ha-CRM1 WT or Ha-CRM1 C528S. Prior to fixation, cells were treated with 15μM 15d-PGJ$_2$, 5nM LMB or ethanol (ETOH) for 1 hour in serum-free medium. Ha-CRM1 was detected with a mouse α Ha. DNA was stained with Hoechst. **(B)** Quantification of (A). For each condition, 100 cells were counted from three independent experiments. Error bars show the standard deviation. **(C)** Rescue of GFP$_2$-NES by CRM1 C528S. HeLa p4 cells were cotransfected with GFP$_2$- NES and Ha-CRM1 WT or Ha-CRM1 C528S. After transfection, cells were treated as described in (A). To detect Ha-CRM1, the same antibody was used as described in (A). **(D)** Quantification of (C) with 100 cells counted for each condition from 3 independent experiments. Error bars show the standard deviation.

the same cysteine residue as LMB. To confirm these data, the experiment was repeated with the artificial CRM1 export substrate GFP$_2$-NES. Again the reporter was cotransfected with either Ha-CRM1 WT or Ha-CRM1 C528S and treated with the respective compounds. Overexpressing CRM1 WT as well as the mutant CRM1 C528S again did not significantly influence the localization of GFP$_2$-NES in the ethanol control (compare figure 8D to 4B). Treatment with LMB again affected the localization of the reporter with coexpressed CRM1 WT by altering the former mainly cytoplasmic localization to a nuclear accumulation. In contrast, overexpression of LMB resistant CRM1 C528S rescued the inhibitory effect on CRM1 export completely (figure 8C/D). In cells cotransfected with GFP$_2$- NES and CRM1 WT treatment with 15d-PGJ$_2$ also influenced the localization of the reporter significantly by shifting the cytoplasmic localization to an equal distribution or even causing a nuclear accumulation. By overexpressing the CRM1 C528S this effect was also rescued completely and the reporter showed a distribution comparable to that seen with the ethanol control (figure 8C/D). This demonstrated that 15d-PGJ$_2$ is able to modify CRM1 at cysteine 528, as is seen with LMB. This experiment also indicates that cysteine 528 is probably the only amino acid to be targeted by the prostaglandin that can be involved in inhibiting export efficiency, since the exchange of this single cysteine to a serine led to a complete rescue of the inhibitory effect of 15d-PGJ$_2$ using the CRM1-dependent reporter GFP$_2$-NES.

All previous experimental data show that prostaglandin 15d-PGJ$_2$, which can be produced endogenously targets the same sensitive cysteine 528 in CRM1 as LMB.

4.2 Analysis of human telomerase reverse transcriptase import

Human telomerase reverse transcriptase is a ribonucleoprotein which consists of a protein subunit (TERT) and a RNA component (TER) (Blackburn et al. 1989; Lamond 1989). Telomerase is a conserved enzyme that is involved in chromosome maintenance and telomere elongation by synthesizing the telomeric TTAGGG repeats (Greider et al., 1989; Morin 1989, Blackburn et al. 1989). It therefore has to enter the nucleus through the nuclear pore. In contrast to very small proteins that can diffuse freely through the pore a protein like hTERT needs to be transported actively.

Here in this work it has been shown that factors such as an import receptor and a distinct region of a nucleoporin protein are involved in nuclear import of *human* TERT.

4.2.1 Overexpressed TERT localized to the nucleus independently of its tag

To determine the subcellular localization of overexpressed TERT in HeLa cells and to investigate possible influences of tags on the localization of the protein, several plasmids coding for differently tagged TERT proteins were used. C-terminally located YFP- GFP- and HA-tags were used to detect TERT localization within the cells. While cells transfected with fluorescent YFP and GFP fusion constructs were fixed and mounted, the HA-tagged version was detected using indirectly immunofluorescence.

The YFP and GFP tagged versions of TERT localized to the nucleus almost exclusively. The smaller TERT-HA protein also showed a nuclear localization (figure 9). This data showed that the size of the tag did not affect the subcellular localization of overexpressed TERT.

This experiment showed that the overexpressed human TERT constructs used in this work localized to the nucleus of human cells similar to the endogenous human TERT (shown in Chung et al., 2012; Haendeler et al., 2003). This indicates the protein therefore needs to be recognized, bound and imported into the nucleus by import receptors, since it is too large to diffuse into the nucleus.

TERT-YFP   TERT-GFP   TERT-HA

merge
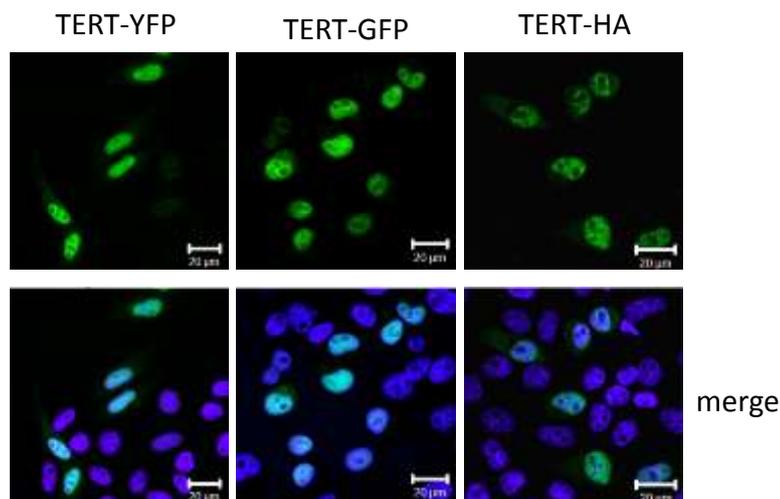
Figure 9: Overexpressed TERT localizes to the nucleus
HeLa cells were transiently transfected with different TERT expression plasmids. Cells transfected with fluorescent YFP- and GFP- tags were fixed and mounted. The HA tag was detected using a specific mouse α Ha antibody. DNA was stained with Hoechst.

4.2.2 Identification of a specific NLS-motif in *human* TERT

Since we observed that overexpressed TERT entered the nucleus it became obvious that it needed to be transported actively. Free diffusion of proteins through the nuclear pore is possible for small proteins of low molecular weight.

To determine which region of TERT is responsible for its import, several truncation mutants of TERT were cloned into a GFP-vector. The construct GFP-TERT NT containing amino acids 1-600 comprised the whole NTE including the TEN- and the TRBD-domains. The truncation mutant GFP-TERT CT comprised the amino acids 601-1132 and included the RT motifs and the C-terminal extension. For a schematic description of the mutants see figure S4.

In HeLa cells the TERT N-terminus as well as the C-terminus localized to the nucleus (figure 10A). This implied the existence of nuclear localization signals or importin docking sites in both truncation mutants. In an attempt to determine a responsible and distinct region for import within the TERT protein, further truncation mutants of the N-terminal region were cloned. For this purpose, several stretches of the proteins N-terminus were fused to a N-terminal GFP or double GFP-tag. GFP/dGFP-TERT 1-150 comprised parts of the N-terminal TEN domain while the truncation mutant 1-300 contains the complete TEN domain and ends

shortly before the telomerase RNA binding site (TRBD). The last N-terminal truncation mutant GFP/dGFP-TERT 301-600 includes the full TRBD and ends before the RT motifs. As shown in figure 10B all of the N-terminal truncation mutants localized to the nucleus exclusively, independently from the size of their tag.
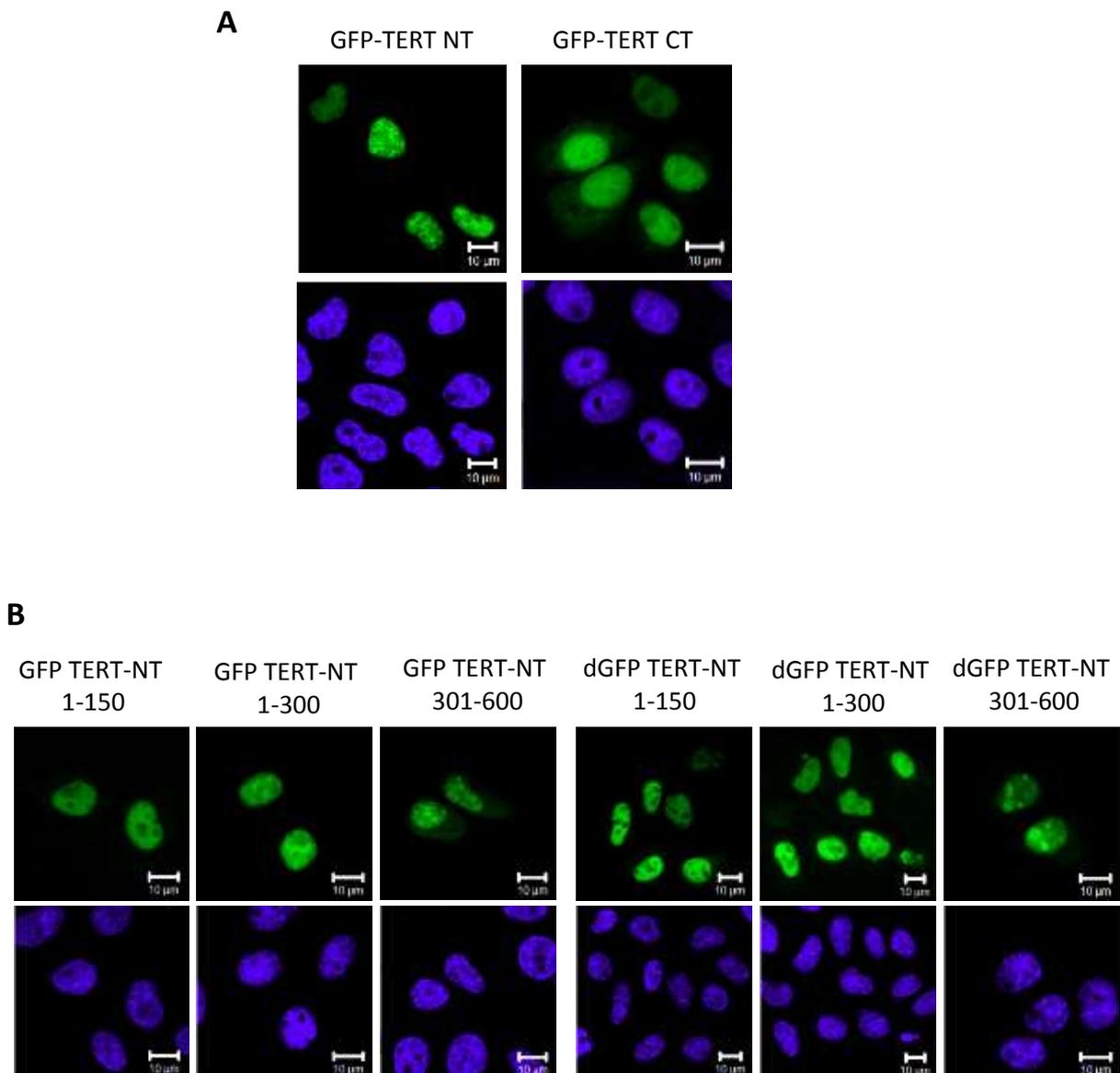
Figure 10: Overexpressed TERT truncation mutants localized to the nucleus exclusively
(A) TERT N-terminus and C-terminus localize to the nucleus. HeLa cells were transiently transfected with the respective GFP fusion plasmids. Cells were fixed and mounted. DNA was stained with Hoechst.
(B) TERT N-terminal fragments localize to the nucleus. HeLa cells were transiently transfected with the respective GFP or dGFP fusion constructs. Cells were fixed and mounted. DNA was stained with Hoechst. In contrast to all other TERT truncation mutants, which localized homogenously to the nucleus, TERT 301-600 strongly localized to the nucleoli.

Based on these observations, we decided not to work with small truncation mutants anymore and to follow a different strategy. A motif scan on the protein sequence of TERT was performed to identify putative recognition motifs for transport receptor binding. Indeed, the motif scan (www.elm.eu.org) identified a NLS motif located within the N-terminal region of TERT stretching from amino acids 235-240 (PKRPRR) similar to the classical NLS (figure 11A).

To validate whether this putative NLS is a functional motif, amino acids 239 and 240 were mutated to alanines (RR $\longrightarrow$ AA). Quantification of the localization of the mutant (GFP-TERT-NT 239) showed no difference in localization compared to wild type GFP-TERT-NT (figure S5). This result led to the conclusion that the two arginine residues were not essential for nuclear import. Next, the residues KR at positions 236 and 237 were also mutated to alanines yielding the sequence KRPAA $\longrightarrow$ AAPAA and destroying the whole putative NLS- site. Quantification of this mutant compared to wild type GFP-TERT-NT gave the first hints for an import defect. Around $^1/_3$ of the analyzed cells showed an equal distribution of the overexpressed protein between nucleus and cytoplasm whereas wild type GFP-TERT-NT was located in the nucleus exclusively (figure S5). This indicated that residues 236 and 237 (KR) could be responsible for the import of GFP-TERT-NT.

To analyze whether these residues also play a role in the import of the full length protein, TERT-GFP was also subjected to site-directed mutagenesis and residues 236 and 237 were mutated to alanines resulting in the sequence (KRPRR $\rightarrow$ AAPRR) leaving the last two arginines intact. After transfection, the mutant showed a severe import defect with predominantly equal distribution of the protein between nucleus and cytoplasm. The number of cells showing a nuclear localization dropped below 10% (figure 11 B/C). This demonstrated that indeed the amino acid sequence 236-240 in TERT is a functional NLS motif with amino acids 236 and 237 as a KR motif required for the import of the full length protein. While this work was in progress the same NLS motif in *human* TERT was discovered by another group (Chung et al., 2012).

4.2.3 Identification of a second NLS in TERT

In the last experiment, the existence of an N-terminal NLS in *human* TERT was demonstrated but mutation of this NLS did not completely lead to exclusion of the protein from the nucleus.

From these results it can be concluded that either residual binding to the NLS occurred or at least one additional NLS motif must exist within the protein. Since the residues KR were predominantly responsible for import in the N-terminally identified motif, a manual search for other KR motifs within the protein sequence was carried out. Indeed two other sites were found. The first one is located at amino acids 594-599 (KRVQLR) and the second one was found at position 649-653 (KRAER) (figure 11D). Also here KR motifs were mutated separately to establish whether they are functional NLS sites and contribute to import of TERT.

First, the KR motif at 594-595 was mutated to alanines by site-directed mutagenesis. The corresponding protein was overexpressed in HeLa cells and accumulated in the nucleus predominantly (data not shown) demonstrating that the KR motif at position 594/595 does not form a functional NLS motif in TERT-GFP.

Next, the downstream KR motif at position 649/650 was mutated to alanines by site directed mutagenesis. HeLa cells were transiently transfected with the resultant mutant and quantification of transfected cells showed a defect in nuclear accumulation of the mutant. Only 63% of cells showed a nuclear accumulation of TERT 649 KR-AA-GFP while the rest showed an equal distribution between nucleus and cytoplasm (25%) or a cytoplasmic localization (11.5%, figure 11 B/C). This result suggested that *human* TERT-GFP exhibits more than one NLS although the newly identified NLS seemed to be a much weaker one than the motif at position 236/ 237.

To investigate whether the import defect enhances after mutation of both motifs a double mutant was created. The N-terminal (236/237) as well as the C-terminal (649/650) motif was mutated resulting in the clone TERT KR 236/237 AA KR 649/650 AA- GFP (TERT 236 649 KR-AA-GFP). Quantification of this mutant resulted in an enhanced cytoplasmic localization of the double mutant compared to the N-terminal single mutant TERT 236 KR-AA-GFP (figure 11 B/C).

To further analyze the import inhibition by the destroyed motifs and to demonstrate the reduced kinetics, a FLIP experiment was performed. HeLa cells were transiently transfected with either TERT-GFP, TERT 236 KR-AA-GFP or TERT 236 649 KR-AA-GFP. Living cells were bleached in the nucleus and the loss of fluorescence from the cytoplasm caused by import of the protein was determined.

A TERT homo sapiens NP_937983.2

1) aa 220-250   GARRRGGSASRSLPLPKRPRRGAAPEPERTP

2) aa 222-240   RRRGGSASRSLPLPKRPRR   Bipartite cNLS

3) aa 235-240   PKRPRR   Monopartite cNLS

B

TERT-GFP   TERT 236 KR-AA-GFP   TERT 649 KR-AA-GFP   TERT 236 649 KR-AA GFP

DNA

C

TERT NLS mutants

D

NLS

236 KRPRR 240   594 KRVQLR 599   649 KRAER 653

1   1132
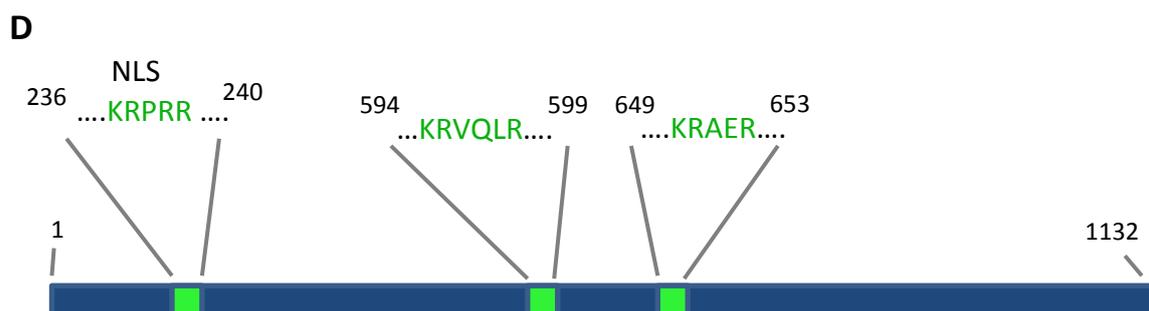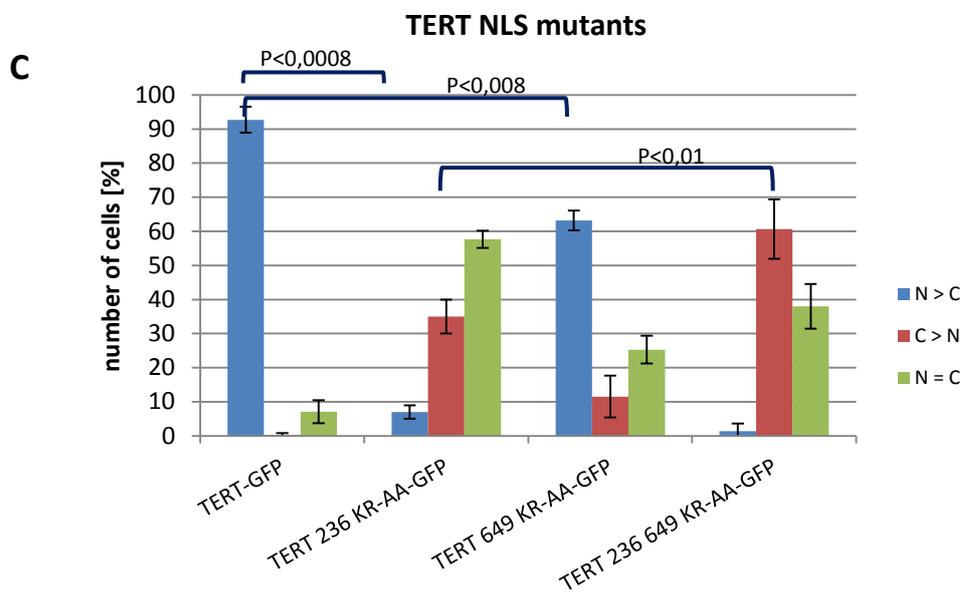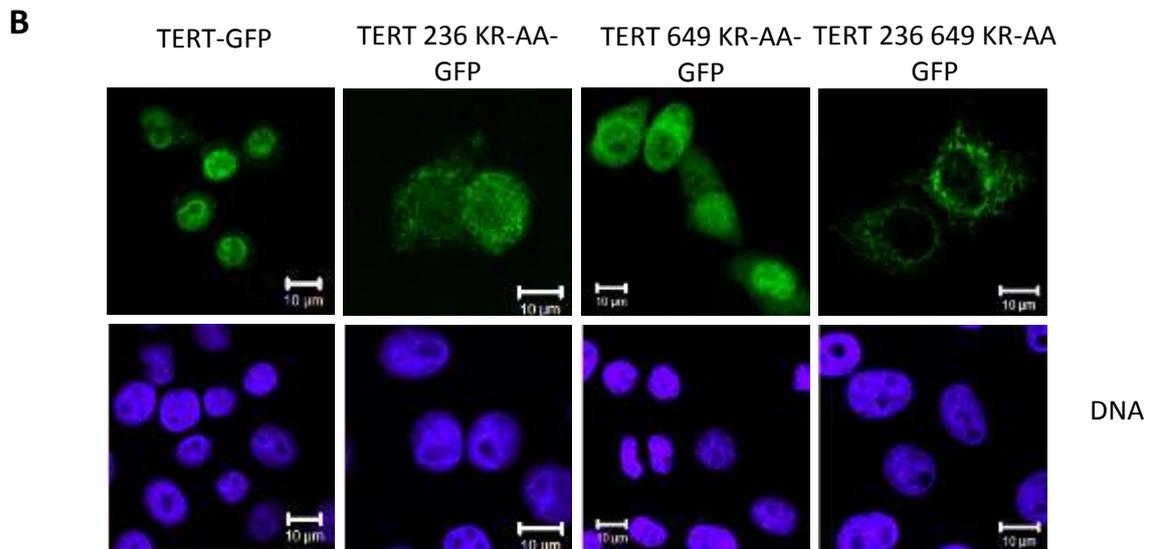
Figure 11: Identification of a second NLS motif in TERT
(A) The amino acid sequence of *human* TERT was run in a protein motif scan (www.elm.eu.org) and a putative NLS was discovered. 1) N-terminal sequence in *human* TERT from amino acids 220-250. 2) Bipartite NLS motif that was found through the in silico scan comprising amino acids 222-240. 3) Monopartite NLS motif within the bipartite motif, which was also discovered by the bioinformatics analysis. **(B)** HeLa p4 cells were transiently transfected with TERT-GFP or the mutants TERT 236 KR-AA-GFP, TERT 619 KR-AA-GFP or the double mutant TERT 236 649 KR-AA-GFP. After fixation DNA was stained with Hoechst and cells were subjected to quantification and imaging. The white arrow points to cells showing an import defect of TERT 649 KR-AA-GFP transfected cells. The red arrow points to a cell classified as nuclear accumulation but compared to wild type TERT-GFP it becomes obvious that a lot of protein resides in the cytoplasm suggesting a slower import than wild type TERT-GFP. **(C)** Quantification of TERT-GFP and the NLS mutants mentioned above. TERT-GFP was quantified from 14 independent experiments. Quantifications were fused and shown as a mean value with standard deviations from all these experiments. TERT 236 KR-AA-GFP and TERT 236 649 KR-AA-GFP were quantified from 3 independent experiments counting 100 cells each. TERT 649 KR-AA-GFP was quantified counting 800 cells from 3 independent experiments. Error bars show the standard deviation of three experiments. **(D)** Schematic description of *human* TERT with its putative NLS sites.

Mean values of 45 measured cells for each time point and condition are shown in figure 12. After t=146 seconds, TERT-GFP fluorescence was reduced from the initial level of 1.0 to 0.36, a great loss of fluorescence suggesting a high import rate (figure 12). At the same timepoint, the remaining fluorescence of TERT 236-KR-AA-GFP was still 0.61. This demonstrated that import kinetics decreased after destruction of the NLS site compared to WT TERT-GFP.

In the double mutant TERT 236 649 KR-AA-GFP this effect was even enhanced, resulting in a value of 0.72 after 146 seconds, showing that import further decreased after mutation of the second KR motif (figure 12). These findings led to the conclusion that TERT-GFP contains another NLS site at position 649/650. However, the strongest NLS motif in TERT is the one found at 236-240 with the KR motif responsible for its import.

Regarding the export rate of TERT-GFP (see figure S7), it became obvious that the protein does not underlie a strong export rate during analysis. Studies suggested that TERT is exported by CRM1 (Seimiya et al., 2000), but after incubation with LMB, export rate did not change much. This led us to the assumption that export of TERT-GFP does not occur at a fast rate.
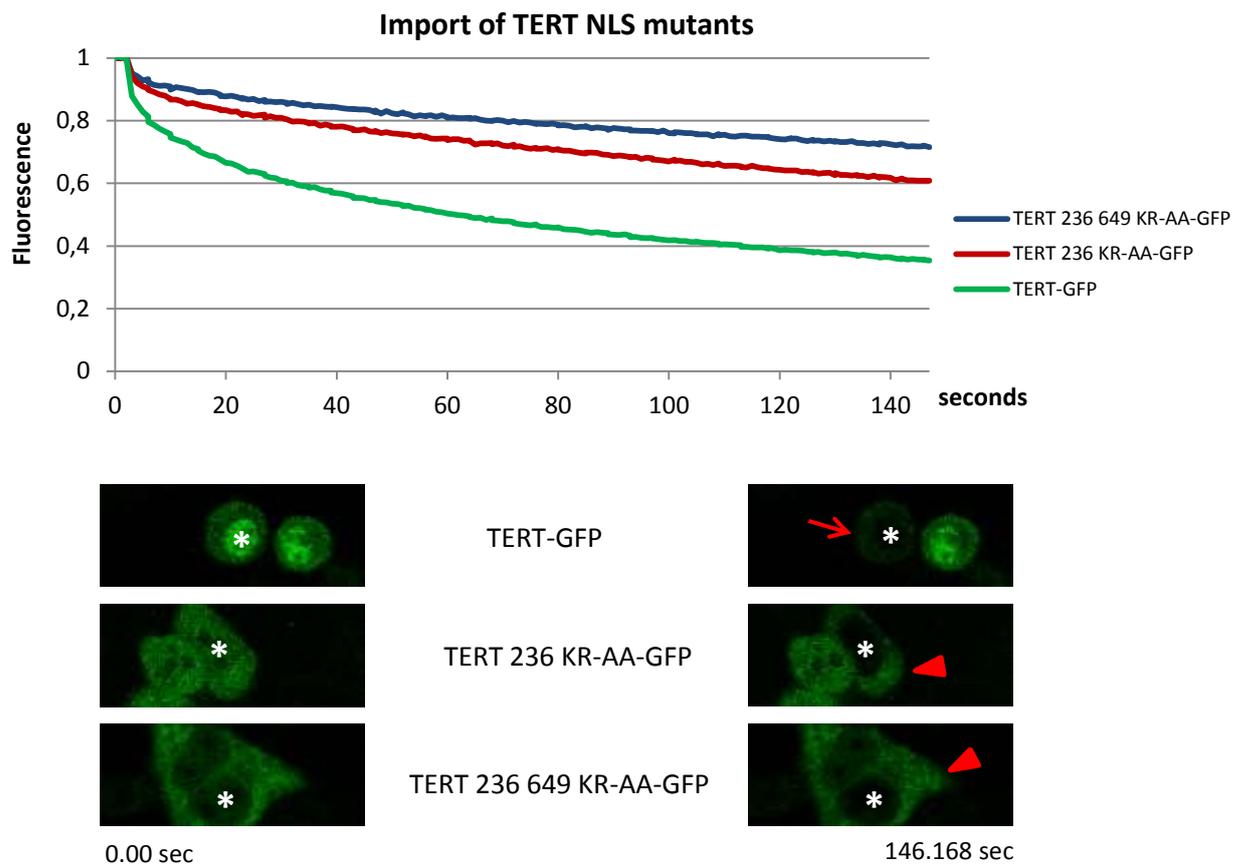
Figure 12: Inhibited import of the NLS mutants can be demonstrated in living cells
HeLa cells were transiently transfected with TERT-GFP, TERT 236 KR-AA-GFP or TERT 236 649 KR-AA-GFP. White asterisks in the nuclei indicate the bleached regions. For every condition 45 cells were analyzed. Error bars in the diagram were left out for better clarity of experimental data (Error bars shown in figure S11). In order to gain comparable data, cells with equal levels of fluorescence in their cytoplasm were chosen in mock as well as in KD cells (figure S6). The red arrow marks the darkened cytoplasm of the bleached TERT-GFP transfected cell after 146 seconds. The red arrowheads point to the relatively bright cytoplasm of cells transfected with the mutants at 146s compared to the start of analysis and to wild type TERT-GFP.

4.2.4 Knock-down of Nup358 results in TERT import defects

Nup358 (RanBP2) is a 358 kDa protein located at the cytoplasmic filaments of the nuclear pore complex (Wu et al., 1995). In recent data it has been shown that this nucleoporin is involved in import of some proteins because depletion of Nup358 led to a cytoplasmic localization of a subset of import substrates (Wälde et al., 2012). As already described, the depletion of Nup358 also led to a cytoplasmic or equal distribution of overexpressed TERT-myc (Hutten 2007) suggesting that the lack of Nup358 led to impaired import of TERT. In the experiment shown in this work former data was reproducible.

Endogenous Nup358 was depleted by siRNA treatment. Cells were then transiently transfected with TERT-GFP and subjected to immunofluorescence. Nup358 was stained with a specific antibody to determine knock-down efficiency. Only cells with significantly reduced Nup358 were analyzed.

Figure 13B and the quantification (figure 13C) show a typical localization of TERT-GFP in mock and Nup358 depleted cells. In control cells (white asterisk) TERT-GFP accumulated in the nucleus almost exclusively while in Nup358 depleted cells (red arrow) TERT-GFP either localized to the cytoplasm or was equally distributed.

4.2.5 Overexpressed Nup358 fragments containing the zinc-fingers efficiently rescued TERT

From the previous experiment, it was known that Nup358 was required for TERT nuclear import. The question arose, which region of Nup358 is responsible for the import of TERT-GFP. In previous work, Nup358 siRNA resistant truncation mutants of the nucleoporin have been cloned and certain domains of its N-terminus containing aa 1-1170 (ending before the Ran-binding domain1 (RB1) and including three FG-repeats) were described as the region responsible for import of DBC-1, (Wälde 2010). Using the same approach, a similar rescue experiment for TERT-GFP was carried out using different fragments of Nup358. Endogenous Nup358 was depleted by siRNA treatment and cells were cotransfected with Ha-tagged Nup358 fragments (figure 13 A) and TERT-GFP. The siRNA treatment against Nup358 again showed a severe impact on TERT-GFP nuclear localization (figure 13 B/C). Less than 30% of the analyzed cells showed a nuclear accumulation of TERT-GFP in knock-down cells. In mock cells more than 90% of the analyzed cells showed a nuclear accumulation of TERT-GFP. Cells cotransfected with Nup358 fragments showed different localizations of TERT-GFP depending on the fragment. The largest fragment without any rescue effect was Nup358 1-1306 containing the leucine rich N-terminus, the coiled-coil domain, FG-repeats (I) and the Ran-binding domain1 (figure 13 A/C). In contrast to the data for DBC-1 this fragment was not able to rescue the import of TERT-GFP in cells depleted of endogenous NUP358. Nuclear accumulation of TERT-GFP was observed only in 35.3% (mean value) of the cells (figure 13 B/C). A longer fragment was analyzed Nup358 1-1810
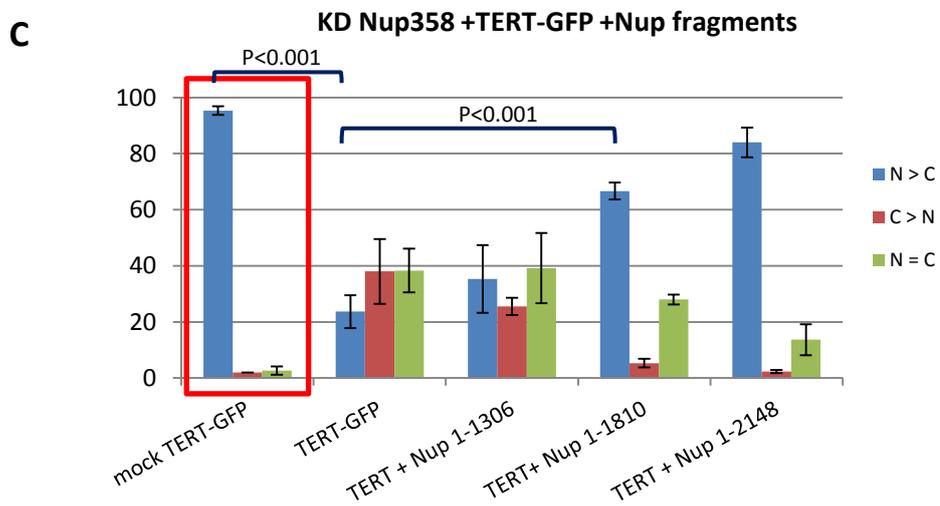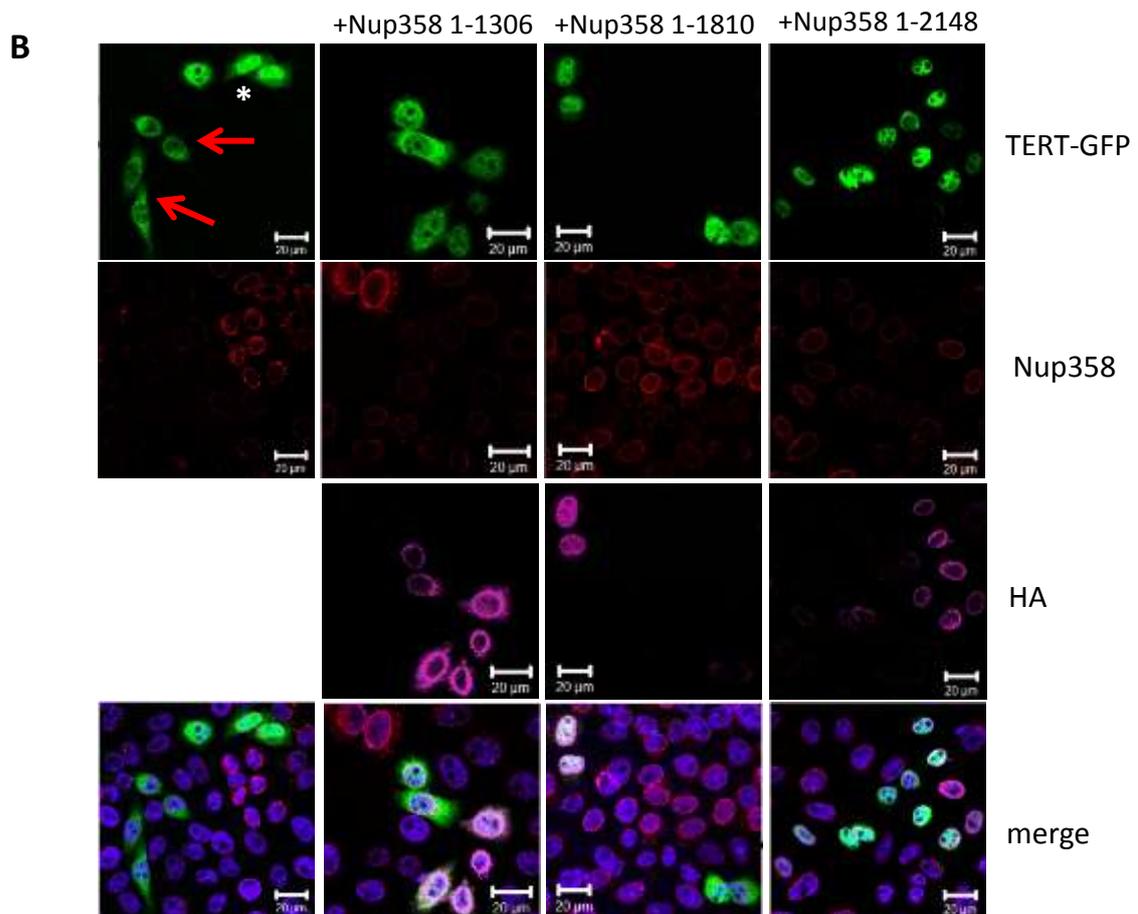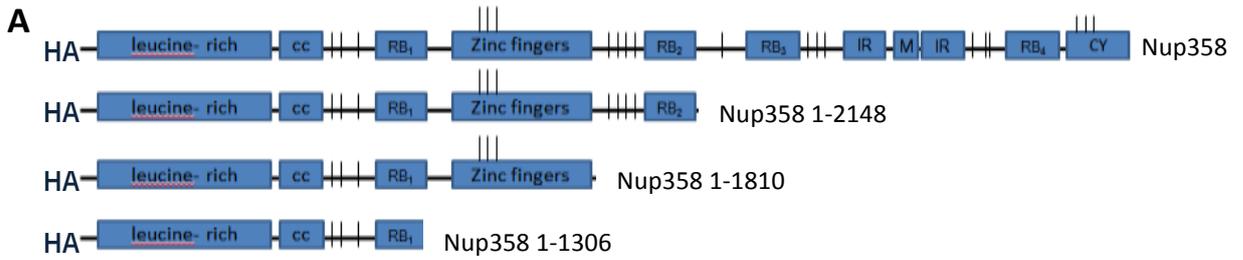
**Figure 13: Overexpression of Nup358 fragments can rescue TERT-GFP**
(A) Schematic description of full length Nup358 and the N-terminal Ha tagged fragments and their domains. CC= coiled coil domain, I= FG-repeat, RB= Ran binding domain. **(B)** HeLa p4 cells were subjected twice to siRNA treatment against Nup358 and were then cotransfected with TERT-GFP and Ha-Nup358 fragments respectively. Following fixation endogenous Nup358 was detected with a goat α Nup358 antibody and stained with a donkey α goat 594 antibody. Ha-Nup358 fragments were detected using a mouse α Ha antibody and stained with a donkey α goat 647 antibody. The red arrows point to a group of cells depleted for Nup358 showing the import defect on overexpressed TERT-GFP. The white asterisk marks two cells without Nup358 depletion and correct localization of TERT-GFP. **(C)** Quantification of cells from three independent experiments counting 100 cells each was done. Knock down efficiency was controlled visually in the immunofluorescence by analyzing cells with clearly reduced expression levels of Nup358. Error bars indicate the standard deviation from the mean value of the experiments.

containing the zinc finger domain, which showed the ability to rescue TERT-GFP localization. Around 66% of the analyzed cotransfected cells showed a nuclear accumulation of TERT-GFP. The percentage of cells with cytoplasmic localization was also decreased to an average value of 5.3 % (figure 13 B). Transfection of a larger Nup358 fragment containing aa 1-2148 and the Ran-binding domain2 enhanced the rescue effect on TERT-GFP resulting in 84% of cells showing nuclear accumulation of TERT-GFP (figure 13 B). This experiment showed that indeed Nup358 is involved in TERT-GFP nuclear import since the import defect can be specifically rescued by overexpression of zinc finger domain containing Nup358 fragments after Nup358 depletion. This also showed that although various proteins depend on Nup358 for efficient import individually they require different regions on Nup358.

4.2.6 Importin-7 is the major import receptor for *human* TERT

It was shown that TERT exhibits functional NLSs and its import is dependent on the presence of Nup358 (Hutten 2007). The question arose, which import receptor is responsible for the import of TERT. In the computational motif scan the N-terminal NLS in TERT was classified as a classical NLS (cNLS) basically recognized by importin-β or the importin-β/-α heterodimer (Adam et al., 1994). It would be therefore possible that importin-β or the importin-β/-α heterodimer serves as the responsible import factor for TERT.

To identify the import receptor of TERT, knock down experiments using siRNAs directed against the import receptors importin-β/ -7/ -9 were performed. HeLa cells were treated with siRNAs to reduce the expression level of the import receptors. Control cells were either treated with a random non-targeting siRNA or left untreated (mock), were transiently

A

	TERT-GFP	EZI	NES-GFP$_2$-M9	NES-GFP$_2$-NLS

Mock

DNA

siRNA IPO 9

DNA

siRNA IPO β

DNA

siRNA TPO

DNA

siRNA IPO 7

DNA

B

p-values (n/ n)
TERT-GFP, Mock/KD IPO7 <0,002
NES-GFP$_2$-NLS, Mock/KD IPOβ <0,02
GFP$_2$-NES-M9, Mock/KD transp. <0,02
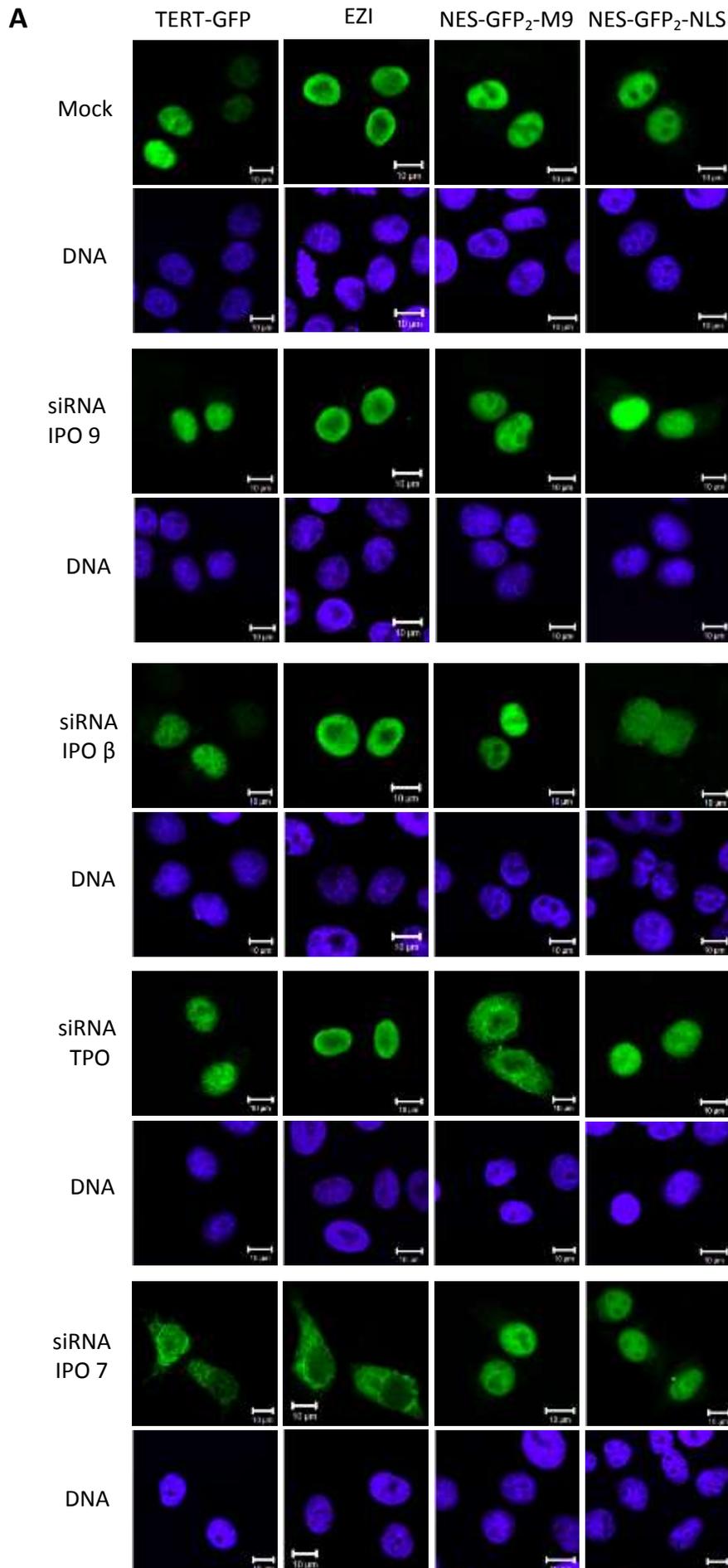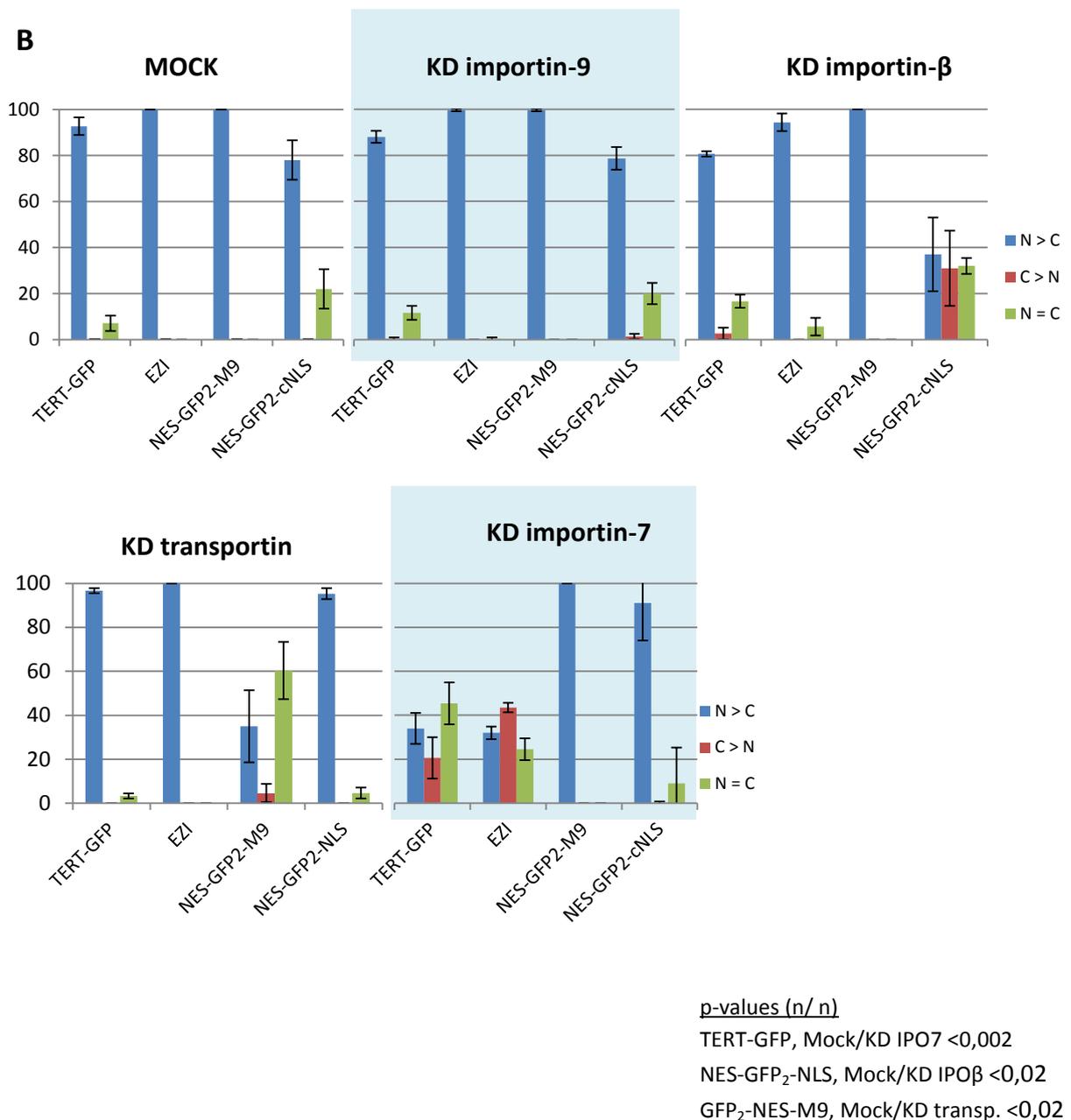
Figure 14: importin-7 is the import receptor for *human* TERT
(A) HeLa cells were transfected with siRNAs for different import receptors and incubated for 72 hours. Cells were transiently transfected with the following plasmids: TERT-GFP, myc-EZI, NES-GFP$_2$-M9 and NES-GFP$_2$-NLS. The artificial import substrate NES-GFP$_2$-NLS also served as a visual control for importin-β knock down. Knock down efficiency for transportin was controlled by quantification of NES-GFP$_2$-M9 localization. **(B)** Quantification of (A). For every condition at least three independent experiments were analyzed counting at least 100 cells each. Mean values from these experiments with its subdivisions are shown in the diagrams. Standard deviations are shown as error bars.

transfected with either TERT-GFP or control plasmids such as EZI or the artificial import substrates NES-GFP$_2$-cNLS and NES-GFP$_2$-M9. The zinc finger transcription factor EZI is imported by importin-7 and serves as a positive control for importin-7 (Saijou et al., 2007).

The artificial import substrate NES-GFP$_2$-NLS is recognized by importin-β and was used here as a control to visualize the effect of the importin-β knock down. In contrast, NES-GFP$_2$-M9 is imported by transportin. The substrate was used as a control for transportin knock down and also to quantify the efficiency of the knock-down. For importin-9 no control plasmid was available. The efficiency of importin-β /-7 /-9 knock-downs was controlled by Western blot (figure 15 B).

Under mock conditions, TERT-GFP, the artificial import substrates and EZI all localized to the nucleus (figure 14 A/B). Depletion of importin-9 did not affect the localization of any reporter protein. Also TERT-GFP was not affected in its nuclear localization, suggesting that importin-9 is not involved in its import (Figure 14 A/B).

Depletion of importin-β also did not lead to a significant mislocalization of TERT-GFP. EZI and NES-GFP$_2$-M9 were also not affected by importin-β depletion. The importin-β dependent substrate NES-GFP$_2$-NLS predominantly localized either to the cytoplasm or was distributed equally throughout the cell (figure 14 A/B).

The transportin knock-down resulted in a cytoplasmic or equal distribution of the reporter NES-GFP$_2$-M9, showing that the knock-down was efficient (figure 14 A/B). TERT-GFP was not affected by the knock-down, suggesting that also transportin is not the import receptor of TERT. Also the localization of EZI and NES-GFP$_2$-NLS did not change.

By contrast, the importin-7 knock down showed a clear effect on TERT-GFP localization. The protein was localized either in the cytoplasm or was distributed homogenously throughout the whole cell (figure 14 A/B). Also the positive control EZI localized to the cytoplasm in the importin-7 knock down. This result suggested that importin-7 serves as an import receptor for TERT. Importin-7 also seems to act independently from importin-β as import receptor of TERT-GFP. Another siRNA against importin-7 (siRNA importin-7-1), targeting the importin-7 mRNA at a more downstream site was tested to confirm the results (figure S2). This siRNA also led to the already described import defects on TERT-GFP. The C-terminus of TERT (aa 601-1132) also responded to the depletion of importin-7 and resulted in a decrease of nuclear localization.

As a second approach and to confirm the results of the siRNA experiments, an immunoprecipitation (IP) using the GFP-nanotrap was performed. HEK-293T cells were transiently transfected with TERT-GFP or with GFP as a control. GFP-tagged proteins were precipitated and samples were subjected to SDS-PAGE and Western blotting.

Input   IP

A

GFP 0,5%
TERT-GFP 1,5%
GFP
TERT-GFP
GFP
TERT-GFP
TERT 236 KR-AA-GFP
TERT 236/649 KR-AA-GFP

150 kDa

25 kDa

α GFP

*

*

120 kDa

α IPO7

80 kDa

α IPOβ

B

mock
KD IPO β
KD IPO 9
mock
KD IPO7

120 kDa
100 kDa

*
*

50 kDa

tubulin

*= IPO9
*= IPOß
*= IPO7
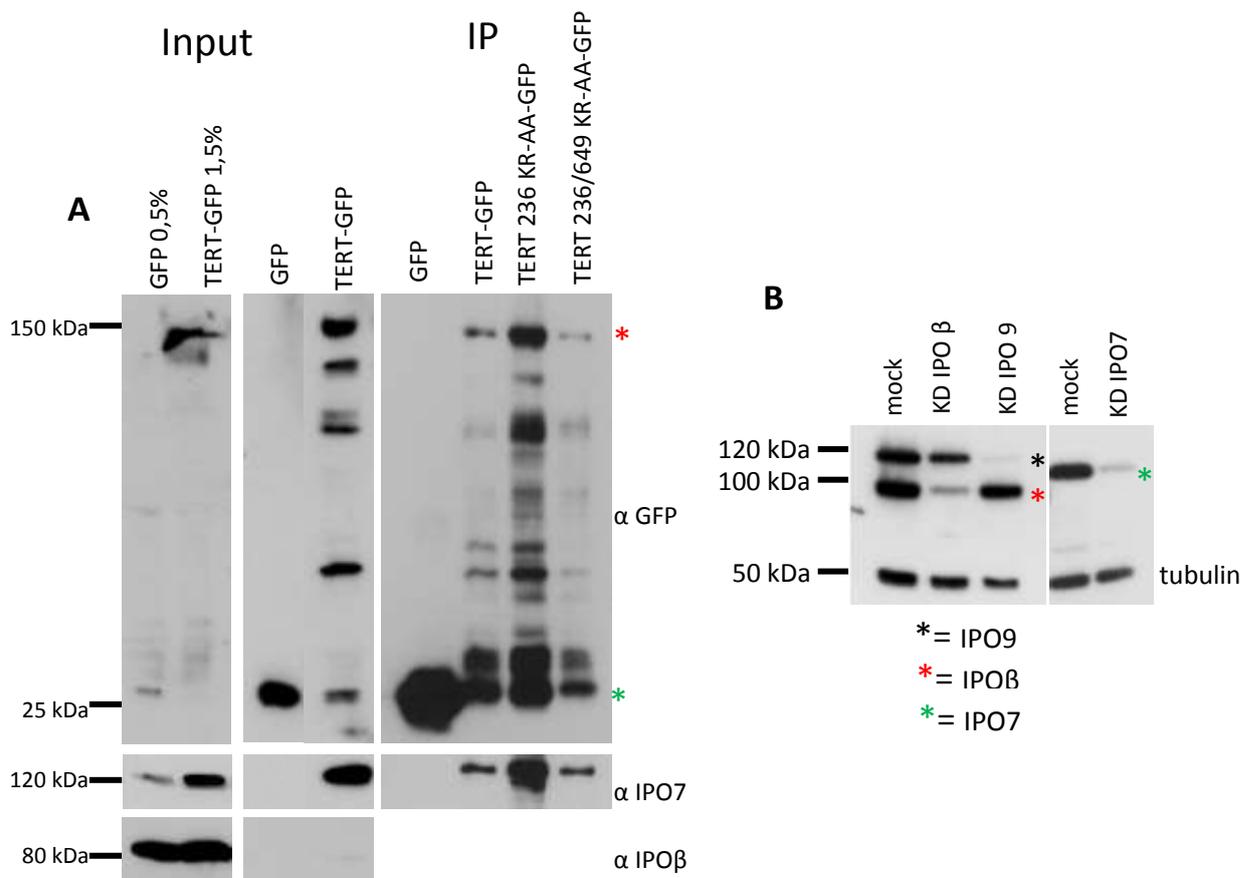
Figure 15: Immunoprecipitation of TERT-GFP and TERT mutants
(A) Immunoprecipitation (IP) from TERT-GFP and TERT-NLS mutants using the GFP-nanotrap. 293T cells were transiently transfected with TERT-GFP or TERT NLS mutants or GFP alone serving as a control. Cells were lysed and subjected to the IP. Inputs were taken from the lysate to confirm expression rate and full length protein expression. First, the TERT bait proteins (151kDa) and the control protein GFP (26kDa) were detected using a rabbit α-GFP antibody to confirm its size and expression. Both proteins were detectable in the input as well as in the IP on the membrane. Red asterisks mark the band resulting from TERT proteins while the green asterisks show GFP. **(B)** Western blot control of knock down efficiency for importin-9, importin-β and importin-7 using the respective antibodies. Tubulin was detected as a loading control.

If TERT interacts with an import receptor, the respective receptor should also be detectable on the membrane. Therefore, the blot was probed with antibodies against different import receptors. As shown on the blot TERT-GFP was efficiently precipitated in the IP (figure 15 A). In the IP importin-β did not coprecipitate, indicating that importin-β is either not an import receptor of TERT or not able to bind under the IP conditions. However, binding of importin-7 (119 kDa) to TERT-GFP was detectable (figure 15 A).

In the control lane of precipitated GFP, no importin-7 was detectable, suggesting that importin-7 binding to TERT is specific and that this importin, could be the specific receptor for

TERT. Other transport factors tested e.g. importin-9 or CRM1 either did not significantly bind in the IP or bound unspecifically to the GFP control (data not shown).

The NLS mutants of TERT were also tested for importin-7 binding (figure 15 A) to investigate whether importin-7 uses these NLS sites for import of TERT. The IP showed that importin-7 also bound to the mutants (figure 15 A), suggesting that importin-7 either might not bind the identified NLS motifs or is sticky on TERT under the given IP conditions. Another explanation for the coprecipitation of importin-7 with the mutants could be residual binding of importin-7 to the mutants at the residing intact residues of the NLSs. However, depletion of different major import receptors revealed importin-7, as the only promising candidate for TERT nuclear import.

4.2.7 Localization of TERT-GFP can be rescued by importin-7 overexpression after depletion of endogenous importin-7

To confirm the specificity of the TERT-GFP import defects after importin-7 knock down, rescue experiments with siRNA resistant importin-7 were carried out. For that purpose, *Xenopus laevis* importin-7, which is 96% homologous to human importin-7 was used. *Xenopus* importin-7 already carried a base substitution compared to *human* importin-7 at the siRNA target site. Two further silent base substitutions were introduced by site directed mutagenesis to achieve siRNA resistance. HeLa cells were treated with importin-7 siRNA for 72 hours and were then transfected with plasmids as mentioned below. Control cells (mock) were transfected with a scrambled non-targeting siRNA. Knock down efficiency of importin-7 was confirmed by Western blotting (figure 16C). EZI was again used as a positive control for importin-7 knock-down and for the rescue experiment to demonstrate the functionality of overexpressed importin-7-HA.

In mock cells, and in presence of overexpressed importin-7-HA, EZI and TERT-GFP localized to the nucleus exclusively as seen in previous experiments. Upon importin-7 knock down, TERT-GFP and EZI showed a clear import defect resulting in a predominantly cytoplasmic localization or an equal distribution of EZI or TERT-GFP, respectively (figure 16A/B). Only 35.5% of the cells transfected with EZI showed a nuclear localization of EZI and 32% of the analyzed cells showed a nuclear accumulation of TERT-GFP.
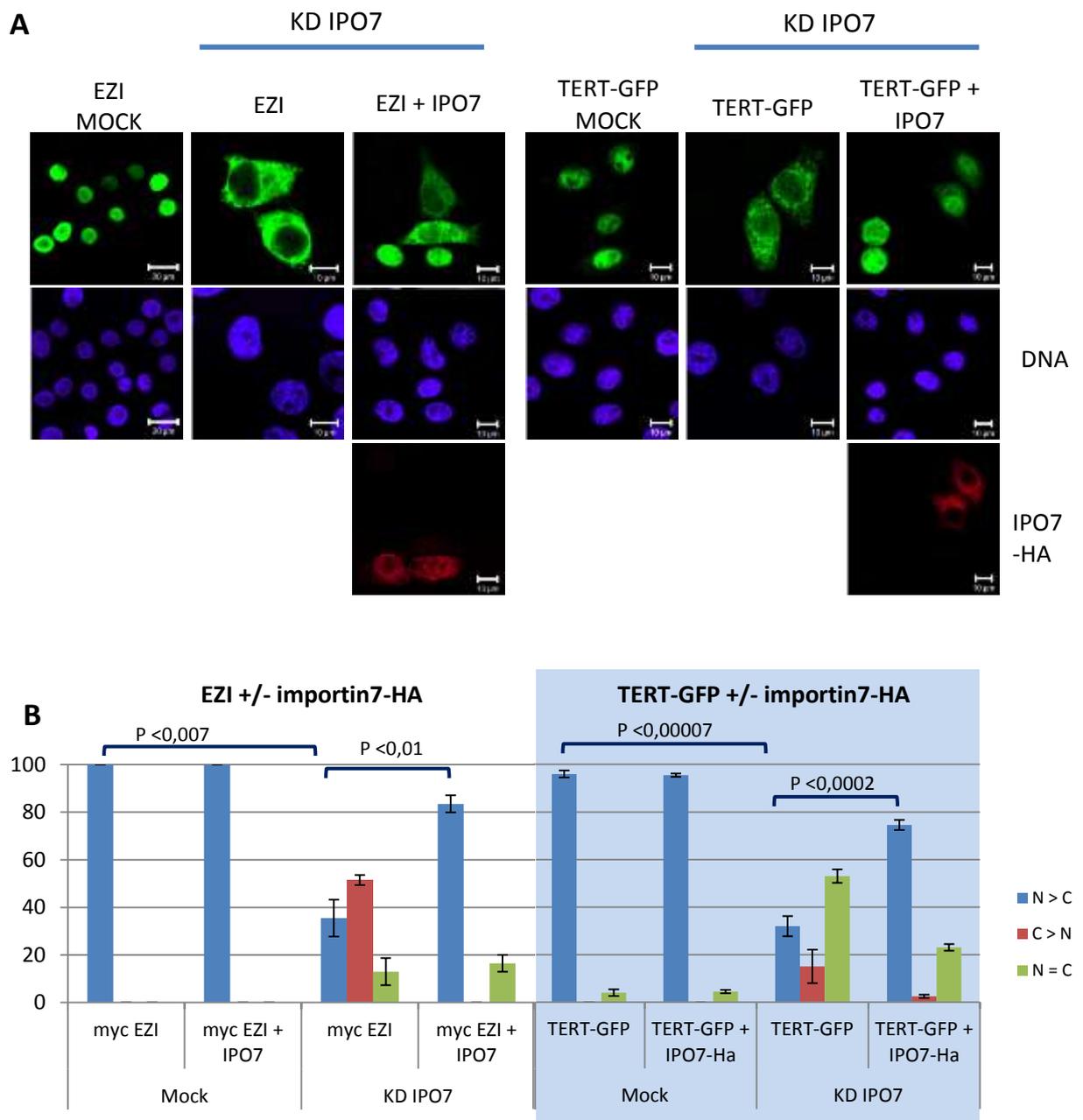
Figure 16: TERT-GFP import defects by importin-7 knock down can be rescued by importin-7 overexpression
(A) HeLa cells were incubated with importin-7 siRNA for 72 hours and were then transiently transfected with TERT-GFP or myc-EZI plasmid DNA. For rescuing the importin-7 import defect, cells were cotransfeced with a siRNA resistant importin-7-HA plasmid. Cells were then subjected to immunofluorescence. Myc-EZI was detected using a mouse α myc antibody while Ha-Importin7 was detected by using a mouse α Ha antibody. **(B)** Quantification of transfected cells. TERT-GFP mock was quantified by counting 100 cells from 14 independent experiments. TERT-GFP importin-7 knock down was analyzed using counts from 11 independent experiments with 100 cells each. The remaining conditions were quantified by counting 100 cells from three independent experiments each. Error bars show the standard deviation from the mean of the experiments. For confirmation of knock-down efficiency of importin-7 see figure 17.

The import defect of both overexpressed proteins could be rescued by overexpression of siRNA resistant importin-7-HA significantly (figure 16A/B). After cotransfection with the importin-7 siRNA resistant importin-7-HA plasmid an average of 47.5% of the analyzed cells showed a rescue effect resulting in 83% of cells in which a nuclear accumulation of EZI was observed. For TERT-GFP nuclear accumulation of the protein could be detected in 74% of cells after cotransfection with importin-7-HA, resulting in a rescue effect of 42% after overexpression of siRNA resistant importin-7-HA (figure 16B). This experiment validated the previous experiments showing that Importin7 plays a key role in TERT-GFP import, because the knock down effect can be reversed by overexpression of importin-7.

The import defect of endogenous TERT after depletion of importin-7 could not be tested in this work because all purchased antibodies failed in detection of endogenous TERT.

4.2.8 In vivo analysis of import inhibition after importin-7 knock down

To demonstrate that import intensity of TERT-GFP was negatively influenced by depletion of importin-7 compared to mock cells, live cell FLIP was performed to measure transport kinetics. For this FLIP experiment, the same settings were used as described before in 3.5.2. HeLa cells were either treated with importin-7 siRNA or a scrambled non-targeting siRNA as a control. Following siRNA treatment, cells were transfected with a plasmid coding for TERT-GFP. Knock down efficiency was confirmed by Western blotting (figure 17B). TERT-GFP transfected live cells were bleached in the nucleus and the import rate was determined by the loss of fluorescence in the cytoplasm. As shown in figure 17A, import of TERT-GFP can be inhibited by depletion of importin-7. Under mock conditions, it took 94.7 seconds until a loss of fluorescence of 50% could be observed. When importin-7 was depleted a loss of fluorescence of only 34.7% could be observed after 146 seconds at the end of the measurement. These measurements showed that under mock conditions, TERT-GFP is imported quickly and its import is significantly reduced when importin-7 is depleted, suggesting that importin-7 is the import receptor of TERT.

A

B
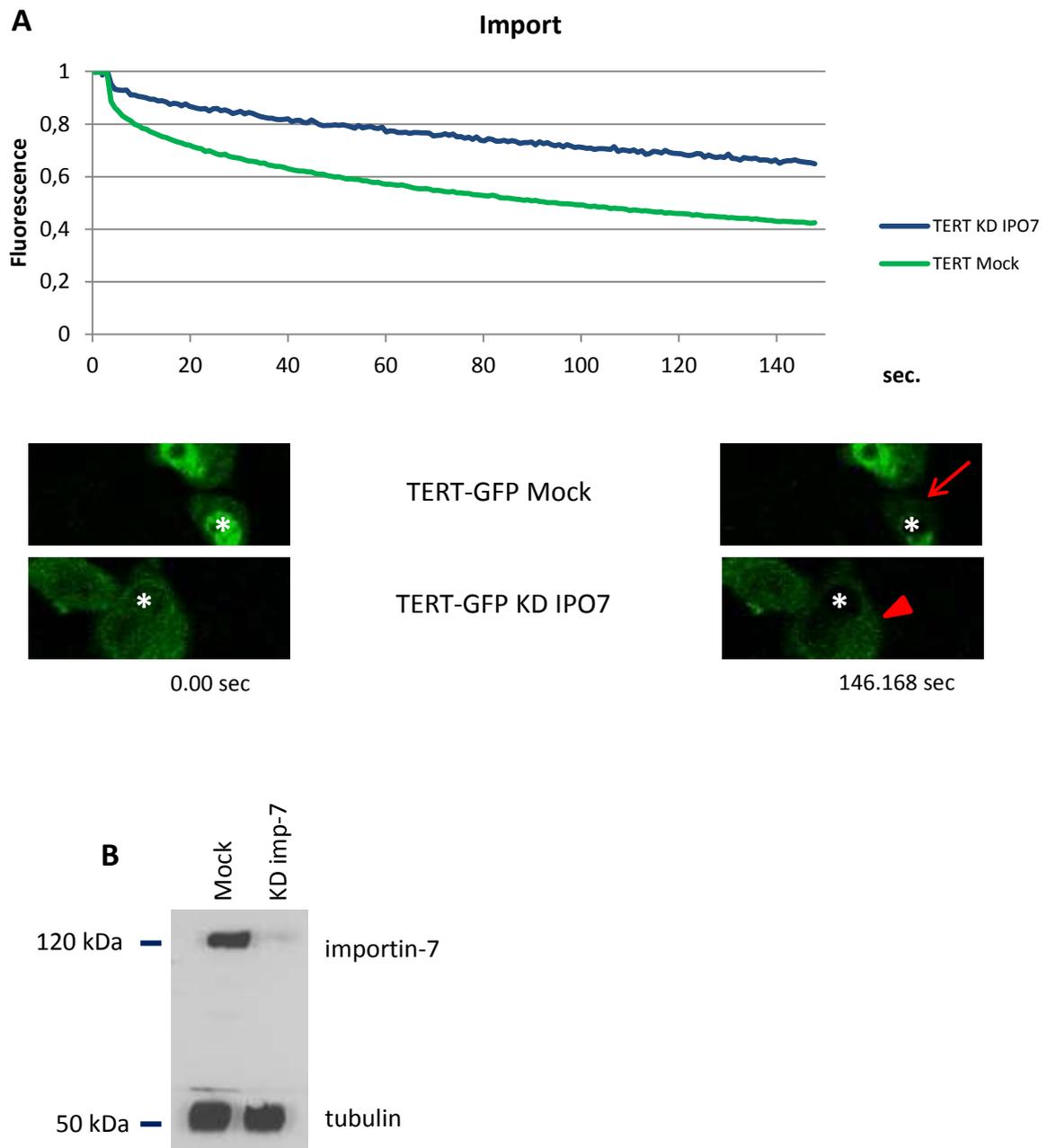
Figure 17: Import inhibition on TERT-GFP after depletion of importin-7 can be demonstrated in living cells
(A) HeLa cells were treated with a siRNA against importin-7 or a scrambled non-targeting siRNA (mock) and incubated for 72 hours. Cells were then transiently transfected with TERT-GFP plasmid DNA. The assay was performed in three independent experiments and 10-15 cells were analyzed per condition. Error bars in the diagram were left out for better clarity (the standard deviation is shown in figure S12). Instead, the mean values of measured cells are shown. Asterisks in the images indicates the bleached region in the nucleus. The red arrow marks the darkened cytoplasm of the bleached control cell after 146 seconds compared to the beginning of the measurement. The arrowhead points at the relatively bright cytoplasm of an Importin7 knock down cell after 146 seconds compared to the start of the analysis. In order to gain comparable data, cells with equal levels of fluorescence in their cytoplasm in mock as well in KD cells were chosen (figure S8). **(B)** Knock down efficiency of importin-7 was determined by Western blotting. Tubulin was used as a loading control.

4.2.9 Importin-7 can bind to Nup358 in a RanGTP dependant manner

Since previous experiments showed a dependency of TERT-GFP import on Nup358 and importin-7, it was interesting to investigate the relationship between importin-7 and the nucleoporin. Nup358 exhibits a number of FG-repeats within its structure which might interact with transport receptors such as importin-β (Delphin et al., 1997). Like Nup358, the import receptor importin-7 contains Ran binding sites (Görlich et al., 1997) which both proteins could use for interaction. To investigate the mechanism of putative interactions between Nup358 and importin-7, immunoprecipitations and in vitro binding assays were performed.

First the *in vivo* context was investigated. Native full length Nup358, was immunoprecipitated from a HeLa cell lysate using a goat α Nup358 antibody. The first sample was wasged with IP-washing buffer, only (sample 1), showing the native binding partners of the nucleoporin under IP conditions. As shown in figure 18A, importin-β clearly bound to Nup358 under native conditions, supporting the idea that it used the nucleoporin FG repeats for binding (Delphin et al., 1997). In contrast, importin-7 was not detectable under these conditions. The binding of importin-β to Nup358 could lead to a competitive situation on the nucleoporin for other importins that have weaker affinities towards Nup358. Therefore, the amount of bound importin-β to the nucleoporin was reduced by the addition of 500mM NaCl to the IP-washing buffer (samples 2 and 3). Afterwards, recombinant importin-7 was added to the beads in the presence or absence of GTP loaded RanQ69L. This Ran mutant cannot hydrolyze its bound GTP (Nachury et al., 1999).

However, reduction of bound importin-β alone to Nup358 did not lead to a binding of importin-7 to the nucleoporin as shown in sample 2. This finding suggested that if importin-7 binding to Nup358 occurs, it requires additional factors. Finally, the addition of RanQ69L lead to a binding of importin-7 to Nup358, suggesting that importin-7 does not interact with Nup358 through FG binding but uses the cofactor Ran for interaction with the nucleoporin.

To further investigate this interaction, a recombinant in vitro binding assay was performed. Recombinantly expressed GST-tagged Nup fragments (figure 18C) were coupled to GST-beads and incubated with recombinant His-tagged importin-7 with or without addition of GTP loaded RanQ69L.

A

Protein-G control	+				
Nup358		+	+	+	
Importin-7			+	+	
RanQ69L				+	
Input, 1%					+

200 kDa — Nup358

120 kDa — importin-7

80 kDa — importin-β

1 2 3

NaCl washed

B

Input 500ng

C
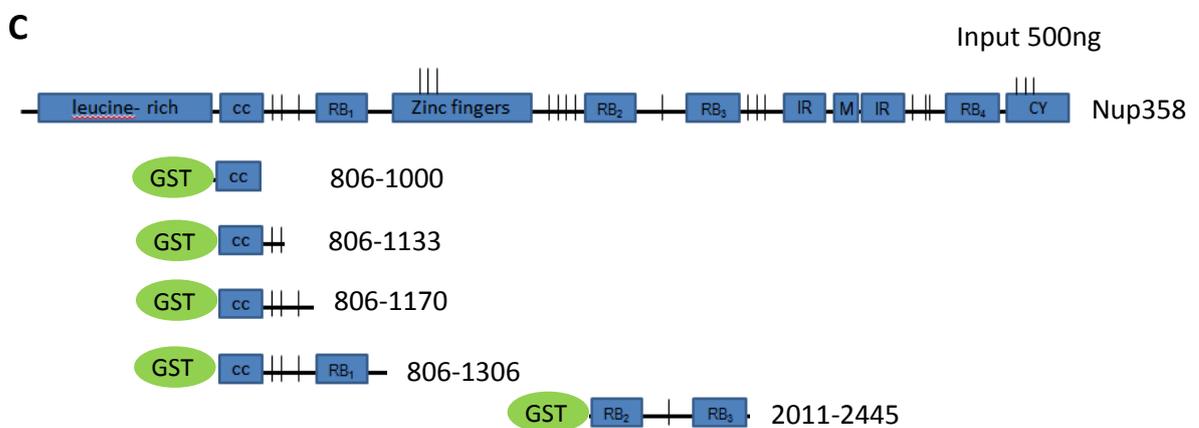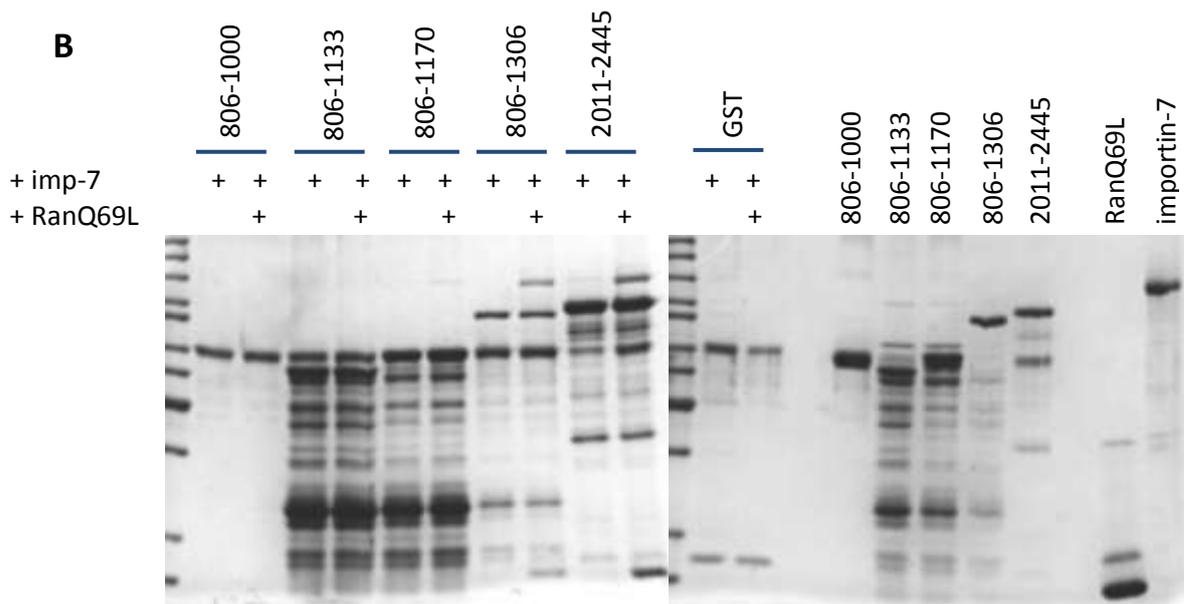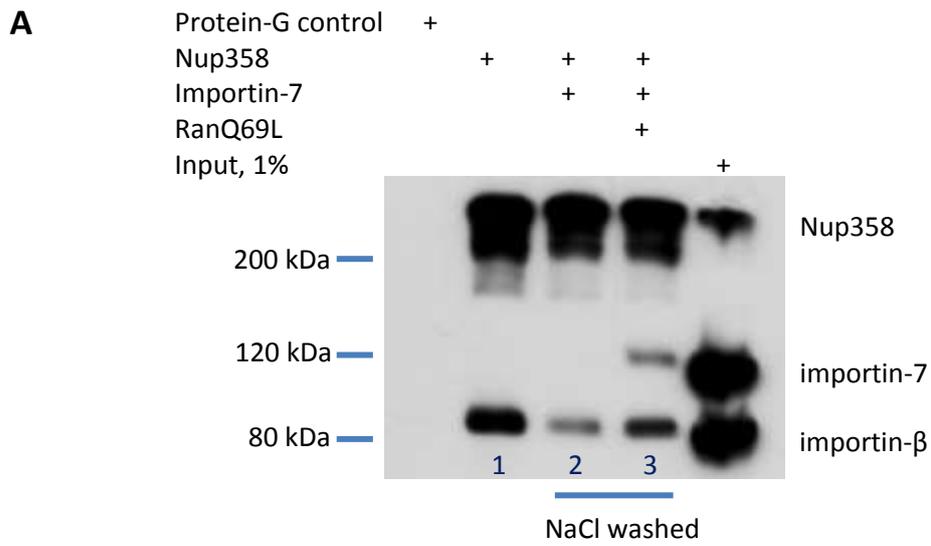
Figure 18: importin-7 binds to recombinant Nup358 fragments and to endogenous Nup358 in a RanGTP dependant manner.
(A) Untransfected HeLa cells were used for an immunoprecipitation (IP) of Nup358 using a specific goat α Nup358 antibody. The total IP volume was split into three samples each of the same volume represented by lanes 1-3. Lane 1 contained the native IP with Nup358 showing its binding partner importin-β. Endogenous importin-7 did not bind to Nup358 under these IP conditions. Samples 2 and 3 were washed with dilution buffer containing 500mM NaCl reducing the amount of bound importin-β on Nup358. Samples 2 and 3 were then incubated with 2µg of recombinant His-importin-7 while sample 3 was additionally incubated with 1µg of GTP loaded RanQ69L. To ensure specific binding to Nup358 a protein-G control was carried out using a HeLa cell lysate. **(B)** Coomassie gel of an in vitro binding assay of recombinant Nup358 fragments and importin-7 showing dependence on RanGTP. 5µg of each GST-Nup358 fragment was coupled to GST-beads and incubated with 5µg His-importin-7 +/-2µg RanQ69L loaded with GTP. GST was used as a control for specific importin-7 binding. **(C)** Schematic description of Nup358 and its recombinant GST-tagged truncation mutants used in (A).

As shown in figure 18B, importin-7 binding to Nup fragments only occurred in those fragments containing a Ran-binding site and in the presence of RanQ69L. In contrast, fragments containing only FG repeats as a putative binding site for importin-7 were not able to bind importin-7 (figure 18B). This could indicate that importin-7 might not use FG repeats to bind to the nucleoporin. Instead, as also demonstrated in the immunoprecipitation, the interaction seemed to be Ran dependent, suggesting that both proteins interact with each other via Ran.

It could be conceivable, that Importin-7 binding to Nup358 is not generally required for the import of the receptor and its cargo. Our findings rather support previous findings that import receptors such as transportin and importin-β complex with RanGTP to release their cargoes and to be exported from the nucleus into the cytoplasm by interaction with the NPC (Jäkel et al., 1998; Izaurralde et al., 1997; Görlich et al., 1997).

However, the release mechanism of importin-7 from TERT-GFP must differ from this known pathway. Experiments with RanQ69L addition after TERT-GFP immunoprecipitation did not show a dissociation of importin-7 from TERT-GFP (figure S9) suggesting an alternative mechanism of cargo release.

4.2.10 TERT-GFP import inhibition can be enhanced by co-depletion of importin-7 and Nup358

Our result described so far showed that, depletion of Nup358 as well as depletion of the importin-7 negatively affect nuclear localization of TERT-GFP. To further analyze whether import inhibition on TERT-GFP can be enhanced by simultaneous depletion of importin-7 and

B

MOCK — KD imp-7

KD Nup358 — KD Nup358/ imp-7

Legend: N > C, C > N, N = C

C
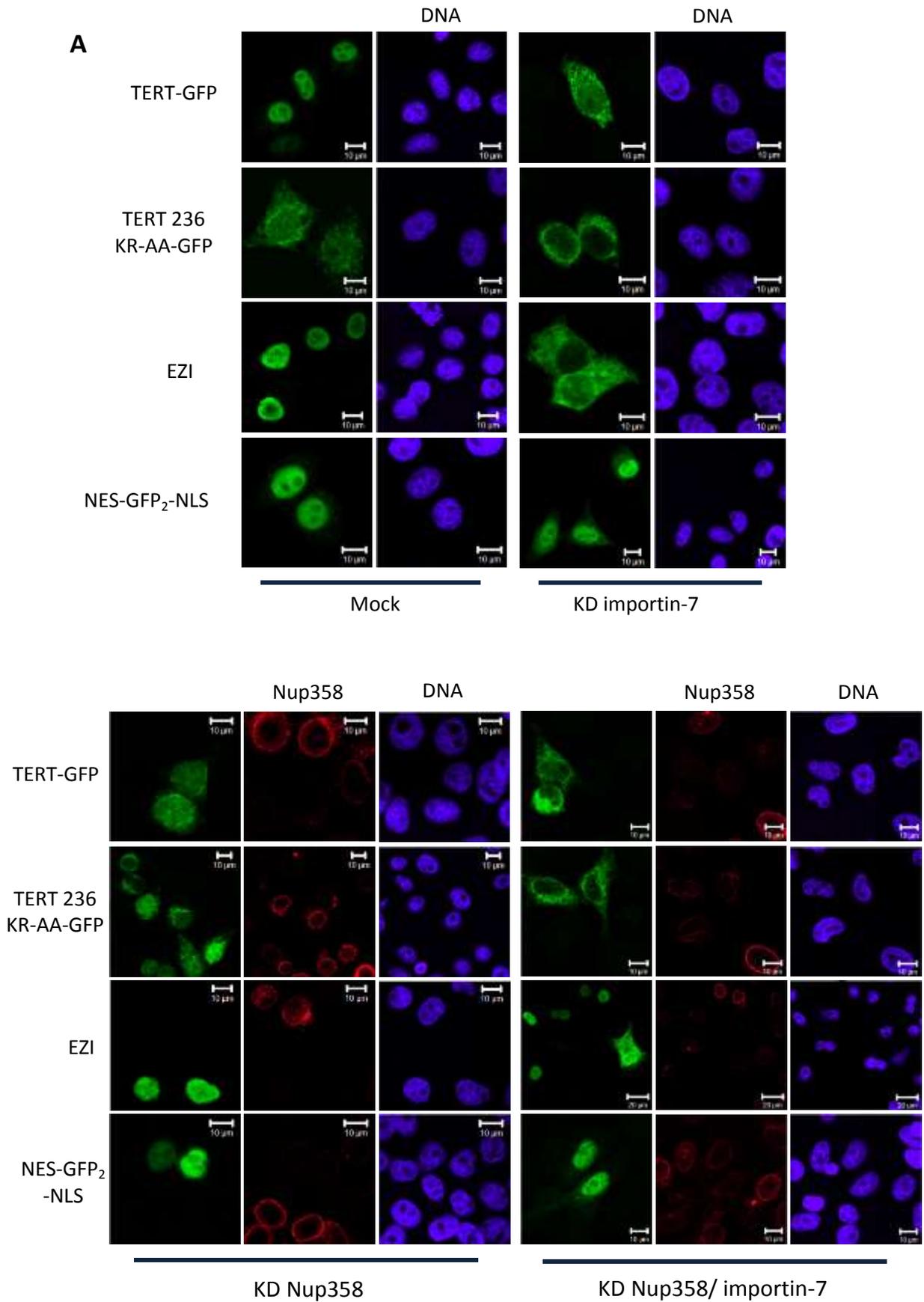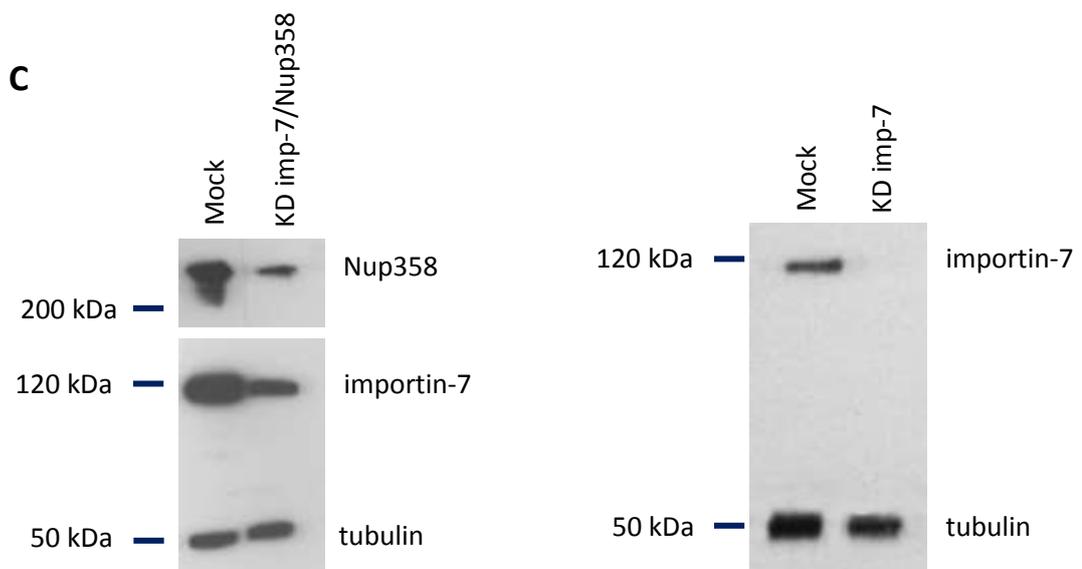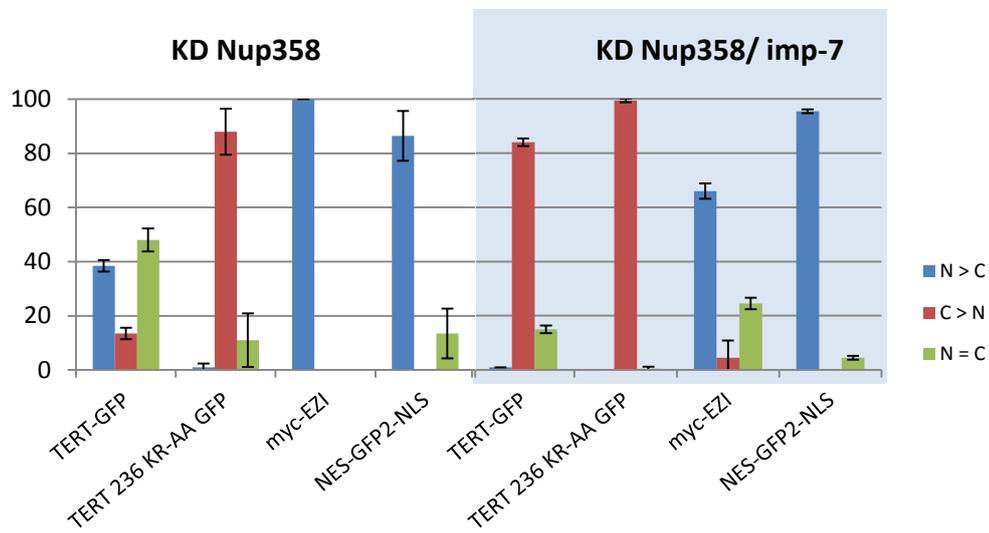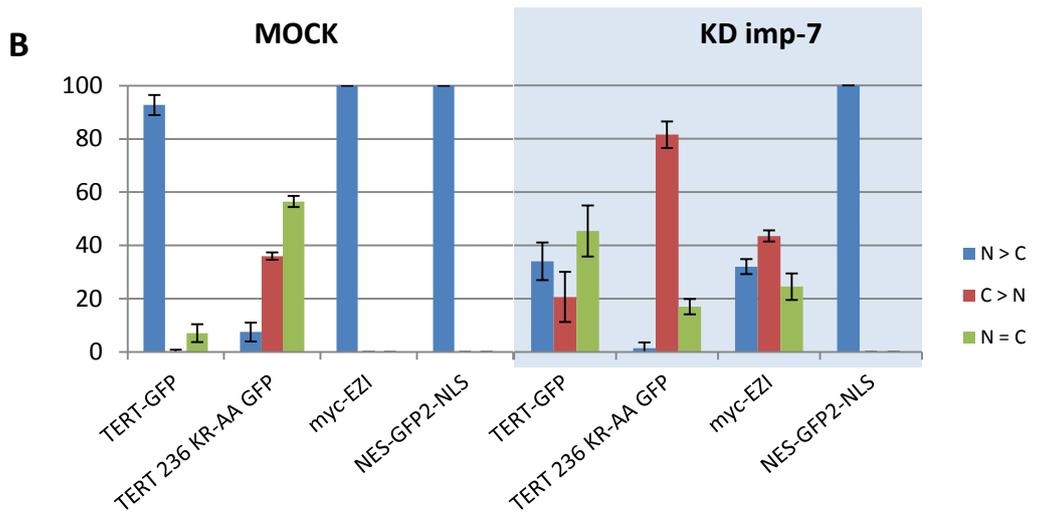
Figure 19: TERT-GFP import inhibition can be enhanced by co-depletion of importin-7 and Nup358
(A) HeLa cells were incubated with either siRNA against importin-7 or a scrambled non-targeting siRNA as a control for 72 hours. Cells were then transiently transfected with following plasmid DNA: TERT-GFP, TERT 236 KR-AA-GFP, myc-EZI or the artificial shuttle substrate NES-GFP$_2$-NLS. Cells were subjected to immunofluorescence and EZI was detected by using a mouse α myc antibody. HeLa cells were used to perform a knock-down against Nup358. KD efficiency was controlled by immunofluorescence, analyzing only cells with a significantly reduced level of Nup358. Double knock down of Nup358 and importin-7 was performed similarly, starting with incubation of siRNA against Nup358 for 48 hours followed by a retransfection of siRNA against Nup358 containing also the siRNA against importin-7. Cells were then incubated for 72 hours to ensure the reduction of importin-7 protein level. Knock down cells were then transiently transfected with plasmid DNA mentioned above. **(B)** Quantifiation of cells mentioned in (B). Quantification was carried out by counting at least 100 cells for each condition from three independent experiments. For quantification of TERT-GFP (mock) counts from 14 experiments were used and after KD of importin-7 counts from 11 experiments were used. Values of the colored bars represent mean values while the error bars represent the standard deviations. **(C)** Western blot control after importin-7 siRNA treatment and double knock down of importin-7 and Nup358. Tubulin served as a loading control.

Nup358, a double knock down of both proteins was performed. Effects of the double knock down were then compared to single knock downs done and to control cells (mock). In mock cells, NES-GFP$_2$-NLS, EZI and TERT-GFP predominantly localized to the nucleus. The import defective mutant TERT 236 KR-AA-GFP showed a predominantly equal distribution between cytoplasm and nucleus (figure 19 A/B). The NLS mutant was used here to investigate if also import defective TERT is still dependent on NUP358.

Knock down of importin-7 resulted in a massive decrease of nuclear accumulation of EZI and TERT-GFP as described above (figure 19 A/B). The import defective mutant of TERT-GFP, TERT 236 KR-AA-GFP resulted in a much greater cytoplasmic localization, when importin-7 was depleted as compared to mock conditions (figure 19 A/B). The artificial shuttle NES-GFP$_2$-NLS remained unaltered in its localization within the importin-7 knock down showing that importin α/-β mediated import remained unaffected by importin-7 depletion (figure 19A). Single knock down of Nup358 resulted in less nuclear accumulation of TERT-GFP as described before (see figure 13). The import defective mutant also resulted in increased cytoplasmic localization. Interestingly, the localization of EZI was not affected by Nup358 depletion (figure 19 A/B), suggesting that defects in protein nuclear accumulation following Nup358 depletion is specific for TERT or other Nup358-dependent proteins and does not affect all proteins imported by importin-7 in general.

Previous work showed a dependency of importin-α/-β mediated transport on Nup358 (Hutten et al., 2008). In cells depleted of Nup358 an impaired import of the artificial importin-α/-β dependent import substrate NES-GFP$_2$-cNLS was detected (Wälde 2010; Hutten et al., 2008).

In contrast to these previous findings a strong dependency of the artificial import substrate NES-GFP$_2$-cNLS on Nup358 could not be detected in this work. Only a slight reduction of nuclear accumulation of NES-GFP$_2$-cNLS after depletion of Nup358 of about 15-20% could be observed. This might be due to a different charge of HeLap4 cells used in this work compared to previous work or resulted from different KD efficiencies of Nup358.

Double knock down of the import receptor importin-7 and Nup358 resulted in an enhanced cytoplasmic localization of TERT-GFP, showing that the import defect was enhanced when both factors involved in TERT-GFP import are depleted. Corresponding to the importin-7 knock down, EZI showed a reduction of only 34% in nuclear accumulation (figure 19 B). This could be explained by a weaker effect of the importin-7 siRNA during simultaneous performance of a knock-down against two proteins.

Taken together, these results show that import of TERT-GFP depends on the presence of both, importin-7 and Nup358. These results also show that depletion of Nup358 seemed not to influence importin-7 mediated import in general and that the nucleoporin is not rate limiting for importin-7-mediated import.

5) Discussion

The prostaglandin 15d-PGJ$_2$ inhibits CRM1 mediated protein export

Leptomycin B is a highly specific, inhibitor for CRM1 mediated protein export, produced by the fungus *Streptomyces*. It binds to a sensitive cysteine residue (at aa position 528 in the human sequence) (Kudo et al., 1999). LMB contains a reactive ring with a free electron pair connected to a fatty acid tail (figure 4A). In light of the strong inhibition of nuclear export that can be obtained with LMB as an exogenous substance, it was interesting to investigate putative endogenous factors which could potentially be produced by the eukaryotic cell itself. The prostaglandin 15d-PGJ$_2$ was a promising candidate since it has a similar structure to LMB. In this work, we investigated the ability of 15d-PGJ$_2$ to impair CRM1 mediated protein export and we were able to identify CRM1 as one of several targets of 15d-PGJ$_2$.

Accumulation of the prostaglandin 15d-PGJ$_2$ in the nucleus

Prostaglandins normally bind to specific transmembrane receptors at the plasma membrane, but it is known for 15d-PGJ$_2$ that it can cross the cell membrane to act intracellular (reviewed in Scher et al., 2009). Although import pathways of 15d-PGJ$_2$ through plasma membranes still remain unclear (reviewed in Scher et al., 2009) we were able to show that biotinylated 15d-PGJ$_2$ can enter the cell. This means that the prostaglandin has to cross the plasma membrane. It might be conceivable that 15d-PGJ$_2$ diffuses through the plasma membrane. As a membrane derivative, 15d-PGJ$_2$ contains a fatty acid tail which could be used to be integrated into the membrane and to cross it by diffusion until the prostaglandin reaches the cytoplasm. The biotinylated 15d-PGJ$_2$ used in this work translocates to the nucleus and accumulates there. The prostaglandin therefore either diffuses passively through the nuclear pore or targets proteins that accumulate in the nucleus, for example transport factors or their substrates. Our data also show that biotinylated 15d-PGJ$_2$ accumulates in the nucleus after only a short incubation time, suggesting that after translocation to the nucleus the prostaglandin is retained there, which leads to the hypothesis that 15d-PGJ$_2$ specifically targets nuclear proteins (figure 1). A binding approach using biotinylated 15d-PGJ$_2$ with cell lysate identified several nuclear proteins and CRM1 as targets of 15d-PGJ$_2$ (data not shown).

It is also known that the prostaglandin also targets and modifies the nuclear protein and transcription factor PPARγ. After modification, the 15d-PGJ$_2$/PPARγ complex translocates into the nucleus (reviewed in Scher et al., 2004). 15d-PGJ$_2$ has also other targets like the IκB kinase (Straus et al., 2000; Rossi et al., 2000) or the HIV transactivating protein Tat, (Kalantari et al., 2009) and it also targets cysteine 184 in the GTP-binding protein H-Ras (Oliva et al., 2003). It is therefore likely that many other proteins including nuclear proteins are also 15d-PGJ$_2$ targets, which could explain the strong nuclear accumulation of the prostaglandin.

It remained unclear whether CRM1 is also retained in the nucleus during the time of export blockade, or whether the blocked CRM1 is also able to leave the nucleus without a cargo.

A reduced ability for export after 15d-PGJ$_2$ modification of the main export factor CRM1 might contribute to retention of other putative 15d-PGJ$_2$ targets in the nucleus. Proteins to be exported to the cytoplasm are kept in the nucleus and might bind to other proteins and form complexes that might not occur without an inhibition of their export factor CRM1, thus enhancing nuclear accumulation of the prostaglandin by providing potentially new targets.

Previous studies detected several CRM1 specific inhibitors, but all of the discovered CRM1 inhibitors such as LMB are exogenous substances (Sun et al., 2013). In contrast, 15d-PGJ$_2$ is an endogenous product of higher eukaryotic cells and has the ability to regulate CRM1 mediated protein export as an endogenous inhibitor (Hilliard et al., 2010).

Several CRM1 substrates show different sensitivities towards CRM1 export inhibition by 15d-PGJ$_2$

We were able to identify CRM1 as a target of 15d-PGJ$_2$ in vitro by mass spectrometry. We were also able to show that 15d-PGJ$_2$ is capable to inhibit CRM1 mediated protein export. Export of CRM1 specific substrates to the cytoplasm e.g. the reporter proteins NES-GFP$_2$-cNLS/ -M9 or NC2β can be inhibited after incubation with 15d-PGJ$_2$, as demonstrated in quantification analysis and in living cells, as indicated by the FLIP experiments. Rescue experiments, using the LMB resistant CRM1 mutant C528S showed that 15d-PGJ$_2$ can indeed modify wild type CRM1 at this sensitive cysteine and therefore blocks its export function. CRM1 C528S was able to export its substrates after incubation of 15d-PGJ$_2$, suggesting that the mutant is resistant towards 15d-PGJ$_2$ modification (figure 8).

Our data showed that not all CRM1 substrates were inhibited equally. The CRM1 substrate TFIIAα for example could be retained in the nucleus only after application of high levels of 15d-PGJ$_2$. In contrast, the export of the CRM1 substrate NC2β could be inhibited at nanomolar concentrations of the prostaglandin (figure 6). This could be due to different affinities of the substrates for CRM1. For NC2β it was suggested that it exhibits a low affinity towards CRM1 (Kahle et al., 2009). The level of export inhibition could also depend on the position where the substrate binds within the NES binding groove of CRM1. For the CRM1 export substrate snurportin1 it could be shown that it uses more than one binding site in the CRM1 molecule (Monecke et al., 2009). It is therefore likely that different substrates use different binding sites within the CRM1 molecule. Although CRM1 export substrates bind at the NES binding groove in the hydrophobic cleft, they can possess different affinities in CRM1 binding which can influence the inhibitory effect of 15d-PGJ$_2$ on CRM1 mediated protein export. This could help to explain different behaviors of CRM1 substrates towards CRM1 inhibition by 15d-PGJ$_2$. Another explanation for reduced inhibitory effect of 15d-PGJ$_2$ could be the difference in structure of LMB and 15d-PGJ$_2$. LMB contains a longer carbon-rich tail than 15d-PGJ$_2$. This could help to inhibit CRM1 mediated protein export more efficiently than this could be achieved by 15d-PGJ$_2$, which exhibits a much shorter tail. LMB occupies 70% of the NES binding groove and therefore blocks the interaction of NES with CRM1 very strongly (Sun et al., 2013). The structure of bound 15d-PGJ$_2$ to CRM1 has not been solved yet. The fungal CRM1 inhibitor also helps to open and deepen the CRM1 NES binding groove by interaction. Interestingly, CRM1 was also found to enhance lactone hydrolysis of LMB by conformational changes of other residues and therefore drives modification by itself (Sun et al., 2013). This mechanism can contribute to the high potency of LMB as a CRM1 inhibitor and to the low concentrations needed of LMB to inhibit CRM1 mediated protein export effectively. For 15d-PGJ$_2$ none of these supporting mechanisms could be shown yet.

It also remains unclear how efficiently extracellular added 15d-PGJ$_2$ enters the cell or even the nucleus, since its import pathways into the cells and also the amount of imported 15d-PGJ$_2$ after extracellular addition remains unclear (Hilliard et al., 2010). Unbound endogenously produced 15d-PGJ$_2$ could be detected in a concentration of 16 nanomolar in a cell lysate (Rajakaria et al., 2007), but 15d-PGJ$_2$ which was already bound to targets could not be included in the measurement (Hilliard et al., 2010). Phospholipase A2, the arachidonic releasing enzyme as well as PGHS, which processes arachidonic acids to PGH$_2$, a precursor

prostaglandin of 15d-PGJ$_2$ were detected at both nuclear membranes (Spencer et al., 1998; Perisic et al., 1999). It is therefore likely, that bioactive concentrations of 15d-PGJ$_2$ can be much higher at the cytoplasmic periphery of the nucleus to modify CRM1 and inhibit its nuclear protein export.

Also, in contrast to LMB which is a highly specific target of CRM1, 15d-PGJ$_2$ has more than one target in the cell. It is known that besides CRM1 the prostaglandin can target several other proteins such as BSA, IκB kinase and PPARγ (Straus et al., 2000; Rossi et al., 2000). This can also explain why higher initial concentrations of 15d-PGJ$_2$ are needed to visualize its inhibitory effect on CRM1 mediated protein export.

This study showed that at least one additional prostaglandin in addition to 15d-PGJ$_2$ has the ability to inhibit CRM1 mediated protein export besides 15d-PGJ$_2$. PGA for example contains a cyclopentenone ring with a free reactive group and was also shown to have a certain potential to inhibit CRM1 mediated protein export (figure 4 A/B). Apart from 15d-PGJ$_2$ and PGA other prostaglandins also exist which contain a cyclopentenone ring containing a free electron pair. During an inflammation, cells of inflammatory response produce a subset of prostaglandins and a certain number of those have a reactive cyclopentenone ring. In this situation, CRM1 could be targeted by other prostaglandins similar to 15d-PGJ$_2$. This could then lead to a stronger inhibition of CRM1 mediated protein export by endogenously produced prostaglandins than shown in this work where only single prostaglandins were incubated with the cells.

15d-PGJ$_2$ can be processed from precursor prostaglandins within the cell, while other prostaglandins first need extracellular receptors to influence the cell. It can therefore act as an intracellular and as an extracellular prostaglandin (Scher et al., 2004).

Taken together, these results show that the inhibitory effect on CRM1 mediated export could endogenously be enhanced by the cooperative action of several cyclopentenone prostaglandins. We found that 15d-PGJ$_2$ has the ability to inhibit CRM1 mediated nuclear protein export, although a higher concentration, extracellularly added, is required to see the same effects as with LMB. Genes that are CRM1 dependently expressed may also be influenced by the inhibition of CRM1 mediated export. Regarding this aspect, also little changes in CRM1 activity mediated by endogenous as also exogenous 15d-PGJ$_2$ might have severe effects on cellular functions (Hilliard et al., 2010).

15d-PGJ$_2$ has anti-inflammatory effects

Modification of CRM1 by 15d-PGJ$_2$ and the resulting inhibition of CRM1 mediated protein export might contribute to its anti-inflammatory effects. During the cell cycle many different proteins are imported into the nucleus. Many of them are also exported again by CRM1. Transcription factors, for example are exported when their function is not required any more. In the case of an export blockade all these proteins are retained in the nucleus and might contribute to damaging effects on the cell. Long-term CRM1 export blockade with LMB at a CRM1 saturating concentration prevents cells from dividing and induces apoptosis (Mutka et al, 2009).

15d-PGJ$_2$ with its inhibitory effect on CRM1, can in the same way contribute to cell cycle arrest and later on enhance cell death or apoptosis (Shin et al., 2009). The inhibition of CRM1 mediated protein export marks a negative influence on pathways in cells and may change cell fate dramatically. This can also contribute to the previously described anti-inflammatory effect of 15d-PGJ$_2$.

For the highly specific CRM1 inhibitor LMB it was reported that it is a potent anti-cancer drug in cell culture (Mutka et al., 2009; Shao et al. 2011). However, the high toxicity of LMB prevents it from being used as such. For 15d-PGJ$_2$ an anti-cancer activity was reported in a study that showed induction of apoptosis in leukemia and colorectal cancer cells (Shin et al., 2009). It therefore may be that in this case the inhibition of CRM1 mediated export in fast growing cancer cells also contributes to this anti-cancer effect of the prostaglandin.

Outlook

The inhibitory effect of 15d-PGJ$_2$ on CRM1 mediated export could be shown in this work only after application of exogenous 15d-PGJ$_2$. It would be interesting to investigate whether endogenous 15d-PGJ$_2$ would have the same effect. It also remained unclear how much of endogenously produced 15d-PGJ$_2$ is needed to show comparable effects. The strength of export inhibition on different CRM1 substrates varied a lot during this work. There are substrates such as NC2β whose export can be inhibited efficiently following application of low levels of 15d-PGJ$_2$. In contrast, only physiologically irrelevant concentrations of the prostaglandin lead to export inhibition of certain CRM1 substrates e.g. RanBP1. Therefore,

further studies on structural changes within the CRM1 molecule, especially in the NES binding site after 15d-PGJ$_2$ modification are essential. Following the example of LMB-studies (Sun et al., 2013), precise studies about binding mechanisms of 15d-PGJ$_2$ at the cysteine 528 in the CRM1 molecule have to be performed. To better understand the mechanisms of export inhibition it needs to be revealed which conformational changes the export factor undergoes after modification by 15d-PGJ$_2$.

Import of *Human* TERT import depends on importin-7 and a zinc finger region in Nup358

Human TERT localizes to the nucleus

Endogenous TERT as well as overexpressed TERT localize to the nucleus (Wong et al., 2002). In this work overexpressed GFP-tagged *human* TERT showed an intranuclear homogenous localization. TERT is a 126 kDa protein (Mitchell et al., 1999; Harley et al., 1990) which is too large to translocate through the nuclear pore and enter the nucleus by diffusion alone, it needs to be actively transported.

Very few details about transport of the TERT protein were known. The best studied transport direction of *human* TERT is export which is described to be mediated by CRM1 and also triggered by oxidative stress via Src kinase family-dependent phosphorylation of tyrosine 707 (Seimiya et al., 2000; Haendeler et al., 2003). Import pathways and receptors involved in TERT nuclear import remained unknown, so far. It was reported that the interaction of 14-3-3 proteins with the C-terminus of TERT is required for nuclear import of the protein (Seimiya et al., 2000).

TERT is involved in ageing and its expression is upregulated in many cancer cells, suggesting a role in cancer development and progression (Mitchell et al., 1999; Harley et al., 1990). It is therefore an interesting topic to investigate the factors involved in import of TERT into the nucleus.

Fragments of TERT localize to the nucleus

To investigate which region of TERT is responsible for the import of the protein, several regions have been cloned into GFP fusion vectors. However, as shown in this work, cloned fragments of TERT always localized to the nucleus although no NLS motifs were detected in the respective sequences. It is possible that in every cloned N-terminal TERT fragment an unknown NLS motif could be hidden, but perhaps the fragments could rather bind to secondary proteins to be transported into the nucleus.

Those proteins that complex with TERT later in the nucleus, especially the N-terminal and TR binding H/ACA proteins dyskerin, NOP10, NHP2 which complex in the cytoplasm (reviewed in

Hukezalie et al., 2013), could bind especially the short TRBD (telomerase-RNA- binding-domain) containing fragment and translocate it to the nucleus. Due to their truncation, N-terminal TERT fragments could also be disrupted in their structure compared to the full length protein. It might be conceivable that certain regions are ectopically exposed to the surface of the N-terminal fragments which would be hidden in full length context, attracting import receptors to transport the mutants into the nucleus.

Another explanation for the nuclear localization of the fragments could be that the N-terminal fragments bind to other truncated TERT molecules. It is unknown how much and at which concentration different truncated TERT proteins are present in a cell. Assembly and complementation studies suggested that the RID1 (also called TEN domain) containing N-terminal part of *human* TERT can interact with truncated parts of TERT containing RID2-RT-CTE domain (reviewed in Autexier et al., 2006). These observations also fit to our findings that most of the tested cloned fragments of TERT localized to the nucleus, therefore this study was continued using full-length TERT only.

Importin-7 is an import receptor of *human* TERT

In vivo FLIP experiments demonstrated an influence of importin-7 in TERT import kinetics, as import rate of TERT decreased significantly after importin-7 knock-down compared to control cells (figure 17). Additionally, knock-down experiments with siRNAs for major import receptors like importin-β, transportin and importin-9, revealed that only importin-7 depletion had a major impact on the localization of TERT (figure 14).

Although we cannot completely exclude the involvement of other import factors on nuclear import of TERT since we tested only a subset of available import receptors in a cell, we can demonstrate a strong and specific role for importin-7 in TERTs nuclear import. Rescue experiments based on a siRNA resistant importin-7 construct showed that importin-7 overexpression can indeed specifically rescue TERTs nuclear localization after depletion of its import receptor importin-7 (figure 14). Taken together, these findings demonstrate a significant role for importin-7 in nuclear import of TERT.

After import into the nucleus the substrate has to be released from its import receptor. This usually is achieved by binding of RanGTP to the import receptor. In this work the cargo release by RanGTP from importin-7 was also tested (figure S9). Release of importin-7 from

TERT could not be achieved by addition of RanQ69L, suggesting that TERT-importin-7 interaction in the nucleus is disrupted by either an unknown nuclear factor or by higher affinity of TERT towards other nuclear components. The resistance of importin-7 cargos to their release from the receptor by RanGTP was described previously. For example, the ribosomal protein rpL23a cannot be completely released from importin-7 by RanGTP (Jäkel et al., 1998). The author mentioned a 30 fold lower affinity of importin-7 for RanGTP, compared to importin-β, as a possible reason for this finding (Jäkel et al., 1998). The same effect could also be shown for the substrates c-Jun and HIV-1 Rev which are imported by multiple import receptors via an arginine rich sequence (Waldmann et al., 2007; Arnold et al., 2006). The addition of RanQ69L led to a significant disassembly of importin-substrate complexes with the exception of importin-7, which was obviously resistant towards RanQ69L addition and still bound its substrate.

For histone H1, which is imported by an importin-β- importin-7 heterodimer, it was shown that RanGTP is required for its import to finally complete NPC passage and to induce the release of importin-β at the terminal transport step at the nuclear pore (Jäkel et al., 1999). But experimental data led to the suggestion that the H1- importin-7 complex still exists in the nucleus. RanGTP than later aids the histone transfer from importin-7 to the DNA where H1 is incorporated into chromatin (Jäkel et al., 1999).

It could therefore be that TERT dissociation from importin-7 can also be facilitated by interaction of RanGTP with the import receptor. Due to the reduced affinity of RanGTP towards importin-7, other factors with a higher affinity towards TERT than importin-7 might be required to completely dissolve this cargo-receptor complex. These factors might be nucleolar proteins e.g. nucleolar transport factors. It is known that TERT can also be found in nucleoli (Tomlinson et al., 2006). Telomeric proteins such as TPP1 and TIN2 which recruit telomerase to the telomeres (reviewed in Egan et al., 2012) could also help RanGTP to dissolve the import complex.

A previous study mentioned CRM1 as the export factor of TERT (Seimiya et al., 2000). In our study FLIP experiments with and without LMB indicated that export of TERT in general does not occur at a fast rate (figure S7). Incubation of TERT and TERT NLS mutants transfected cells with LMB also did not change localization of the relevant proteins much (Chung et al., 2012), indicating that also here TERT is not exported with a high rate.

TERTs NLS motifs and their role in import

A motive scan of the protein sequence of *human* TERT indicated the existence of a putative NLS motif at position 236-240 (KRPRR). Following mutation of the amino acids KR to alanines (TERT KR 236/237 AA-GFP) TERT showed a homogenous distribution all over the cell, or localized to the cytoplasm, indicating the existence of a functional NLS. This NLS site was also shown independently from this work by Chung et al., 2012. The still high percentage of cells (60%) showing an equal distribution of overexpressed TERT KR 236/237 AA-GFP in this work, suggested the existence of at least one additional NLS motif or a larger importin binding site in the protein sequence of the telomerase protein. It is also possible that TERT complexes with other proteins which drive the import of TERT into the nucleus or that residual binding of the import receptor at the two intact residues (aa at position 239/240) occurs.

Also Chung et al., 2012 reported that ~ 30% of the analyzed cells still show a non-cytoplasmic localization of a mutant whose NLS is completely mutated (236-KRPRR-240 $\longrightarrow$ 236-AAPAA-240), indicating that also in their work either a yet unidentified NLS or a TERT interacting protein promotes import of TERT.

We showed the KR motif in the NLS is necessary for import. Thus, we started to search for other existing KR motifs within the protein. However, around 40% of the analyzed cells expressing the double mutant TERT KR 236/237 AA; KR 649/650 AA-GFP still showed a homogenous localization of the protein throughout the cell (figure 11), suggesting that TERT has additional unknown NLS motifs or importin binding regions.

Our data identified importin-7 as an import receptor for *human* TERT. The question arose whether importin-7 binds to the identified NLSs. It could be conceivable that importin-7 binds to the already identified NLS sites in the protein and therefore drives its import into the nucleus. To test this hypothesis immunoprecipitation experiments with both point mutants and the wild type (WT) TERT were performed (figure 15), but no reduced binding of importin-7 compared to WT TERT could be detected in the mutants. This would be expected when importin-7 binds the identified NLS motifs.

In contrast, it is known that importin-7 mostly binds long stretches of amino acids within its substrate. EZI for example is bound by importin-7 at several of its zinc-finger regions over a stretch of 52 amino acids and no distinct NLS motif could have been found within this protein (Saijou et al., 2007). Other importin-7 substrates are also bound by importin-7 via long stretches of amino acids. In the case of the histone protein H1, for example, the whole

protein seems to be involved in its import (Bäuerle et al., 2002). The binding region in HIV-integrase, which is also imported by importin-7, consists of 76 amino acids stretching from amino acids 212-288. Interestingly, this protein is also imported by many other import receptors (reviewed in Chook et al., 2011). Considering the results in other importin-7 substrates it is possible that TERT also uses long stretches of amino acids that serve as an importin-7 docking site. It could be that importin-7 binds great parts of the TERT protein. The identified motifs could then act as initial docking sites for importin-7 binding while other regions of the protein also contribute to import.

On the other hand, due to the known problem of insolubility of TERT during recombinant expression in *E.coli*, we were never able to show a direct interaction of TERT or TERT-NLS mutants with importin-7. In a cell lysate, barriers that separate the organelles such as the nuclear membrane which separates the nucleus from the cytoplasm no longer exist, allowing proteins to have contact with each other that would not occur under native cellular conditions. It could therefore be that TERT interacting proteins which might also be bound and imported by importin-7 now have access also to the NLS mutated TERTs because they use a different binding region on the protein than the import receptor. This could lead to an indirect importin-7 binding of the NLS-mutated TERT proteins.

However, overexpressed GFP-TERT CT (aa 601-1132) and GFP TERT NT (aa 1-600) both showed a reduced nuclear localization after knock down of importin-7, suggesting a role of importin-7 in nuclear import of both truncation mutants (figure S 10). Under mock conditions localization of these TERT truncation mutants is predominant nuclear (figure S 10).

The influence of Nup358 on TERT import

The data from this work and previous work (Hutten 2007) show a dependency of TERT import on the nucleoporin Nup358. The question arose whether a specific region in Nup358 is required for an efficient transport of TERT or whether only the full length Nup can mediate import of TERT. It was already known from previous studies that Nup358 is required for the import of a certain subset of proteins, for example DBC-1 or HIV-1 Rev (Waelde 2010; Hutten et al., 2009). For DBC-1, a Nup region containing aa 1-1170 (ending in front of Ran-binding domain1 (RB1) including 3 FG-repeats) was described as the region responsible for its import

(Wälde et al., 2012). In contrast to these findings, TERT import depends on a region further downstream (aa 1-1810) containing the zinc-fingers region of Nup358.

A region in TERT responsible for Nup358 dependency could not be defined, since TERT fragments always localized to the nucleus after depletion of Nup358 (data not shown). The dependency of TERT on the nucleoporin could only be shown for the full length TERT.

It can be concluded that there is no general region or motif in Nup358 specifically responsible for the import of the group of Nup358 dependent proteins. Furthermore, proteins seem to require different and very defined and independent regions on the Nup for their import. It was suggested that Nup358 provides a platform for substrate binding prior to their import (Wälde et a., 2012; Pante et al., 1993).

TERT nuclear import is dependent on the presence of both, importin-7 and Nup358. It was therefore interesting to investigate whether importin-7 mediated protein import in general depends on the presence of the nucleoporin. EZI was shown to be specifically imported by importin-7 (Saijou et al., 2007). In Nup358 depleted cells EZI still localized to the nucleus, suggesting that importin-7 mediated import in general is not affected by Nup358 depletion and therefore not dependent on Nup358. It is therefore TERT itself that is dependent on Nup358, supporting the already mentioned theory that Nup358 provides an assembly platform for certain substrates. Proteins may therefore interact with different parts of Nup358 to be correctly assembled with their import receptor.

The finding that importin-7 mediated import of proteins does not generally depend on Nup358 might be also supported by the finding that importin-7 does not interact with Nup358 without RanGTP as a cofactor (figure 18). It might not interact strongly with the Nups FG repeats. Also, the observed binding of importin-7 to Nup358 mediated by RanGTP seems to be weak under the immunoprecipitation conditions (figure 18 A), although RanGTP-mediated binding of importin-7 to Nup358 fragments was stronger in vitro (figure 18 B). Ran dependant binding of importin-7 to a nucleoporin rather supports the suggestion that complexing of Ran with an import receptor leads to its export from the nucleus (Görlich et al., 1997).

Inhibition of TERT import can be enhanced by co-depletion of importin-7 and Nup358

One could argue that the cytoplasmic localization of TERT after Nup358 depletion could also result from enhanced or accelerated export of the protein instead of impaired import. It was already shown, in previous work that depletion of Nup358 does not lead to accelerated export of the affected proteins (Wälde 2010). FLIP experiments also showed an impaired import after depletion of importin-7. Considering these data, it seems likely that in this case also depletion of Nup358 results in an impaired import of TERT.

The detailed mechanism of Nup358 responsibility in import of TERT still remains unclear. It is also unclear whether Nup358 binds to TERT and if yes, whether other proteins are also involved in assembly. It also remains unclear where importin-7 binding to TERT occurs and whether it is affected by Nup358.

From these findings the question arises why transport of certain proteins depend on the presence of single Nups? It will need further investigation to discover the molecular mechanisms behind this specific behavior.

The model shown below (figure 21) describes a putative mechanism of nuclear import of TERT by importin-7 and Nup358. TERT could use the zinc finger region of Nup358 as a platform prior to its import. Importin-7 could bind the telomerase protein there and deliveres it into the nucleus. RanGTP and TERT interacting factors could help to disolve the importin-substrate complex in the nucleus. The newly formed importin-7-RanGTP complex could then leave the nucleus again by binding to nucleoporins e.g. Nup358, to be recycled back to the cytoplasm for another round of import.

Model
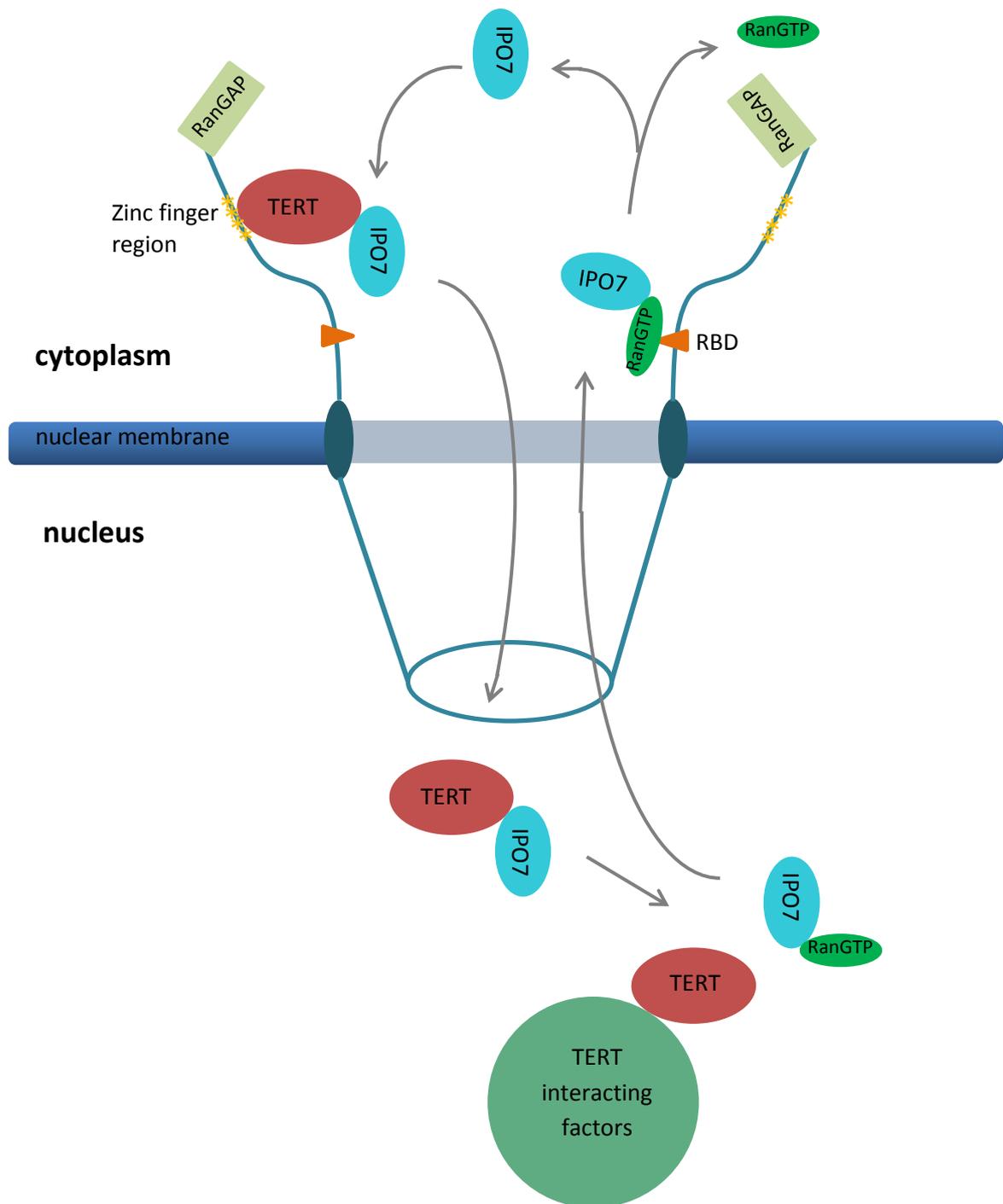
Figure 21: Model of TERT recognition by importin-7 and later dissociation of the complex
TERT could be recruited to Nup358, which provides a platform for proteins prior to their import. TERT can be there recognized and bound to importin-7 which transports it through the pore into the nucleus. Once in the nucleus, RanGTP together with other TERT interacting factors triggers the dissociation of the import complex. The importin-7- RanGTP complex leaves the nucleus by interaction of RanGTP with nucleoporins (e.g. Nup358). In the cytoplasm RanGAP dissolves the complex again- ensuring a new round of import for the receptor.

Outlook

Within the course of this study the import of overexpressed *human* TERT into the nucleus was examined. We found the import receptor importin-7 to be essential for TERT nuclear import. The filamentous nucleoporin Nup358 also plays a role in import of TERT. First of all, the binding of TERT to importin-7 has to be further investigated. Although, we found NLS motifs within the protein sequence which strongly influenced its localization it remained unclear whether importin-7 directly binds these motifs. To answer this question, the big problem of recombinant expression of TERT in *E.coli* or in insect cells first has to be solved. With recombinantly expressed TERT, many problems hindering this work could be solved. The interaction between importin-7 and TERT could be further investigated. It can be distinguished whether it is a direct interaction or mediated by binding of secondary proteins. A putative role of the TERT RNA component in nuclear import or in disassembly of the receptor-substrate complex in the nucleus could be investigated. Import assays provide an option to investigate import pathways of proteins and still provide the barrier of the nuclear membrane combined with selective transport of proteins through the pore. These assays could then be performed to gain further insights into TERT nuclear import. Also the RanGTP dependant disassembly of TERT-importin-7 complex in the nucleus can be further investigated using purified proteins. Furthermore, the ability of importin-7 to bind to NLS mutated TERTs could be observed without the influence of other proteins derived from a cell lysate.

It would also be interesting to see whether endogenous TERT responds in a similarly manner to overexpressed TERT towards an importin-7 knock-down. For this, a specific antibody against human TERT is required, combined with cells expressing rather high levels of endogenous TERT.

The influence of Nup358 on TERT nuclear import could also benefit from the availability of recombinant TERT and a TERT specific antibody. The specific role of the zinc finger region of Nup358 on TERT nuclear import, can be further investigated using binding assays or with immunofluorescence.

Taken together, these approaches could contribute to gain further insights into the precise import mechanism of this protein.

Appendix
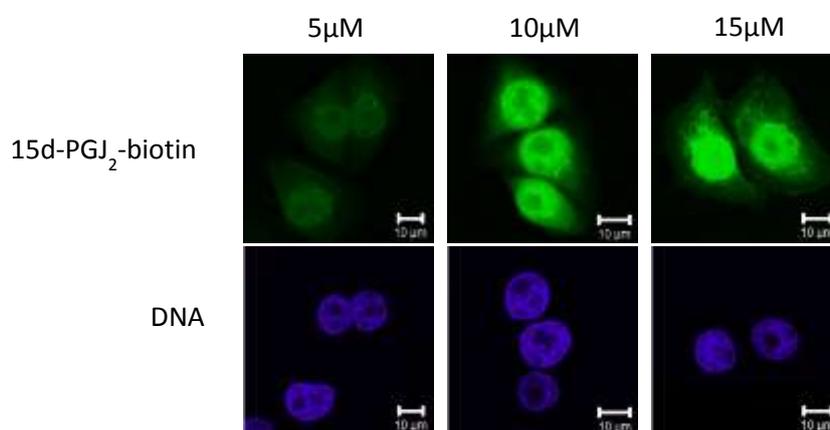
S1: Concentration dependency approach of 15d-PGJ$_2$

HeLa p4 cells were grown on coverslides. Prior to incubation with biotinylated 15d-PGJ$_2$ medium was changed to 400µl serum free medium per 24-well. Cells were incubated with either 5µM, 10µM or 15µM of biotinylated 15d-PGJ$_2$ for 15 minutes to test the ability of 15d-PGJ$_2$ to be imported into the nucleus. Biotin was visualized after fixation by using Streptavidin coupled to a fluorophore with an excitation at 488nm. Images were taken by using the reuse function to retain the same settings throughout the experiment. As shown in the images already lower concentrations of 15d-PGJ$_2$ e.g. 5µM are detectable in the nucleus after 15 minutes of incubation. The amount of detectable 15d-PGJ$_2$ in the nucleus increased with increasing concentration.
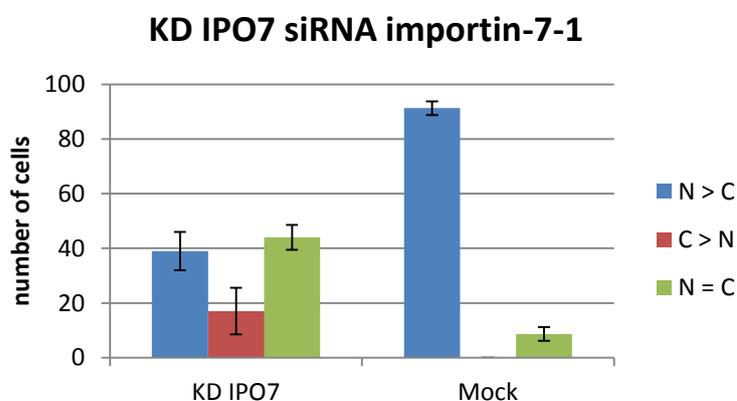

S2: Inhibition of TERT import after importin-7 depletion with siRNA importin-7-1

A second siRNA against importin-7 was tested. The siRNA importin-7-1 was purchased to validate the effects of the siRNA used in the rest of the work. It targets a different region in the importin-7 mRNA.

Import of NES-GFP2-M9
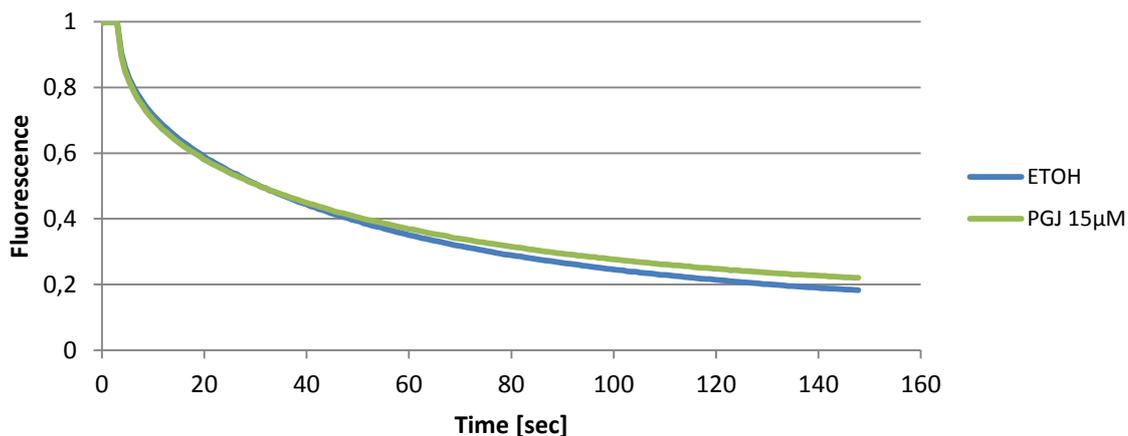
S3: Live cell imaging using FLIP showing no inhibition of import after 15d-PGJ₂ application

HeLa p4 cells were transiently transfected with the artificial import substrate NES-GFP$_2$-M9. The M9 sequence is recognized by the import receptor transportin, in contrast, CRM1 recognized the NES motif. Prior to FLIP analysis cells were incubated with either 15µM of 15d-PGJ$_2$ or Ethanol as a solvent control, for 1 hour in serum-free medium. Cell medium was later changed to CO_2-independent medium and FLIP was carried out in a preheated microscope chamber at 37°C. As shown in the diagram, import in the analyzed cells was not affected by application of 15d-PGJ$_2$. For this analysis 20 cells were analyzed for each condition.
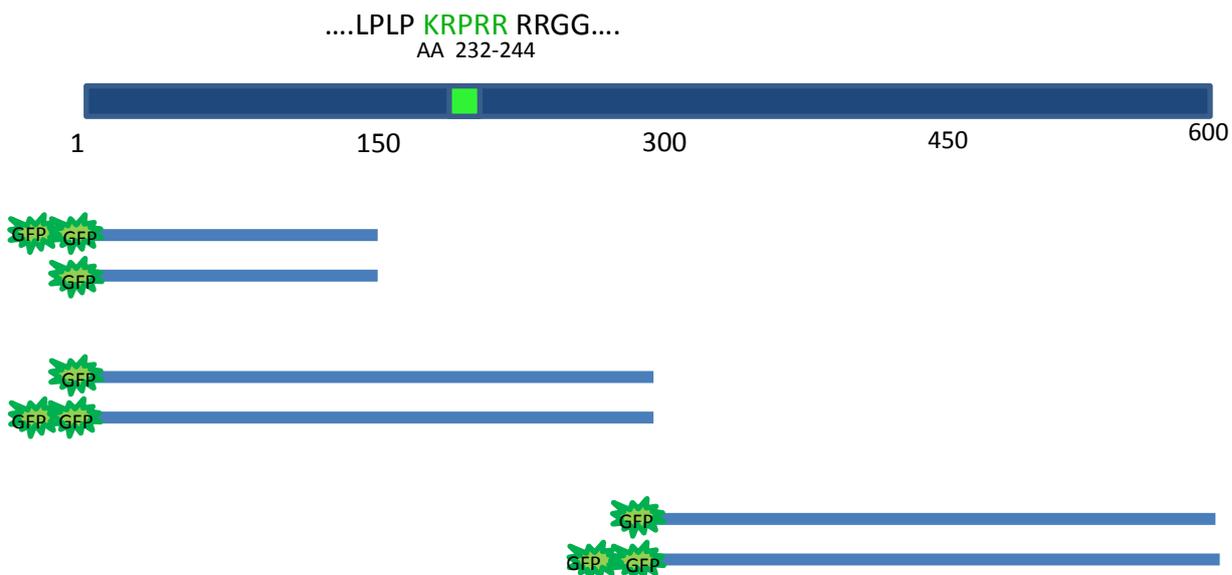
S4: Localization of TERT N-terminal truncation mutants

Schematic description of TERT-N-terminus and the cloned truncation mutants fused to GFP-tags.

TERT NT NLS mutants

P <0,0009

legend:
- N > C (blue)
- C > N (red)
- N = C (green)
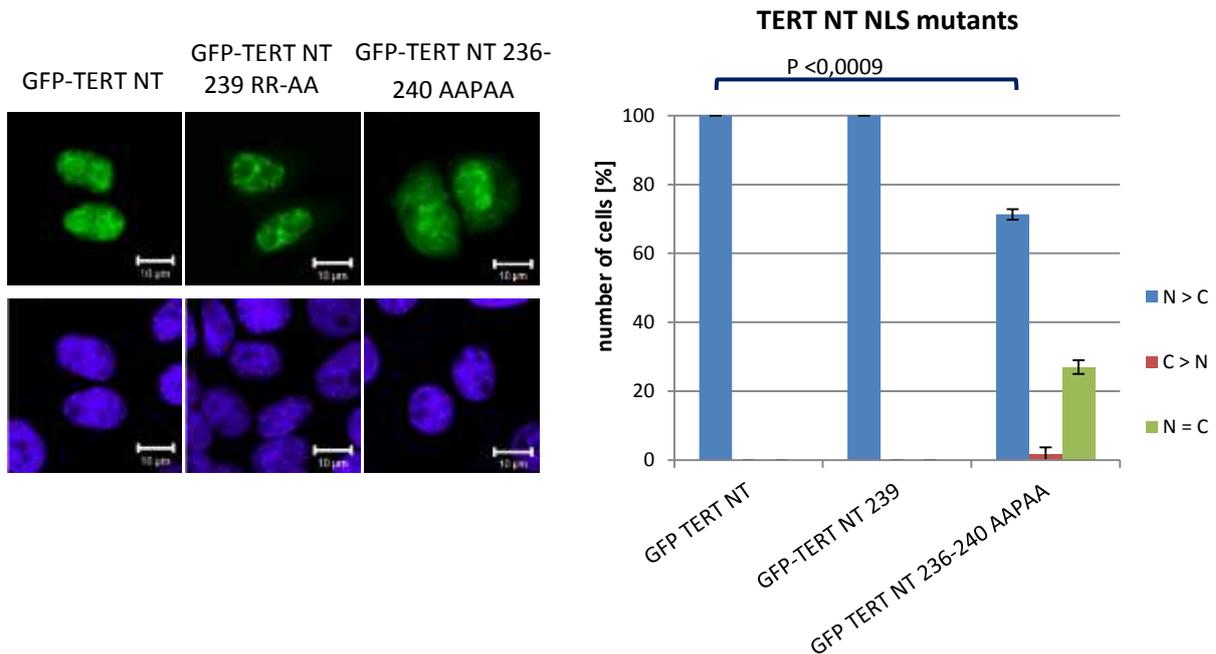
S5: Mutation of the NLS-motif in TERT N-terminus

GFP-TERT N-terminus (GFP-TERT NT) contained the NLS-motif at position 236-240 and localized to the nucleus exclusively. Mutation of the last 2 arginines (239/240) to alanines did not change localization of the TERT truncation mutant GFP-TERT NT 239 RR-AA indicating that the last 2 residues are not essential for its import. Mutation of the full NLS-site (GFP-TERT NT 236-240 AAPAA) indeed changed localization of the construct. More than 25% of the analyzed cells showed an equal localization of this TERT N-terminal mutant between nucleus and cytoplasm. This gave the first hints for the existence of a functional NLS in human TERT.

TERT-GFP (Roi2)

time (sec)	Cell 1	Cell 2	Cell 3	Cell 4	Cell 5	Cell 6	Cell 7	Cell 8	Cell 9	Cell 10
0	1005,4	780	1463,6	917,8	1294,8	1181	1084,5	1187,3	964,2	1216,6
0,154	992,7	755	1422,2	886,1	1273,4	1174,4	1061,9	1179,4	952	1200,2
0,309	981,4	764,9	1424,3	902,5	1276,9	1164,5	1058	1187,8	944,2	1185,6
0,463	962,6	760,2	1412,2	870,8	1258,9	1151,4	1036,7	1202,6	934,5	1193,9

TERT 236 KR-AA-GFP (Roi2)

time (sec)	Cell 1	Cell 2	Cell 3	Cell 4	Cell 5	Cell 6	Cell 7	Cell 8	Cell 9	Cell 10
0	840,2	990,9	1537,9	910,6	1734,5	925,4	970,6	1697	1205,2	1374,9
0,154	825,5	979,8	1554,8	897,7	1736,3	928,2	974	1688,7	1218,9	1360,5
0,309	814,2	964,7	1529,1	884,4	1697,7	917,4	953,3	1691,7	1176,2	1382,2
0,463	806,9	970,2	1514,5	868,2	1680,6	908,5	966,2	1675,9	1173,8	1368

TERT 236 649 KR-AA-GFP (Roi2)

time (sec)	Cell 1	Cell 2	Cell 3	Cell 4	Cell 5	Cell 6	Cell 7	Cell 8	Cell 9	Cell10
0	1372,1	1014,3	1095,2	1222,8	1142,4	1331	1297,5	916,9	1007,3	988
0,154	1342,5	993,1	1081,5	1191,2	1131,7	1324,8	1297,8	923,6	978,4	988,2
0,309	1324,2	985,1	1094,9	1172,7	1126,6	1319,9	1280,4	931,2	983,5	970,2
0,463	1321,8	982,1	1093	1190,2	1103,2	1302,4	1277,4	906,6	984,6	967,8
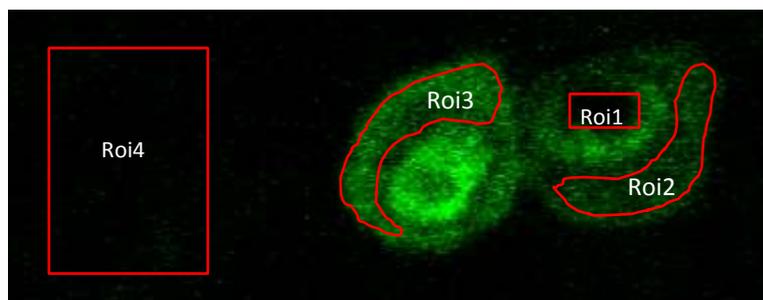
S6: Raw FLIP data from the first 10 FLIPs of Roi2 from each mutant
The tables show the raw FLIP data of the first five fluorescence intensities taken in a FLIP measurement. They show the fluorescence measured in pixels of Roi2 (region of interest2) from the first 10 FLIPs performed in each mutant. These pixel intensities show that the initial fluorescence in the cytoplasm of the analyzed cells was comparable.
The picture below the tables shows a typical example of the localization of the different Rois used in the FLIP measurements. Roi1 marks the bleaching region of the analyzed cell, while Roi2 is the region in the cytoplasm where loss of fluorescence is measured. Roi3 indicates a comparable region to Roi2 in the reference cell. In Roi4 the background of the measurement is taken.
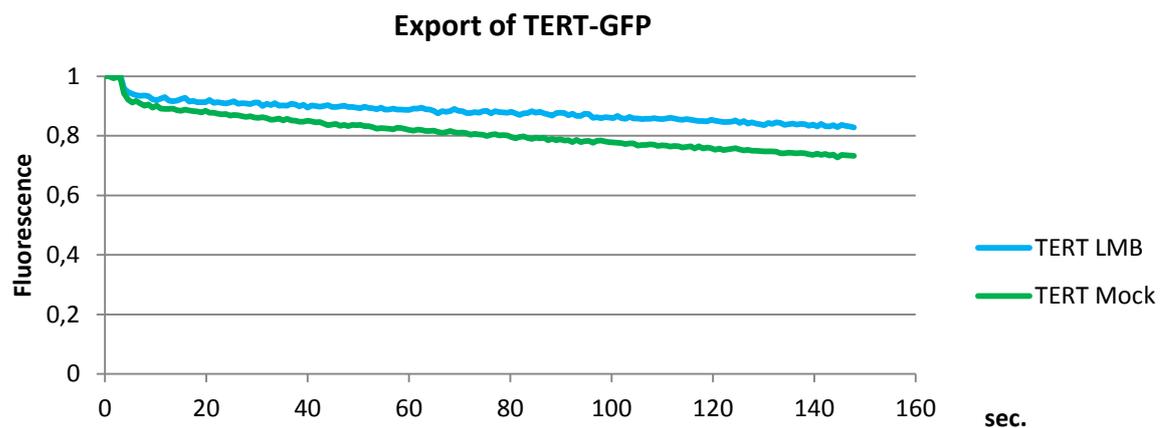
Export of TERT-GFP

S7: FLIP analysis of TERT-GFP export +/- LMB

Human TERT is exported by CRM1 (Seimiya et al., 2000). To illustrate and to compare transport kinetics of TERT-GFP in general TERT-GFP export was analyzed by FLIP. To measure Crm1 mediated export of TERT-GFP, cells were either treated with 5nM of the specific Crm1 inhibitor LMB for 2 hours prior to FLIP analysis or were left untreated (mock). To guarantee viability of cells throughout the whole measurement CO_2 independent medium was used during analysis.

Compared to import rates of TERT-GFP (figure 12, figure17) export of TERT-GFP occurs at a much slower rate.

TERT-GFP mock (non-targeting siRNA)

time (sec)	Cell 1	Cell 2	Cell 3	Cell 4	Cell 5	Cell 6	Cell 7	Cell 8	Cell 9	Cell 10
0	1069,3	1404,6	882,5	1166,7	1080,2	998,5	1021,6	1191,6	852,3	1181,6
0,154	1041,6	1395,3	870,2	1141,9	1091,9	982,5	1030,6	1195,6	864,7	1176,1
0,309	1030,6	1375,2	849,5	1135,5	1069,1	970,5	1016,9	1155,7	847,1	1147,6
0,463	1026,2	1360,8	854,7	1121,7	1045,2	967,2	990,3	1149,4	835,6	1148,4

TERT-GFP knock down importin-7

time (sec)	Cell 1	Cell 2	Cell 3	Cell 4	Cell 5	Cell 6	Cell 7	Cell 8	Cell 9	Cell 10
0	969,1	753,1	707,2	1035,4	1003,8	939,3	1346,5	1006,9	1005,2	996,2
0,154	929	728,1	683,2	1035,1	1003,2	911,2	1344	983,3	995,8	964,8
0,309	931	728,4	675,6	1006,9	986,7	925,1	1362,7	985,4	963	967,5
0,463	926,9	718,3	674,5	1005	982	885,4	1321,6	991,4	959,2	972,9

S8: Raw FLIP data of TERT-GFP from the first 10 FLIPs of Roi2 after knock down of importin-7 or mock

The tables show the raw FLIP data of the first 5 pictures taken in a FLIP measurement. They show the fluorescence measured in pixels of Roi2 (region of interest2) from the first 10 FLIPs performed in both conditions. These pixel data show that the starting fluorescences in the cytoplasm (Roi2) of the cells was comparable.

Immunoprecipitation   **Inputs**
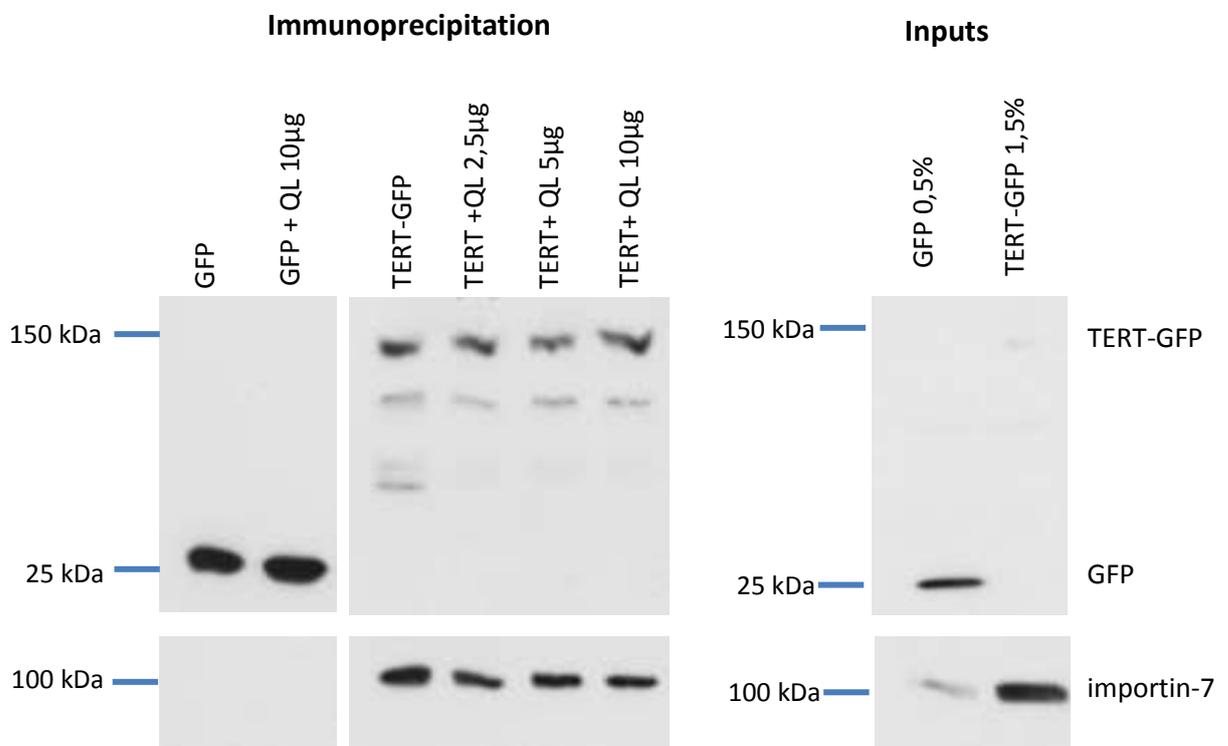
S9: Importin-7 did not dissociate from TERT-GFP by addition of GTP loaded RanQ69L

293T cells were transiently transfected with either TERT-GFP (TERT) or an empty GFP-vector as a control. After immunoprecipitation(IP) using the GFP nanotrap the IP was washed and divided into 4 samples. The first sample was left untreated (TERT-GFP) showing the endogenous bound importin-7. To the three remaining IP samples different concentrations of previous GTP loaded RanQ69L (QL) were added and incubated on the beads for 30 minutes, at 4°C with rotation followed by washing with GFP- dilution buffer. Even the application of high levels of RanGTP (10µg) was not sufficient to reduce the amount of endogenous Importin7 bound to TERT-GFP. Only a very slight reduction of bound importin-7 could be achieved.
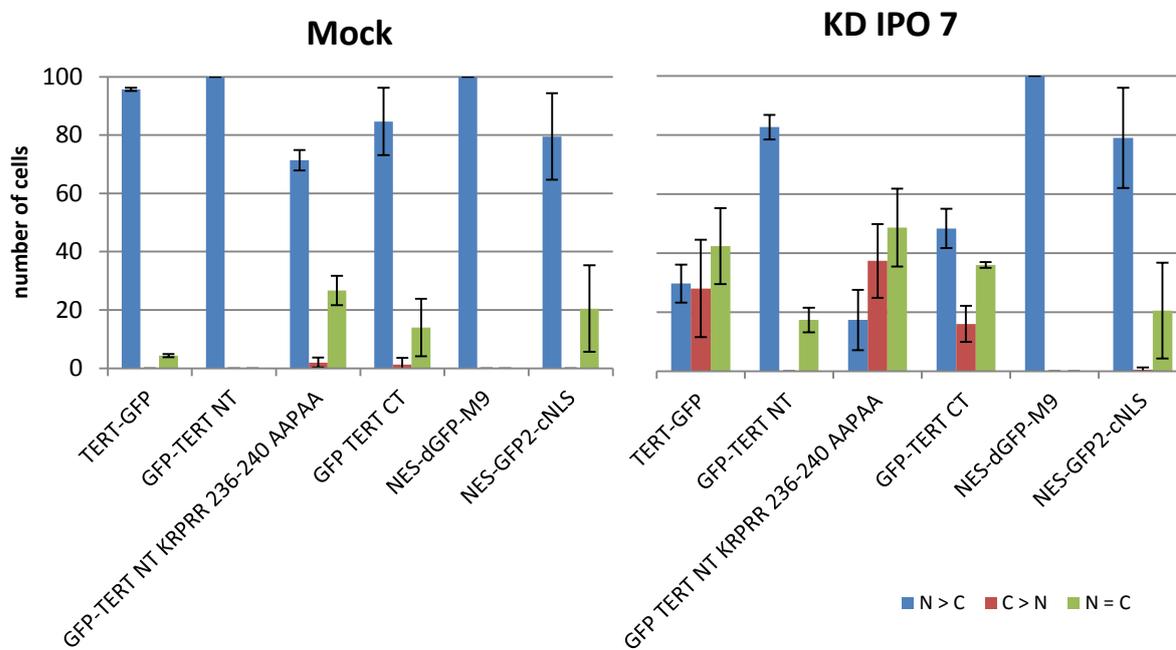
Figure S10: Comparison of TERT truncation constructs and the NT-import defective mutant in Mock and importin-7 knock-down conditions.

Full length TERT-GFP shows the characteristic import defect after importin-7 depletion. The WT TERT-NT truncation mutant also shows a reduced nuclear localization, indicating that importin-7 is involved in its import.

Under mock conditions the N-terminal NLS mutant GFP-TERT NT KRPRR 236-240 AAPAA already shows a reduced nuclear localization which was enhanced under knock-down conditions.

The TERT CT construct (aa601-1132) also responded to the knock-down of importin-7, suggesting another binding site for importin-7.

The control plasmids NES-GFP$_2$-cNLS/-M9 were not affected by the importin-7 knock-down.
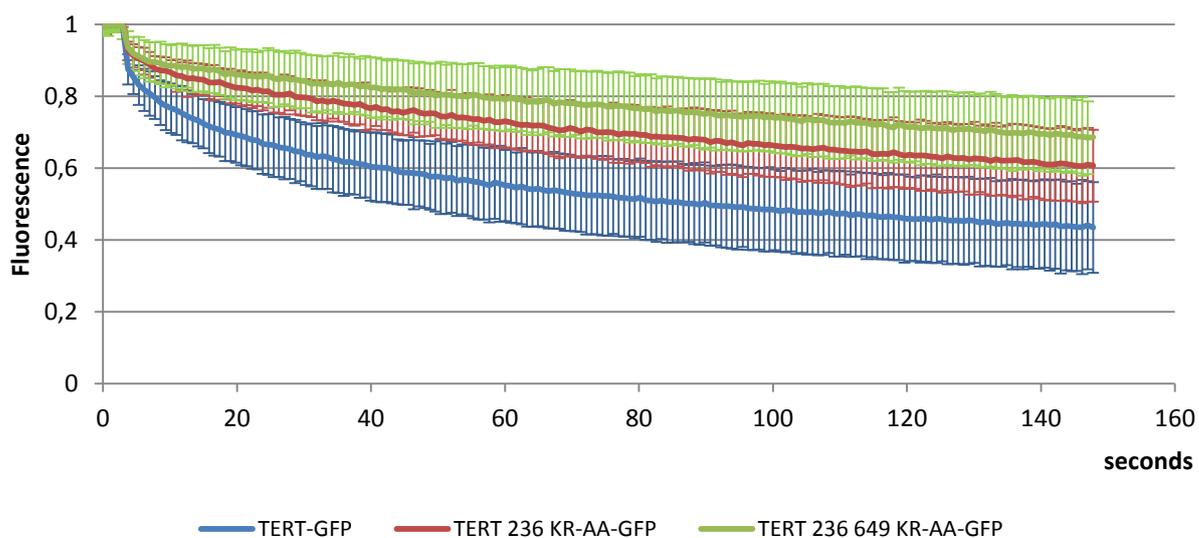
Figure S11: Original FLIP data with standard deviation of TERT-NLS mutants
The data with the error bars representing the standard deviation corresponds to the graph shown in figure 12.
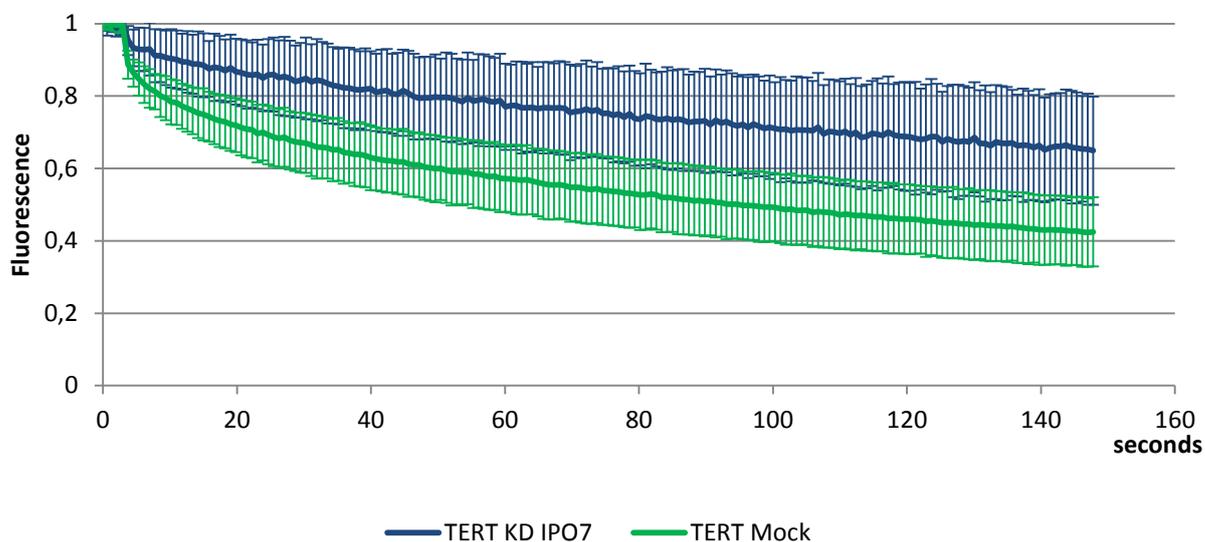
Figure S12: Original FLIP data with standard deviation of TERT-GFP
The data with the error bars representing the standard deviation corresponds to the graph shown in figure 17.

References

Adam E.J.H., Adam S., (1994). **Identification of Cytosolic Factors Required for Nuclear Location Sequence-mediated Binding to the Nuclear Envelope.**
JBC; vol. 125: 547-555

Akey C.W., Radermacher M. (1993). **Architecture of the** *Xenopus* **Nuclear Pore Complex Revealed by Three-Dimensional Cryo-Electron Microscopy.**
JBC; vol. 122: 1-19

Alber F., Dokudovskaya S., Veenhoff L.M., Zhang W., Kipper J., DevosD., Suprapto A., Karni-Schmidt O., Williams R., Chait B.T., Sali A., Rout M.P (2007a). **The molecular architecture of the nuclear pore Complex.**
Nature; 450: 695-701

Alber F., Dokudovskaya S., Veenhoff L.M., Zhang W., Kipper J., Devos D., Suprapto A., Karni-Schmidt O., Williams R., Chait B.T., Rout M.P., and Sali A. (2007b). **Determining the architectures of macromolecular assemblies.**
Nature; 450:683-94.

Arai K., Masutomi K., Khurts S., Kaneko S., Kobayashi K., Murakami S. (2002). **Two independent regions of human telomerase reverse transcriptase are important for ist oligomerization and telomerase activity.**
JBC; 277:8538–44

Arnold M., Nath A., Hauber J., Kehkenbach R.H. (2006). **Multiple Importins Function as Nuclear Transport Receptors for the Rev Protein of Human Immunodeficiency Virus Type 1.**
JBC; 281:20883–20890

Autexier C., Lue N. F. (2006). **The Structure and Function of Telomerase Reverse Transcriptase.**
Annu. Rev. Biochem.; 75:493-517

Avilion A.A., Harrington L.A., Greider C.W. (1992). *Tetrahymena* **Telomerase RNA Levels Increase During Macronuclear Development.**
Dev. Genetics; 13: 80-86

Bachand F., Autexier C. (2001). **Functional regions of human telomerase reverse transcriptase and human telomerase RNA required for telomerase activity and RNA-protein interactions.**
Mol. Cell. Biol.; 21:1888–1897.

Banik S. S. R., Counter C. M. (2004). **Characterization of interactions between PinX1 and human telomerase subunits hTERT and hTR.**
JBC; 279: 51745-51748

Bäuerle M., Doenecke D., Albig W. (2002). **The requirement of H1 histones for a heterodimeric nuclear import receptor.**
JBC.; 277:32480–32489

Beattie T.L., Zhou W., Robinson M.O., Harrington L. (2001). **Functional multimerization of the human telomerase reverse transcriptase.**
Mol. Cell. Biol.; 21:6151–6160

Bernad R., van der Velde H., Fornerod M., Pickersgill H. (2004) **Nup358/RanBP2 Attaches to the Nuclear Pore Complex via Association with Nup88 and Nup214/CAN and Plays a Supporting Role in CRM1-Mediated Nuclear Protein Export.**
Mol. Cell. Biol.; 24: 2373-2384

Bhattacharyya A., Blackburn E.H. (1994). **Architecture of telomerase RNA.**
The EMBO J.; 13: 5721-5731

Birnboim H.C., Doly J., (1979). **A rapid alkaline extraction procedure for screening recombinant plasmid DNA.**
Nucl. Acids Res.; 7:1513-1524

Bischoff F.R., Ponstingl H. (1991). **Catalysis of guanine nucleotide exchange on Ran by the mitotic regulator RCC1.**
Nature; 354:80-82.

Bischoff F.R., Ponstingl H. (1991a). **Mitotic regulator protein RCC1 is complexed with a nuclear ras-related polypeptide.**
Proc. Natl. Acad. Sci. USA.; 88:10830-10834

Bischoff R.F., Klebet C., Kretschmer J., Witringhofer A., Ponstingl H. (1994). **RanGAP1 induces GTPase activity of nuclear Ras-related Ran.**
Proc. Natl. Acad. Sci. USA; 91:2587-2591

Bischoff F.R., Görlich D. (1997). **RanBP1 is crucial for the release of RanGTP from importin beta-related nuclear transport factors.**
FEBS Letter; 419:249-254

Black B.E., Holaska J.M., Levesque L., Ossareh-Nazari B., Gwizdek C., Dargemont C., Paschal B.M. (2001). **NXT1 is necessary for the terminal step of Crm1-mediated nuclear export.**
JCB; 152:141-155

Blackburn E. H., Greider C. W., Henderson E., Lee M. S. , Shampay J., Shippen-Lentz D., (1989). **Recognition and elongation of telomeres by telomerase.**
Genome; 31:553-560

Burns L.T., Wente S.R. (2012). **Trafficking to uncharted territory of the nuclear envelope.**
Curr. Op. in Cell Biol.; 24:341–349

Carmody S.R., Wente S.R., (2009). **mRNA nuclear export at a glance.**
J. of Cell Sci.; 122: 1933-1937

Cingolani G., Petosa C., Weis K., Müller C.W., (1999). **Structure of importin-β bound to the IBB domain of importin-α.**
Nature; 399:221-229; May 20, 1999

Cingolani G., Bednenko J., Gillespie M.T., Gerace L. (2002). **Molecular Basis for the Recognition of a Nonclassical Nuclear Localization Signal by Importinβ.**
Mol. Cell; 10:1345–1353

Chook Y.M., Süel K.E. (2011). **Nuclear import by Karyopherin-βs: recognition and inhibition**
Biochim. Biophys. Acta; 9: 1593–1606

Chuderland D., Konson A., Seger R. (2008) **Identification and characterization of a general nuclear translocation signal in signaling proteins.**
Mol. Cell.; 31: 850–861

Chung J., Khadka P., Chung I.K., (2012). **Nuclear import of hTERT requires a bipartite nuclear localization signal mediated by Akt phosphorylation.**
J. of Cell Sci.; epup February 24, 2012

Collins K. (2006). **The biogenesis and regulation of telomerase holoenzymes.**
Nat. Rev. Mol. Cell Biol. ; 7: 484–494

Conti E., Kuriyan J. (2000). **Crystallographic analysis of the specific yet versatile recognition of distinct nuclear localization signals by karyopherinα.**
Structure; 8: 329-338

Counter C.M., Avilion A.A., LeFeuvrel C.E., Stewart N.G., Greider C.W., Harley C.B., Bacchetti S. (1992). **Telomere shortening associated with chromosome instability is arrested in immortal cells which express telomerase activity.**
The EMBO J.; 5: 1921 - 1929

Dasso, M. (2002). **The Ran GTPase: theme and variations.**
Curr Biol. ;12:R502-508.

Darzac, X., Kittur N., Roy S., Shav-Tal Y., Singer R. H., Meier U. T. (2006) **Stepwise RNP assembly at the site of H/ACA RNA transcription in human cells**.
JCB.; 173, 207-218.

Delphin, C., Guan, T., Melchior, F., and Gerace, L. (1997). **RanGTP targets p97 to RanBP2, a filamentous protein localized at the cytoplasmic periphery of the nuclear porecomplex.**
Mol. Biol. Cell.; 8:2379–2390

Dingwall C., Sharnick S.V, Laskey R.A. (1982**). A polypeptide domain that specifies migration of nucleoplasmin into the nucleus.**
Cell; 30:449-458.

Dong X., Biswas A., Chook Y.M. (2009). **Structural basis for assembly and disassembly of the CRM1 nuclear export complex.**
Struct. Mol. Biol.; 16: 558-560

Egan E., Collins K. (2012). **Biogenesis of telomerase ribonucleoproteins.**
RNA; 18: 1747-1759

Egan E. D., Collins K. (2012a). **An enhanced H/ACA RNP assembly mechanism for human telomerase RNA**.
Mol. Cell Biol.; 32, 2428-2439

Faberge, A. C. (1973). **Direct demonstration of eightfold symmetry in nuclear *pores.***
Z. Zellforsch Mikrask. Anat.; 136:183-190

Ferrezuelo F., Steiner B., Aldea M., Futcher B. (2002). **Biogenesis of Yeast Telomerase Depends on the Importin Mtr10.**
Mol. Cell Biol.; 22: 6046–6055

Fischer U., Huber J., Boelens W.C., Mattaj I.W., Lührmann R. (1995). **The HIV-1 Rev activation domain is a nuclear export signal that accesses an export pathway used by specific cellular RNAs.**
Cell; 82: 475-483

Floer M., Blobel G., Rexach M. (1997). **Disassembly of RanGTP-karyopherin beta complex, an intermediate in nuclear protein import.**
JBC; 272:19538-19546

Fontes M.R., Teh T., Kobe B. (2000). **Structural basis of recognition of monopartite and bipartite nuclear localization sequences by mammalian importinα.**
J. of Mol. Biol.; 297: 1183-1194

Fornerod M., van Deursen J., van Baal S., Reynolds A., Davis D., Murti K.G., Fransen J., Grosveld G. (1997). **The human homologue of yeast CRM1 is in a dynamic subcomplex with CAN/Nup214 and a novel nuclear pore component Nup88.**
The Embo J.; 16:807-816

Fornerod M., Ohno M., Yoshida M., Mattaj I.W. (1997a). **CRM1 is an export receptor for leucine-rich nuclear export signals.**
Cell; 90:1051-1060

Fox A.M., Ciziene D., McLaughlin S.H., Steward M. (2011). **Electrostatic Interactions Involving the Extreme C Terminus of Nuclear Export Factor CRM1 Modulate Its Affinity for Cargo.**
Biol. Chem.; 286: 29325-29335

Frey S., Görlich, D. (2007**). A saturated FG-repeat hydrogel can reproduce the permeability properties of nuclear pore complexes.**
 Cell; 130:512-23

Frey S., Richter R.P., Görlich, D. (2006). **FG-rich repeats of nuclear pore proteins form a three-dimensional meshwork with hydrogel-like properties.**
Science; 314:815-7.

Fried H., Kutay U. (2003) **Nucleocytoplasmic transport: taking an inventory**
Cell. and Mol. Life Sci.; 60:1659–1688

Gadal O., Strauss D., Kessl J., Trumpower B., Tollervey D., Hurt E. (2001). **Nuclear export of 60S ribosomal subunits depend on Xpo1p and requires a nuclear export sequence- containing factor, Nmd3p; that associates with the large subunit protein Rp110p.**
Mol. Cell. Biol.; 21:3405-3415

Gallardo F., Olivier C., Dandjinou A.T., Wellinger R.J., Chartrand P. (2008). **TLC1 RNA nucleo-cytoplasmic trafficking links telomerase biogenesis to its recruitment to telomeres.**
The EMBO J.; 27:748-757

Gasteier, J.E., Madrid, R., Krautkramer, E., Schroder, S., Muranyi, W., Benichou, S., Fackler, O.T. (2003.) **Activation of the Rac-binding partner FHOD1 induces actin stress fibers via a ROCK-dependent mechanism.**
JBC; 278:38902-38912. Epub 2003 Jul 10.

Gillis A.J., Schuller A.P., Skordalakes E. (2008). **Structure of the Tribolium castaneum telomerase catalytic subunit TERT.**
Nat. Art.; 455: 633-638

Görlich, D. *et al*. (1995). **Two different subunits of importin cooperate to recognize nuclear localization signals and bind them to the nuclear envelope.**
Curr. Biol.; 5: 383–392

Görlich D., Henklein P., Laskey R. A., Hartmann E. A (1996). **41 amino acid motif in importin-a confers binding to importin-β and hence transit into the nucleus.**
The EMBO J. 15: 1810–1817

Görlich D., Pante N., Kutay U., Aebi U., Bischoff F.R. (1996a). **Identification of different roles for RanGDP and RanGTP in nuclear protein import.**
The Embo J. 15:5584-5594.

Görlich D., Dabrowski M., Bischoff F.R., Kutay U., Bork P., Hartmann E., Prehn S., Izaurralde E. (1997). **A Novel Class of RanGTP Binding Proteins.**
JCB; 138: 65-80

Görlich D., Kutay U. (1999). **Transport between the cell nucleus and the cytoplasm.**
Annu. Rev. Cell. Dev. Biol.; 15:607-660.

Goldberg M.W., Allen T.D. (1996). **The nuclear pore complex and lamina: threedimensional structures and interactions determined by field emission in-lens scanning electron microscopy.**
J. Mol Biol. 257:848-865

Goodwin J.S., Kenworthy A.K. (2005). **Photobleaching approaches to investigate diffusional mobility and Trafficking of Ras in living cells.**
Science; 37: 154-164

Greider C.W., Blackburn E.H. (1989). **A telomeric sequence in the RNA of Tetrahymena telomerase required for telomere pepeat synthesis.**
Nat. Art.; 337:331-337

Greider C.W., Blackburn E.H. (1985). **Identification of a Specific Telomere Terminal Transferase Activity in Tetrahymena Extracts.**
Cell. Vol.; 43: 405-413

Güttler T., Madl T., Neumann P., Deichsel D., Corsini L., Monecke T., Ficner R., Sattler M., Görlich D. (2010). **NES consensus redefined by structures of PKI-type nuclear export signals bound to CRM1.**
Nature; 17: 1367-1377

Haendeler J.,Hoffmann J.,Brandes R.P.,Zeiher A.M.,Dimmeler S. (2003). **Hydrogen Peroxide Triggers Nuclear Export of Telomerase Reverse Transcriptase via Src Kinase Family-Dependent Phosphorylation of Tyrosine 707.**
Mol. Cell. Biol.; 32:4598-4610

Hamamoto T., Gunji S., Tsuji H., Beppu T. (1983a). **Leptomycins A and B, new antifungal antibiotics. I. Taxonomy of the producing strain and their fermentation, purification and characterization.**
J. Antibiotics; 36:639-645

Hamamoto T., Seto H., Beppu T. (1983b). **Leptomycins A and B, new antifungal antibiotics. II. Structure elucidation.**
J. Antibiotics (Tokyo); 36:646-650

Harley C.B., Futcher A.B., Greider C.W., (1990) **Telomeres shorten during ageing of human fibroblasts.**
Letters to Nature; 345:458-460

Harrington L., Zhou W., McPhail T., Oulton R., Yeung D.S., Mar V., Bass M.B., Robinson M.O. (1997) **Human telomerase contains evolutionarily conserved catalytic and structural subunits.**
Gen. Dev.; 11: 3109–3115

Hastie N.D., Dempster M., Dunlop M.G., Thompson A.M., Green D.K., Allshire R.C. (1990). **Telomere reduction in human colorectal carcinoma and with ageing.**
Nature; 346: 866-888

Hilliard M., Frohnert C., Spillner C., Marcone S., Nath A., Lampe T., Fitzgerald D. J., Kehlenbach R. H. (2010). **The Anti-inflammatory Prostaglandin 15-Deoxy-$\Delta^{12,14}$-PGJ$_2$ Inhibits CRM1-dependent Nuclear Protein Export.**
JBC; 285:22202–22210

Ho T.C., Chen S.L., Yang Y.C., Chen C.Y., Feng F.P., Hsieh J.W., Cheng H.C., Tsao Y.P. (2008). **15-Deoxy (12,14)-prostaglandin J2 Induces Vascular Endothelial Cell Apoptosis through the Sequential Activation of MAPKS and p53.**
JBC; 283: 30273–30288

Hoelz A., Debler E.W., Blobel G. (2011). **The Structure of the Nuclear Pore Complex.**
Annu. Rev. Biochem.; 80: 613-643

Hutten S., (2007). **Untersuchungen zur Funktion der cytoplasmatischen Nukleoporine Nup214 und Nup358 im nukleocytoplasmatischen Transport.** Dissertation zur Erlangung des Doktorgrades. Mathematische- Naturwissenschaftliche Fakultät, Ernst-August-Universität, Göttingen

Hutten S., Flotho, A., Melchior, F., Kehlenbach, R.H. (2008). **The Nup358/ RanGAP complex is required for efficient importin α/β-dependent nuclear import.**
Mol. Biol. Cell.; 19:2300-2310.

Hutten S., Wälde S., Spillner C., Hauber J., and Kehlenbach R.H. (2009). **The nuclear pore component Nup358 promotes transportin-dependent nuclear import.**
J. Cell Sci.; 122:1100-10. Epub 2009 Mar 19.

Izaurralde E., Kutay U., von Kobbe C., Mattaj I.W. and Görlich D. (1997). **The asymmetric distribution of the constituents of the Ran system is essential for transport into and out of the nucleus.**
The EMBO J.; 16:6535–6547

Jakob S., Schroeder P., Lukosz M., Büchner N., Spyridopoulos I., Altschmied J., Haendeler J. (2008). **Nuclear Protein Tyrosine Phosphatase Shp-2 Is One Important Negative Regulator of Nuclear Export of Telomerase Reverse Transcriptase.**
JBC; 48: 33155-33161

Jacobs S.A., Podell E.R. Cech T.R. (2006). **Crystal structure of the essential N-terminal domain of telomerase reverse transcriptase.**
Nat. Struct. Mol. Biol., 13: 218–225

Jäkel S., Görlich D. (1998.) **Importin β, transportin, RanBP5 and RanBP7 mediate nuclear import of ribosomal proteins in mammalian cells.**
The EMBO J.; 17:4491–4502

Jäkel S., Albig W., Kutay U., Bischoff F.R., Schwamborn K., Dönecke D., Görlich D. (1999). **The importinβ/ importin 7 heterodimer is a functional nuclear import receptor for histone H1.**
The EMBO J.; 18:2411–2423

Kahle J., Piaia E., Neimanis S., Meisterernst M., Doenecke D., (2009). **Regulation of Nuclear Import and Export of Negative Cofactor 2β.**
JBC; 284:9382–9393

Kalantari P., Narayan V., Henderson A.J., Prabhu K.S. (2009). **15-Deoxy-12,14-prostaglandin J2 inhibits HIV-1 transactivating protein, Tat, through covalent modification.**
FASEB J.; 23: 1-8

Kalderon D., Richardson W.D., Markham A.F., Smith A.E. (1984). **Sequence requirements for nuclear location of simian virus 40 large-T antigen.**
Nature; 311:33-8.

Kondo, M., Oya-Ito, T., Kumagai, T., Osawa, T., and Uchida, K. (2001). **Cyclopentenone prostaglandins as potential inducers of intracellular oxidative stress.**
JBC; 276:12076–12083

Koyama M., Matsuura Y. (2010). **An allosteric mechanism to displace nuclear export cargo from CRM1 and RanGTP by RanBP1.**
The EMBO J.; 29: 2002–2013

Kosugi S., Hasebe M., Tomita M., Yanagawa H. (2008). **Nuclear export signal consensus sequences defined using a localization-based yeast selection system.**
Traffic; 9: 2053-2062

Krishnan V.V., Lau E.Y., Yamada J., Denning D.P., Patel S.S., Colvin M.E., Rexach M.F. (2008). **Intramolecular cohesion of coils mediated by phenylalanine–glycine motifs in the natively unfolded domain of a nucleoporin.**
PLoS Comput. Biol.; 4: e1000145.

Kudo N., Matsumori N., Taoka H., Fujiwara D., Schreiner E. P., Wolff B., Yoshida M., Horinouchi S., (1999). **Leptomycin B inactivates CRM1/exportin1 by covalent modification of a cysteine residue in the central conserved region.**
Proc. Natl. Acad. Sci. USA; 96:9112–9117

Kutay U., Bischoff F.R.,Kostka S., Kraft R., Görlich D. (1997). **Export of Importin [alpha] from the Nucleus Is Mediated by a Specific Nuclear Transport Factor.**
Cell; 90:1061-1071

Lamond A.I., (1989). **Tetrahymena telomerase contains an internal RNA template.**
TIBS; pp. 202-204, June 14, 1989

Lee J.B., Cansizoglu A.E., Süel K.E., Louis T.H., Zhang Z., Chook Y.M. (2006). **Rules for Nuclear Localization Sequence Recognition by Karyopherinβ2.**
Cell; 126: 543-558

Lindsay M.E., Holaska J.M., Welch K., Paschal B.M., Macara I.G. (2001). **Ran-binding protein 3 is a cofactor for Crm1-mediated nuclear protein export.**
JCB; 153:1391-1402

Lingner J., Hughes T.R., Shevchenko A., Mann M., Lundblad V., Cech T.R. (1997). **Reverse transcriptase motifs in the catalytic subunit of telomerase.**
Science; 276: 561–567

Lim R.Y., Fahrenkrog B., Koser J., Schwarz-Herion K., Deng J., Aebi U. (2007a). **Nanomechanical basis of selective gating by the nuclear pore complex.**
Science; 318: 640–643

Lim R.Y., Koser J., Huang N.P., Schwarz-Herion K., Aebi U. (2007b). **Nanomechanical interactions of Phenylalanineglycine nucleoporins studied by single molecule forcevolume spectroscopy.**
J. Struct. Biol.; 159: 277–289

Mahajan R., Delphin C., Guan T., Gerace L., Melchior F. (1997). **A small ubiquitin-related polypeptide involved in targeting RanGAP1 to nuclear pore complex protein RanBP2.**
Cell; 88: 97–107

Mattaj I.W., Englmeier L. (1998). **Nucleocytoplasmic transport: the soluble phase.**
Annu. Rev. Biochem.; 67:265-306

Matunis M.J., Coutavas E., Blobel G. (1996). **A novel ubiquitin- like modification modulates the partitioning of the Ran-GTPase- activating protein RanGAP1 between the cytosol and the nuclear pore complex.**
JCB; 135: 1457–1470

Moore J.D., Yang J., Truant R., Kornbluth S. (1999). **Nuclear import of Cdk/cyclin complexes: identification of distinct mechanisms for import of Cdk2/cyclin E and Cdc2/cyclin B1.**
JCB; 144:213-224

Monecke T., Haselbach D., Voß B., Russek A., Neumann P., Thomson E., Hurt E., Zachariae U., Stark H., Grubmüller H., Dickmanns A., Ficner R. (2013). **Structural basis for cooperativity of CRM1 export complex formation.**
PNAS; 3:960-965

Moriarty T.J., Huard S., Dupuis S., Autexier C. (2002). **Functional Multimerization of Human Telomerase Requires an RNA Interaction Domain in the N Terminus of the Catalytic Subunit.**
Mol. Cell. Biol.; 22:1253–1265

Morin G.B., (1989). **The Human Telomere Terminal Transferase Enzyme Is a Ribonucleoprotein That Synthesizes TTAGGG Repeats.**
Cell; 59:521-529

Moy T.I., Silver P.A. (2002). **Requirements for the nuclear export of the small ribosomal subunit.**
J. Cell. Sci.; 115:2985-2995

Mutka S.C., Yang W.Q., Dong S.D., Ward S.L., Craig D.A., Timmermans P.B.M.W.M., Murli S. (2009). **Identification of nuclear export inhibitors with potent anticancer activity in vivo**
Cancer Res.; 69: 510–517

Nachury M.V., Weis K. (1999). **The direction of transport through the nuclear pore can be inverted.**
Proc. Natl. Acad. Sci.; 96: 9622-9627

Nakamura T.M., Morin G.B., Chapman K.B., Weinrich S.L., Andrews W.H., LingnerJ., Harley C.B., Cech T.R. (1997). **Telomerase catalytic subunit homologs from fission yeast and human.**
Science; 277: 955–959

Nakielny S., Siomi M.C., Siomi H., Michael W.M., Pollard V., Dreyfuss G. (1996). **Transportin: nuclear transport receptor of a novel nuclear protein import pathway.**
Exp. Cell. Res.; 229:261-266

Nemergut M.E., Lindsay M.E., Brownawell A.M., Macara I.G. (2002). **Ran-binding protein 3 links Crm1 to the Ran guanine nucleotide exchange factor.**
JBC; 277:17385-17388.

Ohtsubo M., Okazaki H., Nishimoto T. (1989). **The RCC1 protein, a regulator for the onset of chromosome condensation locates in the nucleus and binds to DNA.**
JCB; 109:1389-1397

Oliva J. L., Pérez-Sala D., Castrillo A., Martínez N., Canada, F. J., Boscá L., and Rojas J. M. (2003). **The cyclopentenone 15-deoxy-delta 12,14-prostaglandin J2 binds to and activates H-Ras.**
Proc. Natl. Acad. Sci. U.S.A.; 100: 4772–4777

Pante N., and Aebi U. (1993). **The nuclear pore complex.**
    JCB; 122:977-985

Paraskeva E., Izzauralde E., Bischoff F.R., Huber J., Kutay U., Hartmann E., Lührmann R., Görlich D. (1999). **CRM1-mediated Recycling of Snurportin 1 to the Cytoplasm.**
    JCB; 145:255-264

Pemberton L.F., Paschal B.M. (2005) **Mechanisms of Receptor-Mediated Nuclear Import and Nuclear Export.**
    Traffic 6: 187-198

Perisic O., Paterson H. F., Mosedale G., Lara-González S., Williams R. L. (1999). **Mapping the phospholipid-binding surface and translocation determinants of the C2 domain from cytosolic phospholipase A2.**
    JBC; 274:14979–14987

Peters R. (2005). **Translocation through the nuclear pore complex: Selectivity and speed by reduction-of-dimensionality.**
    Traffic; 6: 421–427

Pradet-Balade B., Girard C., Boulon S., Paul C., Azzag K., Bordonne´ R. , Bertrand E., C. Verheggen (2011**). CRM1 controls the composition of nucleoplasmic pre-snoRNA complexes to licence them for nucleolar transport.**
    The EMBO J.; 30:2205–2218

Rajakaria R., Hilliard M., Lawrence T., Trivedi S., Colville-Nash P., Bellingan G., Fitzgerald D., Yaqoob M. M., Gilroy D. W. (2007). **Hematopoietic prostaglandin D_2 synthase controls the onset and resolution of acute inflammation through PGD_2 and 15-deoxyΔ^{12-14} PGJ_2.**
    PNAS; 104:20979–20984

Rexach M., Blobel G. (1995). **Protein import into nuclei: association and dissociation reactions involving transport substrate, transport factors, and nucleoporins.**
    Cell; 83:683-692

Ribbeck K., Lipowsky G., Kent H.M., Stewart M., Görlich D. (1998). **NTF2 mediates nuclear import of Ran.**
    The Embo J.; 17:6587-6598

Ribbeck K., Görlich D. (2001). **Kinetic analysis of translocation through nuclear pore complexes.**
    The Embo J.; 20: 1320-1330

Richards S. A., Lounsbury K. M., Carey K. L., and Macara I. G. (1996). **A nuclear export signal is essential for the cytosolic localization of Ran binding protein, RanBP1.**
    JCB; 134: 1157–1168

Richardson W.D., Mills A.D., Dilworth S.M., Laskey R.A., Dingwall C. (1988). **Nuclear protein migration involves two steps: rapid binding at the nuclear envelope followed by slower translocation through nuclear pores.**
    Cell; 52:655-664

Robbins J., Dilworth S.M., Laskey R.A., Dingwall C. (1991). **Two interdependent basic domains in nucleoplasmin nuclear targeting sequence: identification of a class of bipartite nuclear targeting sequence.**
Cell; 64:615-623

Rodriguez M.S., Dargemont C., Stutz F. (2004). **Nuclear export of RNA.**
Biol. Cell.; 96: 639-655

Roloff S., Spillner C., Kehlenbach R.H. (2013). **Several phenylalanine-glycine motives in the nucleoporin Nup214 are essential for binding of the nuclear export receptor CRM1.**
JBC; 288: 3952-3963

Rossi A., Kapahi P., Natoli G., Takahashi T., Chen Y., Karin M., Santoro M.G. (2000**). Anti-inflammatory cyclopentenone prostaglandins are direct inhibitors of IkB kinase.**
Nature; 403: 103-108

Rout M.P., Aitchinson J.D., (2001). **The Nuclear Pore Complex as a Transport Machine.**
JBC; 276: 16593–16596

Rout M.P., Aitchinson J.D., Magnasco M.O., Chait B.T. (2003). **Virtual gating and nuclear transport: the hole picture.**
Trends Cell Biol.; 13:622-628

Rouzer C.A., Jacobs A.T., Nirodi C.S., Kingsley P.J., Morrow J.D., Marnett L.J., (2005). **RAW264.7 cells lack prostaglandin-dependent autoregulation of tumor necrosis factor-α secretion.**
J. Lipid Res.; 46:027-1037

Saijou E., Itoh T., Kim K.W., Iemura S., Natsume T., Myajima A., (2007). **Nucleocytoplasmic Shuttling of the Zinc Finger Protein EZI Is Mediated by Importin-7-dependent Nuclear Import and CRM1-independent Export Mechanisms.**
JBC; 282:32327–3233

Scher J.U., Pillinger M.H. (2004). **15d-PGJ$_2$: The anti-inflammatory prostaglandin?**
Clin. Immunol.; 114:100– 109

Scher J.U., Pillinger M.H. (2009). **The Anti-Inflammatory Effects of Prostaglandins.**
J. Inv. Med.; 57:703-708

Schooley A., Vollmer B., Antonin W. (2012). **Building a nuclear envelope at the end of mitosis: coordinating membrane reorganization, nuclear pore complex assembly, and chromatin de-condensation.**
Chromosoma; 121:539–554

Seimiya H., Sawada H., Muramatsu Y., Shimizu M., Ohko K., Yamane K., Tsuruo T., (2000). **Involvement of 14-3-3 proteins in nuclear localization of telomerase.**
The EMBO J.; 19:2652-2661

Shao C., Lu C., Chen L., Koty P.P., Cobos E., Gao W. (2011). **p53-Dependent anticancer effects of Leptomycin B on lung adenocarcinoma.**
Cancer Chem. Pharmacol.; 67:1369-1380

Shin S.W., Seo C.Y., Han H., Han J.Y., Jeong J.S., Kwak J.Y., Park J.I. (2009). **15d-PGJ2 Induces Apoptosis by Reactive Oxygen Species–mediated Inactivation of Akt in Leukemia and Colorectal Cancer Cells and Shows In vivo Antitumor Activity.**
Clin. Cancer Res.; 15: 5414-5425

Siomi M.C., Eder P.S., Kataoka N., Wan L., Liu Q., Dreyfuss G. (1997). **Transportin mediated Nuclear Import of Heterogeneous Nuclear RNP Proteins.**
JCB; 138:1181-1192

Smith A., Brownawell A., Macara I.G. (1998**). Nuclear import of Ran is mediated by the transport factor NTF2.**
Curr. Biol.; 8:1403-6

Spencer A. G., Woods J. W., Arakawa T., Singer II, Smith W. L. (1998). **Subcellular localization of prostaglandin endoperoxide H synthase-1 and -2 by immunoelectron microscopy.**
JBC; 273:9886–9893

Stade K., Ford C.S., Guthrie C., Weis K. (1997). **Exportin 1 (Crm1p) is an essential nuclear export factor.**
Cell; 90:1041-1050

Stewart M. (2007). **Molecular mechanism of the nuclear protein import cycle.**
Nat. Rev. Mol. Cell. Biol.; 8:195-208. Epub 2007 Feb 7.

Straus D.S., Glass C.K. (2001) **Cyclopentenone prostaglandins: new insights on biological activities and cellular targets.**
Med. Res. Rev.; 21: 185–210

Straus D.S., Pascual G., Li M., Welch J.S., Ricote M., Hsiang C.H., Sengchanthalangsy L.L., Ghosh G., Glass C.K. (2000). **15-Deoxy-$\Delta^{12,14}$-prostaglandin J$_2$ inhibits multiple steps in the NF-kB signaling pathway.**
PNAS; 97: 4844–4849

Suntharalingam M., Wente SR. **Peering through the pore: nuclear pore complex structure, assembly, and function.**
Dev. Cell;4: 775–789

Terry L.J., and Wente S.R. (2009). **Flexible gates: dynamic topologies and functions for FG-nucleoporins in nucleocytoplasmic transport.**
Eukaryot Cell. 8:1814-27. Epub 2009 Oct 2.

Tomlinson R.L., Ziegler T.D., Supakorndej T., Terns R.M., Terns M.P. (2006). **Cell cycle-regulated trafficking of human telomerase to telomeres.**
Mol. Biol. Cell; 17: 955–965

Tran E.J., Wente S.R. (2006). **Dynamic nuclear pore complexes: Life on the edge.**
Cell; 125: 1041–1053

Tuschl T. (2001). **RNA interference and small interfering RNAs.**
Chembiochem.; 2: 239-245

Tuschl T., Zamore P.D., Lehmann R., Bartel D.P., Sharp P.A. (1999). **Targeted mRNA degradation by double-stranded RNA in vitro.**
Genes Dev.; 13: 3191-3197

Venteicher A. S., Abreu E. B., Meng Z., McCann K. E., Terns R. M., Veenstra T. D., Terns M. P., Artandi S. E. (2009.**) A human telomerase holoenzyme protein required for Cajal body localization and telomere synthesis.**
Science; 323: 644-648

Wälde S., Thakar K., Hutten S., Spillner C., Nath A., Rothbauer U., Wiemann S., Kehelnbach R.H., (2012). **The Nucleoporin Nup358/RanBP2 Promotes Nuclear Import in a Cargo-and Transport Receptor-Specific Manner.**
Traffic; 13: 218–233

Wälde S., (2010) **The function of Nup358 in nucleocytoplasmic transport.**
Dissertation for the award of the degree „Doctor rerum naturalium ", Division of Mathematics and Natural Sciences, Georg-August University, Göttingen

Walther T.C., Pickersgill H., Cordes V.C., Goldberg M.W., Allen T.D., Mattaj I.W., Fornerod M. (2002) **The cytoplasmic filaments of the nuclear pore complex are dispensable for selective nuclear protein import.**
JCB; 158:63-77

Weis K. (2003) **Regulating Access to the Genome: Nucleocytoplasmic Transport throughout the Cell Cycle.**
Cell; 112:441–451

Wente S.R., Rout M.P. (2010) **The Nuclear Pore Complex and Nuclear Transport**
Cold Spring Harb. Perspect. Biol.; published online July 14, 2010

White H. (1980). **A heteroskedasticity-consistent covariance matrix estimator and a direct test for heteroskedasticity.**
Econometrica; 48:817-838

Witkin K.L., Prathapam R., Collins K. (2007). **Positive and Negative Regulation of *Tetrahymena* Telomerase Holoenzyme.**
Mol. Cell. Biol.; 27: 2074-2083

Wohlwend, D., Strasser, A., Dickmanns, A., Doenecke, D., and Ficner, R. (2007.9 **Thermodynamic Analysis of H1 Nuclear Import: Receptor tuning of importin β/importin 7.**
JBC; 282:10707-10719. Epub 2007 Jan 26.

Wong J. M. Y., Kusdra L., Collins K. (2002). **Subnuclear shuttling of human telomerase induced by transformation and DNA damage.**
Nat. Cell Biol.; advanced online publication DOI: 10.1038/ncb846; August 27, 2002

Wu .J, Matunis M.J., Kraemer D., Blobel G., Coutavas E. (1995). **Nup358, a cytoplasmically exposed nucleoporin with peptide repeats, Ran-GTP binding sites, zinc fingers, a cyclophilin A homologous domain, and a leucine-rich region.**
JBC; 270:14209-14213

Wyatt H.D.M., West S.C., Beattie T.L. (2010). **InTERTpreting telomerase structure and function.**
Nucl. Acids Res.; 38: 5609–5622

Yamada J., Phillips J.L., Patel S., Goldfien G., Calestagne-Morelli A., Huang H., Reza R., Acheson J., Krishnan V.V., Newsam S., Gopinathan A., Lau E.Y., Colvin M.E., Uversky V.N., Rexach M.F. (2010). **A bimodal distribution of two distinct categories of intrinsically-disordered structures with separate functions in FG-nucleoporins.**
Mol. Cell Proteomics; M000035-MCP201

Yokoyama N., Hayashi N., Seki T., Pante N., Ohba T., Nishii K., Kuma K., Hayashida T., Miyata T., Aebi U., Fukui M., Nishimoto T. (1995). **A giant nucleopore protein that binds Ran/TC4.**
Nature.; 376:184-188.

Zhang M.J., Dayton A.I. (1998). **Tolerance of diverse amino acid substitutions at conserved positions in the nuclear export signal (NES) of HIV-1 Rev.**
Biochem. Biophys. Res. Commun; 243: 113-116

Abbreviations

Physical Units

°C	degree celsius
g	gram
x g	acceleration of gravity on earth
h	hour(s)
l	liter
M	molar (mol/l)
min	minute(s)
m	meter
OD	optical density
pH	potential hydrogen
rpm	rotations per minute
s	second(s)
U	Unit
V	volt

Prefixes

k	kilo-	10^3
c	centi-	10^{-2}
m	mili-	10^{-3}
μ	micro-	10^{-6}
n	nano-	10^{-9}
p	pico-	10^{-12}

Code for amino acids

A	Ala	alanine
C	Cys	cysteine
D	Asp	aspartate
E	Glu	glutamate
F	Phe	phenylalanine
G	Gly	glycine
H	His	histidine
I	Iso	isoleucine
K	Lys	lysine
L	Leu	leucine
M	Met	methionine
N	Asn	asparagine
P	Pro	proline
Q	Gln	glutamine
R	Arg	arginine
S	Ser	serine
T	Thr	threonine
V	Val	valine
W	Trp	tryptophane
Y	Tyr	tyrosine
X	any	
φ	hydrophobic	

General abbreviations

15d-PGJ$_2$	15-deoxy-$^{\Delta12,14}$ prostaglandinJ$_2$
A	adenine (DNA and RNA)
Aa	amino acids
Aff. pur.	affinity purified

ATP	adenosine-5-triphosphate
BIB	beta-like import receptor binding
bp	basepair
BSA	bovine serum albumine
C	cytosine (DNA and RNA)
CRM1	chromosome region maintenance 1
C-terminus	carboxy terminus
Da	Dalton
DBC-1	depleted-in-breast-cancer-1
DMEM	Dulbeccos's modified eagles medium
DMSO	dimethyl sulfoxide
DNA	desoxyribonucleic acid
dNTP	2'-desoxynucleoside-5'-triphosphate
DTT	dithiothreitol
ECL	enhanced chemical luminescence
E. coli	*Escherichia coli*
EDTA	ethylenediaminetetraacetic acid
ETOH	ethanol
FCS	fetal calf serum
FG-repeat	phenylalanine glycine repeat
FLIP	fluorescence loss in photo bleaching
G	guanine (DNA and RNA)
GAP	GTPase-activating protein
GDP	guanosine-5'-diphosphate
GFP	green fluorescent protein
GST	glutathione-S-transferase
GTP	guanosine-5'-triphosphate
GTPase	GTP-hydrolase
HA	hemagglutinin
HCl	hydrochloric acid

HEAT	Huntington, elongation factor 3, 'A' subunit of protein phosphatase 2A and TOR1
HEPES	[4-(2-hydroxyethyl)-1-piperazine]ethanesulfonic
His	histidine tag
HIV	human immunodeficiency virus
IF	immunofluorescence
Imp/ IPO	importin
IP	immunoprecipitation
IPTG	isopropyl-β-D-thiogalactopyranoside
KD	knock-down
LB	Luria-Bertani
LMB	leptomycin B
NC2β	negative-cofactor-2-β
NES	nuclear export signal
cNLS	(classical) nuclear localization signal
NP40	octyl phenoxylpolyethoxylethanol
NPC	nuclear pore complex
NTE	N-terminal extension
N-terminus	amino terminus
Nup	nucleoporin
PAGE	polyacrylamide gel electrophoresis
PBS	phosphate buffered saline
PCR	polymerase chain reaction
PG	prostaglandin
POM	pore membrane protein
PY-NLS	proline tyrosine-NLS, motif for interaction of transportin
pH	negative common logarithm of the proton
PMSF	phenylmethylsulphonyl fluoride
Ran	Ras related nuclear protein
RanBP1	Ran binding protein 1
RanBP2	Ran binding protein 2

RanBD	Ran binding domain
RCC1	regulator of chromosome condensation 1
RFP	red fluorescent protein
RID1	RNA interaction domain1
RNA	ribonucleic acid
ROI	region of interest
RNAi	RNA interference
RNase	ribonuclease
RT	reverse transcriptase
SDS	sodium dodecyl sulfate
siRNA	small interfering RNA
T	thymine, in context of DNA and RNA
TAE	Tris / Acetate / EDTA
TAP	Tip-(Herpesvirus saimiri tyrosine-kinaseinteracting-protein) associated protein
TE	Tris / EDTA
TERT	telomerase reerse transcriptase (protein subunit)
TFIIAα	transcription-factor-II-α
TR	telomerse RNA
TRBD	telomerase RNA binding domain
Triton X-100	4-octylphenol polyethoxylate
Tween20	polyoxyethylene (20) sorbitan monolaurate
U	uracile, in context of RNA
UV	ultraviolet
v/v	volume per volume
WB	western blot
wt	wild type
w/v	weight per volume

Acknowledgements

Curriculum vitae

Personal data

Name:	Cornelia Frohnert
Date of birth:	03.04.1982 (Göttingen)

Education

01.04.2009- 31.03.2012	**pHD thesis** „The prostaglandin 15d-PGJ$_2$ inhibits CRM1 mediated protein export. Analysis of *human* TERT nuclear import." Department of Molecular Biology Center for Biochemistry and Molecular Cell Biology Georg-August University, Göttingen Supervisor: Prof. Dr. Ralph Kehlenbach
01.01.2009- 28.02.2009	Research assistent Department for Developmental Biology, GZMB, Göttingen
01.2008-10.2008	**Diploma thesis** „Molekulare Charakterisierung des Kernmembranproteins Spag4L-2" Department for Developmental Biology GZMB Georg-August University, Göttingen Supervisor: Prof. Dr. Sigrid Hoyer-Fender
10.2001-12.2008	Graduate and undergraduate studies: Biology Georg-August-University, Göttingen
06.2001	University entrance qualification: Abitur Felix-Klein-Gymnasium Göttingen
1988-2001	School education

Publications

Frohnert C., Schweizer S., Hoyer-Fender S. (2010). SPAG4L/SPAG4L-2 are testis-specific SUN domain proteins restricted to the apical nuclear envelope of round spermatids facing the acrosome.
Mol. Hum. Reprod.; December 15, 2010

Hilliard M., **Frohnert C.**, Spillner C., Marcone S., Nath A., Lampe T., Fitzgerald D. J., Kehlenbach R. H. (2010). The Anti-inflammatory Prostaglandin 15-Deoxy-$\Delta^{12,14}$-PGJ$_2$ Inhibits CRM1-dependent Nuclear Protein Export.
JBC; July 16, 2010